MONTHLY NOTICES

OF THE

ROYAL ASTRONOMICAL SOCIETY.

VOL. XCI. JUNE 12, 1931. No. 8

Dr. H. KNOX-SHAW, PRESIDENT, in the Chair.

The election by the Council of the following Fellows was duly confirmed :—

John Robinson Airey, M.A., Sc.D., D.Sc., Queenswood, Beckett Park, Leeds ;

Arthur Coombe, M.A., Headmaster of Chichester School, Chichester ;

Rev. Henry Norman Edge, 11 Groombridge Road, South Hackney, London, E. 9 ;

Henry Patrick Folkard, Curraghmore, Edgwarebury Lane, Edgware, Middlesex ;

Vice-Admiral C. A. Fountaine, C.B., Narford Hall, King's Lynn, Norfolk ;

Miss Colleen B. Orpen, B.Sc., P.O., Afrika's Kop, O.F.S., S. Africa ; and

Laurence Chisholm Young, B.A., Trinity College, Cambridge.

The following candidate was proposed for election as a Fellow of the Society, the name of the proposer from personal knowledge being appended :—

E. C. Bullard, Clare College, Cambridge (proposed by Harold Jeffreys).

Seventy-eight presents were announced as having been received since the last meeting, including :—

M. E. J. Gheury de Bray : Elementary Hyperbolics for Technical and other Students, 2 vols.

No.	Name and D.M. No.	Mag. Vis. Phot.	Type.	R.A., Dec. (1900). h m s	Proper-Motion. R.A. Unit ″·001.	Proper-Motion. Dec. Unit ″·001.	P.E. Unit Weight. Unit ″·001.	Paral-lax. Unit ″·001.	P.E. Unit ″·001.
236	−0° 1987	6·83	Go	8 19 27	+ 81	− 215	22	+ 25	± 8
		7·39		−0° 49′·2	+ 77				±10
237	−22° 2317	7·38	G5	8 29 26	− 333	+ 157	22	+ 37	± 8
		8·3		−23° 1′·1	− 361				± 8
238	−15° 2546	9·4	F5	8 36 11	+ 389	− 500	15	+ 25	± 6
		9·8		−15° 58′·6	+ 353				± 6
239	−42° 4528	8·4	Ko	8 38 37	− 309	− 100	23	+ 46	± 8
		8·6		−42° 34′·1	− 274				± 8
240	−14° 2757	7·26	Go	9 3 46	− 518	− 206	20	+ 44	± 7
		7·82		−14° 44′·1	− 565				± 8
241	−25° 6905	6·81	F8	9 4 16	− 337	− 36	25	+ 41	± 9
		8·3		−25° 26′·1	− 327				±10
242	−24° 8451	9·2	K2	9 42 35	− 18	− 302	19	− 8	± 7
		9·9		−24° 47′·3	+ 2				± 8
243	−37° 7536	6·53	F8	11 49 25	− 320	+ 59	23	+ 48	± 8
		7·2		−37° 11′·7	− 324				± 9
244	−26° 8883	7·16	K5	11 52 58	−1073	− 627	24	+ 96	± 9
		8·0		−27° 8′·0	−1040				± 9
245	−41° 7056	6·28	Ko	12 10 19	− 315	− 190	22	+ 21	± 7
		8·2		−41° 21′·1	− 337				± 8
246	−14° 3521	8·31	G5	12 22 55	− 275	− 100	23	+ 30	± 8
		9·09		−15° 5′·7	− 266				± 9
247	Boss 3316	7·50	Go	12 38 22	− 668	− 230	22	+ 29	± 7
	−37° 8082	8·3		−37° 9′·3	− 545				± 8
248	−17° 4092	9·1	Go	14 21 52	− 71	− 290	22	+ 3	± 7
		9·7		−17° 57′·2	− 67				± 8
249	−25° 10584	10·0	G5	14 46 57	− 253	− 177	23	+ 17	± 7
		10·2		−25° 37′·8	− 145				± 8
250	−59° 5821	9·2	B9	15 0 21	..	..	24	+ 16	± 7
		8·8		−59° 35′·0	− 8				± 8
251	−59° 5823	8·7	Go	15 0 25	− 258	− 160	20	+ 21	± 6
		8·9		−59° 33′·7	− 187				± 7
252	85 G Lupi	5·71	Go	15 15 3	−1639	− 276	20	+ 58	± 6
	−47° 9919	6·9		−47° 57′·0	−1625				± 8

No.	Name and D.M. No.	Mag. Vis. Phot.	Type.	R.A., Dec. (1900).	Proper-Motion. R.A. Unit ″·001.	Proper-Motion. Dec.	P.E. Unit Weight.	Parallax. Unit ″·001.	P.E. Unit ″·001.
				h m s					
253	−10° 4149	7·26	F5	15 37 42	−1150	− 300	20	+ 34	± 7
		7·68		−10° 36′·4	−1150				± 8
254	−70° 2163	7·4	G5	15 58 32	− 217	− 370	21	+ 41	± 7
		8·2		−70° 47′·3	− 172				± 8
255	−47° 10664	9·3	K2	16 13 1	− 410	− 800	19	+ 35	± 5
		9·6		−47° 57′·7	− 416				± 7
256	−53° 7865	8·3	G5	16 14 47	− 364	0	26	+ 11	± 8
		8·6		−53° 39′·9	− 343				±10
257	−12° 4523	9·8	..	16 24 45	0	−1240	22	+264	± 8
		11·8		−12° 25′·1	− 136				± 9
258	β Apodis	4·16	Ko	16 28 47	− 290	− 346	18	+ 23	± 6
	−77° 1221	5·9		−77° 18′·5	− 275				± 8
259	Boss 4372	6·66	K2	17 10 4	− 485	−1123	19	+190	± 5
	−26° 12036	8·1		−26° 24′·1	− 498				± 7
260	41 G Aræ *	5·58	Ko	17 11 28	+ 948	+ 207	24	+116	± 8
	−46° 11370	7·2		−46° 31′·9	+1078				± 9
261	−46° 11539	9·1	G5	17 21 3	..	..	16	− 6	± 5
		9·1		−46° 47′·1	+ 19				± 6
262	−46° 11540 †	9·4	..	17 21 6	+ 544	− 908	19	+237	± 6
		11·0		−46° 46′·9	+ 585				± 8
263	−59° 7063	7·71	Go	17 25 12	0	− 390	24	+ 18	± 6
		8·2		−59° 41′·6	− 68				± 8
264	−42° 12320	7·7	G5	17 30 43	+ 166	− 360	24	+ 34	± 8
		7·4		−42° 29′·7	+ 205				± 9
265	−40° 11755	9·0	F5	17 35 50	− 80	− 440	26	+ 21	± 8
		8·8		−40° 15′·6	− 95				±10
266	−33° 12476	6·95	G5	17 41 22	− 246	− 564	19	+ 48	± 6
		8·2		−33° 57′·9	− 214				± 8
267	−7° 4517	7·60	G5	17 47 33	− 71	− 236	22	+ 15	± 7
		8·38		−7° 53′·3	+ 13				± 8

* Brighter component observed. Derived p.m. in R.A. includes orbital motion.

† The p.m. star is wrongly identified by Innes as H.D. 157931 (Co.D. − 46° 11539) in *U.O.C.*, 58, 1923.

No.	Name and D.M. No.	Mag. Vis. Phot.	Type.	R.A., Dec. (1900).	Proper-Motion. R.A. Unit ″·001.	Proper-Motion. Dec. Unit ″·001.	P.E. Unit Weight.	Paral-lax. Unit ″·001.	P.E. Unit ″·001.
				h m s					
268	−43° 12343	8·1	Ma	18 5 6	+ 76	− 480	17	+ 76	± 5
		9·5		−43° 27′·3	+ 119				± 6
269	−11° 4672	8·8	..	18 27 56	− 264	− 260	18	+ 55	± 6
		11·5		−11° 42′·2	− 286				± 7
270	−66° 3406	8·5	G5	18 51 2	+ 145	− 340	22	+ 36	± 7
		9·3		−66° 19′·0	+ 100				± 9
271	−20° 5385	9·4	Go	18 58 3	− 281	− 650	18	− 9	± 5
		9·8		−20° 35′·4	− 293				± 7
272	−46° 12902	9·3	K5	19 9 22	+ 219	− 410	18	+ 77	± 5
		10·7		−46° 3′·3	+ 191				± 6
273	−45° 13161	9·9	..	19 15 4	+ 138	− 440	25	+ 18	± 8
		11·0		−45° 7′·5	+ 176				± 9
274	−25° 14171	9·3	Go	19 29 5	− 118	− 282	20	+ 14	± 7
		9·4		−25° 20′·6	− 60				± 7
275	−46° 13129	8·7	Go	19 32 49	− 267	− 240	17	+ 17	± 5
		9·6		−46° 44′·9	− 57				± 6
276	242 G Sagittarii	6·28	Ko	19 48 18	− 129	− 411	27	+ 82	± 8
	−24° 15668	7·6		−24° 11′·4	− 193				±11
277	−55° 9370	8·44	G5	20 13 56	− 275	− 130	20	+ 35	± 6
		9·3		−55° 7′·4	− 218				± 7
278	ϱ Capricorni	4·96	Fo	20 23 9	− 14	− 22	21	+ 43	± 7
	−18° 5689	5·24		−18° 8′·7	− 23				± 8
279	Boss 5247	6·69	Ko	20 23 18	+ 40	− 130	18	+ 11	± 6
	−18° 5691	7·69		−18° 12′·2	− 6				± 7
280	Boss 5263	5·81	G5	20 26 55	+ 280	+ 106	16	+ 36	± 5
	−10° 5423	6·59		−10° 11′·7	+ 308				± 7
281	−66° 3496	7·7	G5	20 29 14	+ 136	− 372	16	+ 32	± 6
		8·5		−66° 52′·4	+ 86				± 7
282	−53° 9928	8·3	K5	20 34 58	0	−1085	22	+ 71	± 7
		10·8		−53° 1′·7	+ 84				± 9
283	−55° 9465	9·2	Ko	20 41 38	+ 266	− 230	23	+ 17	± 8
		10·2		−55° 8′·3	+ 157				±10
284	−70° 2814	6·84	G5	20 50 28	+ 411	− 300	20	+ 52	± 7
		7·8		−69° 57′·4	+ 435				± 9

No.	Name and D.M. No.	Mag. Vis. Phot.	Type.	R.A., Dec. (1900).	Proper-Motion. R.A. Unit ″·001.	Proper-Motion. Dec.	P.E. Unit Weight. Unit ″·001.	Parallax. Unit ″·001.	P.E. Unit ″·001.
				h m s					
285	−48° 13728	8·1	F8	20 51 11	+ 208	− 320	25	+ 19	± 8
		8·9		−48° 34′·8	+ 142				± 9
286	Wolf 918	..	..	21 3 43	+ 874	−1955	25	+ 71	± 9
		11·7		−13° 39′·6	+ 687				±11
287	−26° 15541	6·50	G5	21 13 59	− 564	− 353	23	+ 54	± 8
		7·6		−26° 45′·9	− 413				±11
288	−31° 18229	7·9	Go	21 17 5	+ 346	+ 90	24	+ 15	±10
		8·5		−31° 14′·5	+ 327				±11
289	−45° 14340	7·7	Ko	21 20 27	+ 253	+ 190	17	+ 64	± 6
		9·2		−45° 14′·8	+ 257				± 8
290	−28° 17381	9·5	Go	21 31 34	+ 319	− 212	19	+ 31	± 7
		9·3		−28° 4′·7	+ 365				± 8
291	−40° 14498	8·5	Ko	21 41 48	+ 125	− 370	25	+ 46	±10
		9·4		−40° 42′·5	+ 78				±11
292	−74° 2021	7·32	Go	21 45 38	− 250	− 460	21	+ 28	± 8
		8·2		−73° 53′·8	− 200				± 8
293	−23° 17135	6·85	F8	21 45 43	+ 314	− 98	23	+ 40	± 9
		7·7		−23° 44′·2	+ 305				±10
294	ε Indi	4·74	K5	21 55 43	+3915	−2591	24	+288	± 8
	−57° 10015	6·9		−57° 11′·8	+3927				± 9
295	−56° 9825	7·8	Go	22 4 8	+ 311	− 111	22	+ 21	± 7
		7·9		−55° 56′·6	+ 151				± 9
296	−16° 6046	6·60	G5	22 9 13	0	− 357	25	+ 32	± 9
		7·38		−16° 18′·3	− 36				±11
297	37 G Gruis	5·44	Go	22 11 42	+ 404	− 681	26	+ 84	± 9
	−54° 10055	6·5		−54° 6′·5	+ 361				±10
298	−30° 19122	8·1	G5	22 17 4	+ 411	79	13	+ 24	± 5
		8·5		−30° 7′·3	+ 416				± 6
299	−26° 16110	7·84	Go	22 17 37	+ 392	− 122	25	− 5	± 9
		8·5		−26° 20′·7	+ 381				±10
300	−59° 7808	9·5	G5	22 25 58	+ 207	− 460	22	+ 21	± 7
		10·3		−59° 17′·4	+ 212				± 7
301	−44° 14978	6·72	F8	22 30 46	+ 227	− 200	18	+ 34	± 6
		7·6		−43° 59′·3	+ 297				± 7

No.	Name and D.M. No.	Mag. Vis. Phot.	Type.	R.A., Dec. (1900).	Proper-Motion. R.A. Unit ″·001.	Proper-Motion. Dec. Unit ″·001.	P.E. Unit Weight. Unit ″·001.	Parallax. Unit ″·001.	P.E. Unit ″·001.
				h m s					
302	−16° 6152	7·36	Go	22 41 58	+ 352	− 64	19	+ 22	± 7
		7·92		−16° 40′·3	+ 357				± 8
303	−65° 4094	8·5	G5	22 47 42	+ 310	− 172	21	+ 17	± 7
		9·3		−65° 36′·0	+ 283				± 8
304	−27° 16109	8·2	G5	22 50 25	+ 203	− 223	23	+ 33	± 9
		8·7		−27° 11′·2	+ 210				±10
305	−23° 17699	7·6	Ma	22 55 0	− 898	+ 32	25	+137	± 9
		9·1		−23° 3′·8	− 922				±10
306	−67° 3959	9·2	Ko	23 11 1	+ 328	− 380	25	+ 26	±10
		10·2		−67° 28′·3	+ 350				±10
307	−67° 3960	8·9	Ko	23 11 4	+ 115	− 440	20	+ 41	± 8
		9·9		−67° 27′·2	+ 353				± 8
308	−58° 8064	8·6	Go	23 12 45	+ 233	− 120	24	+ 36	± 8
		8·4		−58° 50′·9	+ 193				± 8
309	−17° 6769	8·6	K5	23 27 34	+ 272	− 220	26	+ 65	±10
		9·8		−17° 23′·5	+ 282				±10
310	−18° 6342	9·1	K2	23 31 31	+ 328	+ 100	22	− 12	± 9
		10·2		−17° 47′·4	+ 412				± 8
311	−45° 15114	6·26	G5	23 38 40	+ 307	+ 20	25	+ 14	±11
		7·2		−45° 38′·3	+ 308				±10
312	−42° 16457	7·51	Ao	23 41 15	+ 223	− 850	22	+ 18	± 8
		8·0		−42° 6′·8	+ 221				± 9
313	27 G Phœnicis	6·01	F8	23 49 24	+ 362	+ 22	17	+ 8	± 7
	−40° 15285	6·8		−40° 51′·5	+ 372				± 8
314	−20° 6684	7·45	Ko	23 54 17	+ 520	− 315	20	− 4	± 7
		8·2		−20° 35′·0	+ 511				± 8
315	−29° 18946	8·00	G5	23 58 32	+ 263	− 151	22	+ 8	± 9
		8·9		−28° 56′·9	+ 295				±10

De Sitter's Universe and the Motion of Nebulæ.

By G. Castelnuovo.*

(*Communicated by Prof. H. F. Baker, F.R.S.*)

In recent years several works have appeared dealing with the solution of Einstein's gravitational equations, on the hypothesis of a finite space, which was given by de Sitter in 1917. At present the solution due to Friedman and Lemaître, which assumes the radius of curvature of three-dimensional space to be an increasing function of the time, is preferred to de Sitter's statical solution as being more in harmony with the spirit of general relativity theory; but it seems opportune to re-investigate the universe of de Sitter. A representation of this universe in Euclidean space, which appears preferable to others hitherto adopted, since it transforms geodesics into lines, enables us to discover more simply and rapidly some recent results obtained by different methods, and to correct or clear up several inexact or obscure statements.

The conclusion reached in the present paper is that the modification of the Doppler effect due to the curvature of space does not suffice to explain the *apparent* motion of the extra-galactic nebulæ, if we suppose that their *real* motions are distributed at random † ("disorganised movement"). Nevertheless we may obtain a quantitative explanation of the observed facts by assuming a *real* organised motion, such as would occur if an immense primitive nebula were scattered at a time enormously distant (theoretically at time $-\infty$), so as to give rise to the present system of nebulæ moving freely through curved space.‡ To an observer who does not share this motion, it would have an appearance analogous to that of the stars of an open cluster.

On the above hypothesis the radius of curvature of space is found to be 2×10^9 light years; and it is found that in $1{\cdot}4 \times 10^9$ years the mutual distances between the spiral nebulæ would be doubled (provided these distances do not exceed 10^8 light years). The values agree with those deduced by a different procedure from the assumption of an expanding universe.

1. De Sitter's universe U is a four-dimensional space of constant curvature. Hence, by a theorem of Beltrami's, it admits of a representation on Euclidean space S_4 of four dimensions, in which the geodesics of U have for images the lines of S_4.§ To the points of U

* The author wishes to express his hearty thanks to Mr. L. Roth, of the Imperial College of Science, for translating this paper into English.

† The same conclusion has already been arrived at by R. C. Tolman, in an article in the *Astrophysical Journal*, **69**, 145, 1929.

‡ This hypothesis, which H. Weyl, *Phil. Mag.* (7), **9**, 936, 1930, calls the "common origin of the nebulæ," is at once suggested by the present researches.

§ The same representation has been used by Du Val for the study of a question in topology concerning the universe of de Sitter ("A Geometrical Note," *Phil. Mag.*, **47**, 930, 1924). I have indicated elsewhere the fruitfulness of this method ("L'Universo di de Sitter," *Rendiconti Lincei* (6), **12**, 1930 October); for clearness I recall several results of this note. The correspondence between U and a region of S_4 is supposed birational. It is, however, possible to consider correspondences of a different character.

corresponds the *exterior* of the quadric (the "absolute" of Cayley and Klein), which has for its equation in Cartesian co-ordinates,

$$t^2 - x^2 - y^2 - z^2 = 1. \quad . \quad . \quad . \quad (1)$$

Of the lines of S_4 we consider only those which are external to the quadric, or the external portions of the secant lines. The first are *spatial* lines; two points of the same line represent contemporaneous events with respect to a given observer. The second are *temporal* lines and may be regarded as world lines of points having a free motion. The tangents to the quadric (1) are the world lines of light propagation.

The metric in S_4 is given by the known formulæ of Cayley-Klein. If M, N are the intersections, real or imaginary, of a line AB with (1), and if we write

$$(\mathrm{MNAB}) = \frac{\mathrm{MA}}{\mathrm{NA}} \Big/ \frac{\mathrm{MB}}{\mathrm{NB}},$$

the interval (AB) is measured by

$$(\mathrm{AB}) = \kappa \log (\mathrm{MNAB}) \quad . \quad . \quad . \quad (2)$$

where κ is a constant which depends on the unit of length.

In order that (AB) should be real on a spatial line it is necessary to suppose that κ is purely imaginary; we shall choose $\kappa = i/2$, and assume as unit of length the radius of curvature of a three-dimensional space external to the quadric (*e.g.* $t = 0$). The spatial lines are of finite length π and are closed; the distance between two points can never exceed $\pi/2$.

For a temporal line we shall take $\kappa = \frac{1}{2}$ in (2). The equation (2) then gives the interval of *proper time* between two positions A and B of an observer who has for world line the line AB. The unit of time is chosen so that the velocity of light is 1 in the neighbourhood of the observer.* The time varies from $-\infty$ to $+\infty$ as a given point moves along a temporal line from one to the other of its intersections with the quadric (1).

If A and B are consecutive points on a temporal line we deduce from (2) Beltrami's formula for the line element,

$$ds^2 = \frac{(t\,dt - x\,dx - y\,dy - z\,dz)^2 - (t^2 - x^2 - y^2 - z^2 - 1)(dt^2 - dx^2 - dy^2 - dz^2)}{(t^2 - x^2 - y^2 - z^2 - 1)^2} \quad (3$$

which by a suitable change of variables may be transformed into de Sitter's line element.† The same expression (3) with the sign changed gives the square of the distance between two consecutive points on a spatial line.

Perpendicularity in the universe U is represented in S_4 by polarity with respect to the quadric (1). For an observer who follows a world line in S_4 contemporaneous events are represented by points of a three-dimensional space perpendicular (in a non-Euclidean sense) to the given line.

* It is shown later that the unit of time is 2×10^9 years.

† In this connection see the above-mentioned note in the *Rendiconti dell' Acc. d. Lincei.*

The collineations of the space S_4 which transform (1) into itself represent movements in the space-time U. They form a group ∞^{10} of operations which may be called *Lorentz transformations*, by evident analogy with the operations which bear this name in Minkowski's space-time. The geometrical properties and physical laws of U are invariant with regard to these transformations.*

2. Consider two points in free motion ; suppose that the first moves with the observer, situated (for instance) at the sun, and suppose—as we may without imposing any restrictions—that its world line is represented in S_4 by the t-axis. Let the second represent the position of a star or nebula whose world line has the Cartesian equations

$$x = lt + p, \qquad y = mt + q, \qquad z = nt + r \quad . \qquad (4)$$

The position (4) of the star is contemporaneous, with respect to the observer, with the position (0, 0, 0, t) of the latter. Let τ be the *proper time* of the observer (corresponding to the Euclidean time $t = \tanh \tau$) and σ the (non-Euclidean) distance of the star from the observer at that instant. Then we find that

$$\tan^2 \sigma = \mathrm{E} \sinh^2 \tau + 2\mathrm{F} \sinh \tau \cosh \tau + \mathrm{G} \cosh^2 \tau, \quad . \qquad (5)$$

where for the sake of brevity we have written

$$\mathrm{E} = l^2 + m^2 + n^2, \qquad \mathrm{F} = lp + mq + nr, \qquad \mathrm{G} = p^2 + q^2 + r^2. \quad (6)$$

The radial velocity of the star, measured from the observer, is

$$v_r = \frac{d\sigma}{d\tau} = \left[(\mathrm{E} + \mathrm{G}) \sinh \tau \cosh \tau + \mathrm{F}(\sinh^2 \tau + \cosh^2 \tau)\right] \frac{\cos^3 \sigma}{\sin \sigma} \quad (7)$$

The transverse velocity v_t is obtained by noticing that the angle formed by two observations of the star at the instants t and $t + dt$ of Euclidean time is

$$d\omega = \frac{\sqrt{\mathrm{EG} - \mathrm{F}^2}}{\mathrm{E}t^2 + 2\mathrm{F}t + \mathrm{G}} dt,$$

whence

$$v_t = \frac{d\omega}{d\tau} \sin \sigma = \sqrt{\mathrm{EG} - \mathrm{F}^2} \frac{\cos^2 \sigma}{\sin \sigma} \quad . \quad . \qquad (8)$$

The resultant velocity of the star with respect to the observer is $v = \sqrt{v_r^2 + v_t^2}$. By an easy calculation we find for this expression the simple form

$$v = \sqrt{1 - h^2 \cos^2 \sigma} \,.\, \cos \sigma \quad . \quad . \quad . \qquad (9)$$

where

$$h^2 = 1 - \mathrm{E} + \mathrm{G} - \mathrm{EG} + \mathrm{F}^2 \quad . \quad . \quad . \qquad (10)$$

and where h^2 is a positive constant, as is seen by noting that the line (4)

* The distances on a spatial line and the intervals of time on a temporal line are invariant with respect to these transformations and have the additive property (AB) + (BC) = (AC) ; hence it is seen that the definition (2) is imposed by the very nature of things and cannot be modified, save by a change of the unit of length which effects an alteration in the constant κ.

meets the quadric (1) in real points; $h = 0$ only for the world lines of light propagation, and for these we have, as is known, $v = \cos\sigma$; in the vicinity of the observer $v = 1$ according to our convention.*

It follows from (9) that, for a given star, the velocity $|v|$ with respect to the observer is an increasing function of σ, provided that $\cos^2\sigma > \frac{1}{2h^2}$, *i.e.* that $|v| < \frac{\cos\sigma}{\sqrt{2}}$. Since the distance σ is measured by the radius of curvature and the velocity v by that of light, this inequality is verified for all celestial objects observable with our telescopes.

But it is not permissible to infer, as is generally done, that for the totality of stars the velocity increases with the distance. For a star at distance σ the velocity $|v|$ can, in theory, have any value from 0 to $\cos\sigma$ (the velocity of light); and the mean value of v^2, for a given σ, depends upon that of h^2, and hence upon the statistical hypotheses concerning the distribution of the world lines (4).

3. The radial velocity (7) is that which an observer would obtain by a trigonometrical process if sufficiently precise means were at his disposal. We, however, evaluate the radial velocities of the stars by means of the Doppler effect which, separated from other possible causes of displacement of the spectrum lines, enables us to determine v_r with sufficient accuracy in classical physics as well as in special relativity theory (Minkowski's space-time). In de Sitter's universe the Doppler effect depends not only upon v_r but also upon the distance σ, as we shall now see.

We may suppose without loss of generality that two successive waves of radiation emitted by a star leave at instants 0 and ϵ (in the observer's time) and at points whose Cartesian co-ordinates are

$$(p, 0, 0, 0), \qquad (p + l\epsilon, m\epsilon, 0, \epsilon) \qquad . \qquad . \qquad (11)$$

on the world line

$$x = lt + p, \qquad y = mt, \qquad z = 0.$$

If ϵ is an infinitesimal of the first order, the period of radiation, in the proper time of the star, is by (3)

$$d\tau = \epsilon\sqrt{1 - m^2 - l^2\cos^2\sigma}\,.\,\cos\sigma,$$

where σ is the distance between the star and the observer (*i.e.* the sun) at the instant $t = \tau = 0$.

On the other hand, the period as evaluated by the observer is the (non-Euclidean) interval between the points in which the positive semi-axis of t is met by the tangents to the quadric (1) drawn from the two points (11). This period is easily found to be

$$d\tau_0 = \epsilon(1 + l\cos\sigma).$$

The ratio of the two periods gives the formula for the Doppler

* Taking into account the difference in notation and representation, the formulæ (7), (8), and (9) are equivalent to the formulæ in chap. iv. of Silberstein's work, *The Size of the Universe* (Oxford Univ. Press, 1930).

effect; taking into account the fact that the radial and transverse velocities of the star at the given instant are, by (7) and (8),

$$v_r = l\cos^2\sigma, \qquad v_t = m\cos\sigma,$$

we obtain the formula required,*

$$\frac{d\tau_0}{d\tau} = \frac{1 + v_r/\cos\sigma}{\sqrt{\cos^2\sigma - v_r^2 - v_t^2}} \quad . \quad . \quad . \quad (12)$$

We now expand in series, neglecting powers of σ, v_r, and v_t higher than the second. Writing

$$\mathrm{D} = \frac{d\tau_0 - d\tau}{dr} = \frac{\delta\lambda}{\lambda},$$

where λ is the wave-length, we find

$$\mathrm{D} = v_r + \frac{\sigma^2}{2} + \frac{v_r^2 + v_t^2}{2} \quad . \quad . \quad . \quad (13)$$

4. In discussing this formula we note first that it is difficult to obtain a precise value for D for the sixth place of decimals, which corresponds to a velocity of 300 m./sec. We may, therefore, neglect in (13) all decimal figures beyond the fifth place.

Moreover, the recent discoveries of exceedingly distant spiral nebulæ make it certain that the radius of curvature of space is not less than 2×10^8 light years. For stars in the Milky Way σ, v_r, and v_t are less than 10^{-3}, and hence (13) reduces in practice to the formula $\mathrm{D} = v_r$ of classical physics. From this equality nothing can be inferred concerning the curvature of space.

For the extra-galactic nebulæ which are found at a distance of 10^6 or 10^7 light years and give rise to values of D which are almost all positive (some exceeding 2×10^{-2}), the second order terms of (13) cannot be neglected with safety. But since the value of v_r is always very much greater than the last term of (13), and v_r^2 is negligible, to our order of approximation, for the nearer nebulæ, we may limit the discussion to the simpler formula

$$\mathrm{D} = v_r + \sigma^2/2 \quad . \quad . \quad . \quad . \quad (14)$$

In attempting to deduce, by means of (14), the *true* radial velocity v_r from the *apparent* spectroscopic velocity D, it is necessary to make some assumption concerning the correlation between v_r and σ. At first sight the most plausible is to suppose that the nebulæ are moving at random with respect to the Milky Way (disorganised motion) so that at a given distance positive or negative values of v_r are equally probable; this is also suggested by our geometrical representation. This hypothesis would, however, lead to the value $\bar{\mathrm{D}} = \sigma^2/2$; and the

* It should be remembered that σ is the ratio of the distance to the radius of curvature of space, and that v_r, v_t are measured by taking for unit velocity the velocity of light in the neighbourhood of the observer. If the radius of curvature is supposed infinite, $\sigma = 0$, and (12) gives the Doppler effect of special relativity theory.

mean value of the apparent radial velocity, which is always positive, would vary as the square of the distance. Instead the most recent observations appear to establish the simple proportionality of D to the distance σ.* If this law is confirmed we must conclude that *the hypothesis of de Sitter's universe does not suffice to explain the observed facts concerning the apparent motion of the spiral nebulæ, unless we add some hypothesis relative to a systematic dispersion of these nebulæ from the Milky Way.*†

5. We seek now to determine the nature of this dispersion, or of the corresponding world lines (4), in such a manner as to give $D = \kappa\sigma$, where κ is a positive constant. We shall soon see that κ is nearly equal to unity; but even a crude estimate, based on the fact that for nebulæ at a distance of 10^6 light years (for which we have $\sigma < \frac{1}{300}$) D is of the order $\frac{1}{2000}$, *i.e.* 150 km./sec., assures us that $\kappa > 0{\cdot}1$. From this observation we can neglect the second term in (14) for nebulæ which are not exceedingly distant, and replace the equation by

$$\kappa\sigma = \frac{d\sigma}{d\tau},$$

whence

$$\sigma = Ce^{\kappa\tau} \quad . \quad . \quad . \quad . \quad . \quad (15)$$

With this value, and to the same order of approximation, (5) gives

$$4C^2e^{2\kappa\tau} = (E + 2F + G)e^{2\tau} + (E - 2F + G)e^{-2\tau} + 2(G - E).$$

If we suppose that this holds for the nebulæ under consideration, not only at the instant the light is emitted ($\tau = 0$, say), but for a period long enough for us to differentiate the above relation successively, putting $\tau = 0$ in the results, we obtain

$$E = F = G = C^2, \qquad \kappa = 1.$$

These relations must hold at any rate approximately. If they were exactly true, the world lines (4) in question would become

$$x = l(t + 1), \qquad y = m(t + 1), \qquad z = n(t + 1) \quad . \quad (16)$$

and would pass through the point $(0, 0, 0, -1)$ of the "absolute" (1).

Conversely, the motion which has (16) for world lines has the velocity given by (9), in which now $k^2 = 1$; thus

$$v = \sin\sigma\cos\sigma = \sigma,$$

at least as far as the third-order terms.

We consider here radial velocity only, since for this motion the transverse velocity is always zero. Let us determine the corresponding

* The apparent velocity mentioned above is precisely that determined from the value of D, taking account of the sun's motion due to the rotation of the galactic system. The law D/σ = constant follows from the observations of Hubble and other astronomers. See an article by de Sitter, "On the Magnitudes, Diameters, and Distances . . .," *Bulletin Astronom. Institutes of the Netherlands*, **5** (1930 May).

† *Cf.* Tolman, *loc. cit.*

Doppler effect by means of (13). If σ_0 is the distance of the luminous centre from the sun, *expressed in light years*, and R the radius of curvature of space in the same units, so that $\sigma = \sigma_0/R$, (13) becomes

$$D = \sigma_0/R + \sigma_0^2/R^2.$$

From the data, to which we have referred, furnished by observation ($D = \frac{1}{2000}$ for $\sigma_0 = 10^6$), we obtain

$$R = 2 \times 10^9 \text{ light years} \quad . \quad . \quad . \quad (17)$$

where we have neglected the effect of the last term, which is now less than one thousandth of the preceding.

We conclude that, *if in de Sitter's universe of radius given by* (17) *the Milky Way and the extra-galactic nebulæ were scattered at an exceedingly remote epoch* (*theoretically* $\tau = -\infty$) *by an immense central nebula, thus acquiring a free motion through space, we should receive from their movements precisely the impression which is revealed by spectrum analysis.*

It is interesting to note that an observer situated in any one of the spiral nebulæ would receive the same impression. In fact the ∞^3 world lines passing through a point of the "absolute" (*e.g.* the point (0, 0, 0, − 1)) all have the same relation with respect to one another; for there exists a transitive group of ∞^7 non-Euclidean movements, or Lorentz transformations, which change this system of lines into itself, without altering distance, time, or velocity.*

For two of these world lines, one of which contains the observer and the other a point of a nebula, the formula (15) holds with $\kappa = 1$. This may be written as

$$\sigma_0/R = Ce^{\tau} \quad . \quad . \quad . \quad . \quad (18)$$

The distance σ_0 doubles itself when the time τ of the observer increases by

$$T = \log 2 = 0{\cdot}7 \text{ approximately.}$$

Now since the unit of time is the time required to describe the radius of curvature by light if it were propagated with the velocity which it has in the neighbourhood of the observer, *i.e.* 2×10^9 years, we obtain

$$T = 1{\cdot}4 \times 10^9 \text{ years.}$$

---

* This system of lines is also characterised by the following properties :—

(*a*) There exists a transitive group of movements which transform the system into itself;

(*b*) the group determines a group of ∞^1 movements on an arbitrary line of the system.

It is to this group property that H. Weyl appears to allude on p. 939 of the article previously referred to.

However, Weyl's conclusion is not clear when he speaks of a *zone of influence* of all these stars or nebulæ, as though their world lines could penetrate only a part of space. In reality, since the space at infinity of S_4 does not constitute a frontier (S_4 is a *projective* space of four dimensions) and the two sheets of the quadric (1) must be regarded as connected, as the two hemispheres of a sphere, any point of S_4 external to (1) represents an attainable position of a hypothetical star or nebula which leaves the point (0, 0, 0, − 1) at time $\tau = -\infty$.

In this period all the mutual distances between the spiral nebulæ must be doubled. This holds, at least, provided σ_0 remains sufficiently small compared with R for us to substitute $\sigma = \sigma_0/R$ for $\tan \sigma$, which should appear in the first member of (18).

Leaving aside this last observation, it may be noted that the numerical values of R and T coincide with those deduced (by de Sitter, Eddington, and Tolman) for the present value of the radius of curvature and the period T, on the hypothesis of the expanding universe of Friedman-Lemaître; a deduction from quite different theoretical considerations. It may also be said that the latter hypothesis finds an indirect confirmation in the preceding discussion, if we admit, in accordance with general relativity theory, that the form and the dimensions of space depend upon the distribution of matter contained in it. In fact, on the one hand the hypothesis that R is independent of τ would be compatible, in this theory, only with a homogeneous, extremely tenuous and permanent distribution of matter; and on the other, the same hypothesis disagrees with observation unless we assume a primitive concentration at a very remote time, followed by a progressive diffusion of matter through space.

Model Stellar Atmospheres. By W. H. McCrea, Ph.D.

1. *Introduction.*—This paper makes some attempt to work out the behaviour of stellar atmospheres *from physical data alone.* It deals only with greatly simplified models, but the point of view is different from that of previous approaches to the subject. A semi-empirical absorption coefficient has always been used. When it has been employed to calculate the behaviour of a particular species of atom, the individual contribution of that species to the absorption could not be taken into account. It has been necessary to take an assumed general law for the absorption, and to fix the constants in it by comparison with astronomical observations, which has meant that details of its dependence on ionisation and composition could not be fully allowed for. Now this process is the only one practicable, at any rate at present, for detailed comparison with observation, and is one which leads to the *discovery* of the law of absorption, by testing various possibilities. But if we could know all about the absorption beforehand from pure physics we should get a surer understanding of the atmospheric phenomena, we should be able to allow for the detailed effects just mentioned, and we might get explanations of phenomena not previously accounted for. In point of fact, we have not yet got this knowledge, and even if we had it would be very difficult to carry out the necessary calculations. We can, however, take very simplified models, which we may still expect to provide a check on the other methods and to serve for qualitative comparisons.

If this work can thus give a little fresh physical insight into the

problem it is all that can be hoped for. It is in no sense a criticism of Milne's standard papers * on the subject. That some fresh attack from this angle might be of interest was suggested by Professor Milne after he had noticed the difficulties connected with one-constituent atmospheres referred to in § 9 below.

2. *Model Atmospheres.*—In the first instance the effect of the mixture of gases can be represented by taking just two constituents. The theoretical absorption coefficient, however, has been worked out only for systems of single nuclei and electrons, and so in stellar atmospheres, where elements are mostly only once or twice ionised, it really applies only to hydrogen. Hence, in order to have a proper absorption coefficient to go upon, we shall have to take both elements to be hydrogen-like. We take one actually to be hydrogen (H) with ionisation potential 13·54 volts, and the second to be a hypothetical element (X) with ionisation potential 5 volts. Even for hydrogen, however, this is not expected or intended to reproduce in an exact quantitative manner the behaviour in any actual star.

We therefore set about calculating the " number of atoms above the photosphere," which will predict the main spectroscopic behaviour, and the electron pressure, in model stellar atmospheres composed of mixtures in different proportions of elements H and X.

3. *Calculation of the Absorption Coefficient of a Hydrogen-like Atom.*—We work on the basis of Kramers's theory, the general correctness of which according to the newer quantum theory has been established by Gaunt.† A form suited to the present work has been given by Milne.‡

We shall refer to the element under discussion as " hydrogen," though the work is intended to apply to any hydrogen-like atom. By this we shall mean one differing from hydrogen only in ionisation potential, but having atomic states related in the same way, with the same statistical weights, and having, for simplicity, the same atomic weight.

Our notation will be :

n = total number of hydrogen atoms per cm.^{3}.
n_l = number per cm.^{3} in quantum state l (l = 1, 2, 3 . . .).
N_i = number of hydrogen ions per cm.^{3}.
N_e = *total* number of electrons per cm.^{3}.

We explicitly neglect line absorption. The continuous absorption is in two parts. The first is due to *free* electrons. It gives an atomic absorption coefficient $a_1(\nu)$ per hydrogen ion in the form (Milne, *loc. cit.*)

$$a_1(\nu) = \mathrm{N}_e f(\mathrm{T}) \quad . \quad . \quad . \quad . \quad (1)$$

where ν is the frequency and $f(\mathrm{T})$ a function of the absolute temperature T.

We shall write our coefficients per *normal hydrogen atom, i.e.* per

* E. A. Milne, *M.N.*, **89** (1929), 17, 157 ; *Phil. Trans.*, A, **228** (1929), 421.
† J. A. Gaunt, *Phil. Trans.*, A, **229** (1930), 163.
‡ E. A. Milne, *M.N.*, **85** (1925), 750.

atom in quantum state 1. Then $a_1(\nu)$ gives a contribution per normal atom $a_1(\nu)$ where

$$a_1(\nu) = \frac{N_i}{n_1} a_1(\nu) = \frac{N_i N_e}{n_1} f(T) \quad . \quad . \quad . \quad (2)$$

We shall suppose there is local thermodynamic equilibrium at temperature T, so that the usual ionisation formula gives

$$N_i N_e / n_1 = (2\pi m k T)^{\frac{3}{2}} e^{-\chi_1/kT} / h^3 \quad . \quad . \quad . \quad (3)$$

in the usual notation, where χ_1 is the ionisation potential, being the negative energy corresponding to $l = 1$.

Taking now Milne's value for the function $f(T)$ with the constants appropriate to hydrogen, and making use of (3), we find

$$a_1(\nu) = \frac{16\pi^2}{3\sqrt{3}} \frac{e^6}{ch(h\nu)^3} kT e^{-\chi_1/kT}(1 - e^{-h\nu/kT}) \quad . \quad . \quad (4)$$

These results are true whether or not all the free electrons are due to hydrogen. The quantities N_i, N_e, n_1 enter in such a way that the absorption coefficient per normal atom is a function of T and ν only, and not of the pressure.

The second part of the absorption, and the predominating part in all our applications, is that produced by photoelectric ionisation. Absorption by atoms in state l gives a band of absorption starting at frequency $\nu_l = \chi_1/hl^2$ and extending towards higher frequencies. Hence absorption at frequency ν is the sum of that due to all bands with $l \geqslant \lambda$, where

$$\nu_{\lambda-1} > \nu > \nu_\lambda \quad . \quad . \quad . \quad . \quad (5)$$

Again taking Milne's results appropriate to hydrogen we get for the absorption coefficient per normal atom $a_0(\nu)$ for frequency ν within the limits (5) the value

$$a_0(\nu) = \frac{16\pi^2}{3\sqrt{3}} \frac{e^6 \chi_1}{ch(h\nu)^3} \sum_{l=\lambda}^{\infty} \frac{n_l}{l^2 n_1} \Delta(l) \quad . \quad . \quad . \quad (6)$$

where

$$\Delta(l) = 1/(l - \tfrac{1}{2})^2 - 1/(l + \tfrac{1}{2})^2.$$

In the case of hydrogen we have

$$n_l/n_1 = l^2 e^{(\chi_l - \chi_1)/kT} \quad . \quad . \quad . \quad . \quad (7)$$

where $\chi_l = \chi_1/l^2$.

Combining the results (4) to (7) we have for the total absorption coefficient per normal atom

$$a(\nu) = \frac{16\pi^2}{3\sqrt{3}} \cdot \frac{e^6 \chi_1}{h^4 c} \cdot \frac{e^{-\chi_1/kT}}{\nu^3} \left[\frac{kT}{\chi_1}(1 - e^{-h\nu/kT}) + \sum_{l=\lambda}^{\infty} \Delta(l) e^{\chi_l/kT} \right] \quad (8)$$

for $\nu_{\lambda-1} > \nu > \nu_\lambda$.

Strictly speaking, we require always a *Rosseland mean* for the type

of problem under discussion. For the following reasons we shall, however, content ourselves with the *direct mean*. (*a*) The integrals necessary for the averaging can be worked out explicitly. This lightens the work, since those needed to obtain a Rosseland mean require numerical quadratures. (*b*) For mixtures of different gases we can then take simple averages. For a Rosseland mean, which is in the nature of a harmonic mean, the integrals would have to be worked out afresh in each case. (*c*) The difference between the two means is due to the variation of the absorption with wave-length, Rosseland's mean giving greater weight to low values of the absorption. The difference may be considerable for a single hydrogen-like gas for which the absorption is high at the head ν_l of each series, but falls off like ν^{-3} to a small value before the head ν_{l-1} of the next series is reached. But for a mixture of gases this excessive fluctuation will tend to be smoothed out, since the heads of the series for the different gases will not generally coincide, and the divergence between the means will consequently be reduced. (*d*) In any case the general variation of the mean absorption coefficient with temperature and pressure is what chiefly concerns us, and this will not greatly depend on the particular method of averaging over the frequency.

The mean of $a(\nu)$ over any range ν' to ν'' is consequently taken to be $\left[\overline{a(\nu)}\right]_{\nu'}^{\nu''}$ where

$$\left[\overline{a(\nu)}\right]_{\nu'}^{\nu''} = \int_{\nu'}^{\nu''} a(\nu)\mathrm{I}_\nu d\nu \Big/ \int_{\nu'}^{\nu''} \mathrm{I}_\nu d\nu \quad . \quad . \quad . \quad (9)$$

I_ν being the intensity of black radiation of frequency ν. The mean of $a(\nu)$ given by (8) is

$$\overline{a(\nu)} = \mathrm{C}e^{-\chi_1/k\mathrm{T}}\left[\int_0^\infty \frac{k\mathrm{T}}{\chi_1}\frac{1-e^{-h\nu/k\mathrm{T}}}{e^{h\nu/k\mathrm{T}}-1}d\nu + \sum_l \Delta(l)\int_{\nu_l}^\infty \frac{e^{\chi_l/k\mathrm{T}}d\nu}{e^{h\nu/k\mathrm{T}}-1}\right] \div \int_0^\infty \frac{\nu^3 d\nu}{e^{h\nu/k\mathrm{T}}-1} \quad (10)$$

where C has been written for the factor independent of ν and T in (8).

We follow Milne (*loc. cit.*) in calculating the sums and integrals in (10). We have

$$\int_0^\infty e^{-h\nu/k\mathrm{T}}d\nu \Big/ \int_0^\infty \frac{\nu^3 d\nu}{e^{h\nu/k\mathrm{T}}-1} = \frac{15}{\pi^4}\left(\frac{h}{k\mathrm{T}}\right)^3$$

and

$$\int_{\nu_l}^\infty \frac{d\nu}{e^{h\nu/k\mathrm{T}}-1} \Big/ \int_0^\infty \frac{\nu^3 d\nu}{e^{h\nu/k\mathrm{T}}-1} = -\frac{15}{\pi^4}\left(\frac{h}{k\mathrm{T}}\right)^3 \log\left(1-e^{-y_l}\right)$$

where $y_l = \chi_l/k\mathrm{T}$. We therefore require to evaluate the sum

$$-\sum_l e^{y_l}\Delta(l)\log\left(1-e^{-y_l}\right),$$

where now $\Delta(l) = k\mathrm{T}\Delta y_l/\chi_1$. Milne's method is to approximate by replacing the sum by the corresponding integral, taking the upper

limit Y of y_l to correspond to $l = \frac{1}{2}$, so that $Y = y_{\frac{1}{2}} = 4\chi_1/kT$. This gives

$$\begin{aligned} -\sum_l &\doteq \frac{kT}{\chi_1}\int_0^Y e^y \log\left(\frac{1}{1-e^{-y}}\right)dy \\ &= \frac{kT}{\chi_1}\Big[y - (e^y - 1)\log(1 - e^{-y})\Big]_0^Y \\ &\doteq \frac{kT}{\chi}[1 + Y], \text{ since in practice } e^Y >> 1, \\ &= 4 + \frac{kT}{\chi}. \end{aligned}$$

Combining these results we obtain

$$\overline{a(\nu)} = \frac{320}{\sqrt{3\pi^2}} \cdot \frac{e^6\chi_1}{hc}\left[1 + \frac{kT}{2\chi_1}\right]\frac{e^{-\chi_1/kT}}{k^3T^3} \quad . \quad . \quad (11)$$

It is convenient to express this as the *mass* absorption coefficient $\bar{k}$ for the *un-ionised gas*, giving finally when numerical values of the constants are inserted

$$\bar{k} = \frac{AI(1 + T^*/2{\cdot}32I)}{T^{*3}e^{1{\cdot}16I/T^*}} \quad . \quad . \quad . \quad (12)$$

where I is the ionisation potential in volts, and

$$T^* = 10^{-4}T, \qquad A = 4{\cdot}18 \times 10^8.$$

For hydrogen itself (H) we have I = 13·54 volts, giving for $\bar{k}$ the value

$$\bar{k} = \frac{B_H(1 + 0{\cdot}03185T^*)}{T^{*3}e^{15{\cdot}7/T^*}}, \quad \text{where} \quad B_H = 5{\cdot}66 \times 10^9 \quad . \quad (13)$$

For the gas X we have I = 5 volts, giving for the absorption coefficient (12), which we shall call $\bar{l}$, the value

$$\bar{l} = \frac{B_X(1 + 0{\cdot}08621T^*)}{T^{*3}e^{5{\cdot}798/T^*}} \quad \text{where} \quad B_X = 2{\cdot}09 \times 10^9 \quad . \quad (14)$$

Values of $\bar{k}$ and $\bar{l}$ were calculated for the required range of values of T* and are given in Table I.

4. *Degree of Ionisation.*—The degree of ionisation x is given by

$$\frac{1-x}{x} = \frac{P_e}{K_1} \quad . \quad . \quad . \quad . \quad (15)$$

where P_e is the electron pressure, and for hydrogen-like gases we have the known result

$$\begin{aligned} K_1 &= (2\pi m/h^2)^{\frac{3}{2}}(kT)^{\frac{5}{2}}e^{-\chi/kT} \\ &= CT^{*\frac{5}{2}}e^{-1{\cdot}16I/T^*} \quad . \quad . \quad . \quad . \quad (16) \end{aligned}$$

where $C = 3{\cdot}345 \times 10^9$. For hydrogen (H) we write K for K_1 and for the gas X we write L. Values of K and L are given in Table I.

TABLE I.

T*.	log K.	log $\bar{k}$.	log L.	log $\bar{l}$.
0·2	$\bar{27}$·6849	$\bar{23}$·7606	$\bar{5}$·1869	$\bar{2}$·8347
0·3	$\bar{15}$·4892	$\bar{12}$·5976	$\bar{1}$·8238	2·5067
0·4	$\bar{9}$·4837	$\bar{7}$·9054	2·2347	4·2347
0·5	$\bar{5}$·1351	$\bar{3}$·0261	3·7359	5·2058
0·6	$\bar{3}$·6059	$\bar{1}$·0626	4·7749	5·8128
0·7	$\bar{1}$·3966	0·4867	5·5400	6·2133
0·8	0·7592	1·5314	6·1347	6·4925
0·9	1·8339	2·3267	6·6122	6·6925
1·0	2·7060	2·9483	7·0064	6·8383
1·1	3·4294	3·4452	7·3388	6·9464
1·2	4·0404	3·8499	7·6241	7·0274
1·4	5·0194	4·4631	8·0911	7·1329
1·6	5·7732	4·9007	8·4609	7·1902
1·8	6·4747	5·2233	8·7638	7·2183
2·0	6·8677	5·4675	9·0179	7·2374
2·2	7·2811	5·6558	9·2359	7·2241

5. *The Composition of a Stellar Atmosphere.*—We now consider the equilibrium of a stellar atmosphere composed only of gases H and X in a given proportion. The case is different from those treated by Milne,* since one component is not necessarily present to an excess, and the components considered are themselves responsible for the absorption. His general method is, however, the natural one to follow.

We employ the following notation, all the quantities applying to a depth h below some arbitrary zero level:—

s = total number of atoms per unit volume.
ηs = total number of H-atoms per unit volume.
ϵs = total number of X-atoms per unit volume.
p = total gas pressure.
P = electron pressure.
ρ = density.
x = degree of ionisation of H.
y = degree of ionisation of X.

The temperature T, the value of gravity g, and the fractions η, ϵ are supposed independent of h.

We neglect radiation pressure. The hydrostatic equation is therefore

$$\frac{dp}{dh} = g\rho \quad . \quad . \quad . \quad . \quad (17)$$

* E. A. Milne, *M.N.*, **89** (1929), 17.

and we have

$$\rho = s\mathrm{H}, \quad . \quad . \quad . \quad . \quad (18)$$

since we ascribe to the atoms the same mass H, and

$$p = \{\eta(1 + x) + \epsilon(1 + y)\}sk\mathrm{T} \quad . \quad . \quad . \quad (19)$$

The electron pressure is given by

$$\mathrm{P} = (\eta x + \epsilon y)sk\mathrm{T} \quad . \quad . \quad . \quad (20)$$

For hydrogen the total number N_0 of neutral atoms down to depth h is

$$\mathrm{N}_0 = \eta\int^h (1 - x)sdh \quad . \quad . \quad . \quad (21)$$

and we have

$$\frac{x\mathrm{P}}{1 - x} = \mathrm{K} \quad . \quad . \quad . \quad . \quad (22)$$

For X the total number M_0 of neutral atoms down to depth h is

$$\mathrm{M}_0 = \epsilon\int^h (1 - y)sdh \quad . \quad . \quad . \quad (23)$$

and we have

$$\frac{y\mathrm{P}}{1 - y} = \mathrm{L} \quad . \quad . \quad . \quad . \quad (24)$$

We can now use equations (17) to (20) to change the variable from h to P in (21), (23), and obtain

$$\begin{aligned}\mathrm{N}_0 &= \frac{\eta}{g\mathrm{H}}\int_0^{\mathrm{P}} \frac{\mathrm{P}}{\mathrm{P} + \mathrm{K}}d\left[\left\{1 + \frac{\eta\mathrm{K}}{\mathrm{P} + \mathrm{K}} + \frac{\epsilon\mathrm{L}}{\mathrm{P} + \mathrm{L}}\right\}\frac{\mathrm{P}(\mathrm{P} + \mathrm{K})(\mathrm{P} + \mathrm{L})}{\mathrm{P}(\eta\mathrm{K} + \epsilon\mathrm{L}) + \mathrm{KL}}\right] \\ &= \frac{1}{g\mathrm{H}}\left[\frac{\eta\mathrm{P}^2(\mathrm{P} + \mathrm{L})}{\mathrm{P}(\eta\mathrm{K} + \epsilon\mathrm{L}) + \mathrm{KL}} - \frac{\eta\mathrm{PK}}{\eta\mathrm{K} + \epsilon\mathrm{L}} + \eta\mathrm{P} + \epsilon\mathrm{K}\log\frac{\mathrm{P} + \mathrm{K}}{\mathrm{K}}\right. \\ &\qquad \left. - \frac{\epsilon\mathrm{KL}^2}{(\eta\mathrm{K} + \epsilon\mathrm{L})^2}\log\frac{\mathrm{P}(\eta\mathrm{K} + \epsilon\mathrm{L}) + \mathrm{KL}}{\mathrm{KL}}\right] \quad (25)\end{aligned}$$

after some reduction ; and similarly

$$\begin{aligned}\mathrm{M}_0 &= \frac{1}{g\mathrm{H}}\left[\frac{\epsilon\mathrm{P}^2(\mathrm{P} + \mathrm{K})}{\mathrm{P}(\eta\mathrm{K} + \epsilon\mathrm{L}) + \mathrm{KL}} - \frac{\epsilon\mathrm{PL}}{\eta\mathrm{K} + \epsilon\mathrm{L}} + \epsilon\mathrm{P} + \eta\mathrm{L}\log\frac{\mathrm{P} + \mathrm{L}}{\mathrm{L}}\right. \\ &\qquad \left. - \frac{\eta\mathrm{K}^2\mathrm{L}}{(\eta\mathrm{K} + \epsilon\mathrm{L})^2}\log\frac{\mathrm{P}(\eta\mathrm{K} + \epsilon\mathrm{L}) + \mathrm{KL}}{\mathrm{KL}}\right] \quad (26)\end{aligned}$$

Now for the range of temperatures considered it is not necessary to distinguish between the number of normal atoms and the total number of neutral atoms. Hence, since $\bar{k}$, $\bar{l}$ have been evaluated per normal atom, the optical depth τ corresponding to h, or P, is

$$\tau = \mathrm{H}(\bar{k}\mathrm{N}_0 + \bar{l}\mathrm{M}_0) \quad . \quad . \quad . \quad . \quad (27)$$

Hence (25), (26), (27) give the numbers of neutral atoms down to any optical depth, and the electron pressure at that depth.

6. *Calculation of the Results.*—The numerical computation of M_0, N_0, P is somewhat heavy work. We have taken $\tau = \frac{2}{3}$ to correspond to the depth of the reversing layer in all cases. The precise value is not of vital importance, especially in the comparative results. In what follows we suppose M_0, N_0, and P always to apply to this value of τ.

We recall that K, L, $\bar{k}$, $\bar{l}$ are functions of T alone. The quantities M_0, N_0, P are functions of T and g, and we require their values for a series of values of these two parameters. The calculation depends on choosing the most convenient independent variables at each stage. One of these is always T. Calculations were made with $\eta = \frac{1}{4}, \epsilon = \frac{3}{4}$; $\eta = \frac{1}{2}, \epsilon = \frac{1}{2}$; and $\eta = \frac{3}{4}, \epsilon = \frac{1}{4}$.

In approximations to M_0, N_0 we make use of the fact that, for all T considered, $K \ll L$. It is found that for the smallest T taken we must have $K \ll P \ll L$. This leads easily to approximate expressions for N_0, M_0 in terms of g and P.

For sufficiently small T, $N_0\bar{k} \ll M_0\bar{l}$, so that hydrogen does not contribute appreciably to the general absorption. We have in fact

$$N_0 g_H = \eta(1+\epsilon)P/\epsilon \qquad M_0 g_H = P^2/L \quad . \quad (28)$$

$$\tau = {}_H\bar{l}M_0 = \frac{\bar{l}}{L} \cdot \frac{P^2}{g} \quad . \quad . \quad . \quad . \quad (29)$$

Consequently g can be taken as independent variable.

In these cases X shows no absolute magnitude effect, M_0 being independent of g, *while H shows an absolute magnitude effect such that* $N_0 \propto g^{-\frac{1}{2}}$ *for given T.*

When H first becomes of significance for general absorption, equations (28) continue to hold, but (29) must be replaced by

$$\tau = {}_H(N_0\bar{k} + M_0\bar{l}) = \left\{\eta\frac{(1+\epsilon)}{\epsilon}P\bar{k} + \frac{P^2}{L}\bar{l}\right\} \Big/ g \quad . \quad . \quad (30)$$

so that it is now simplest to use P as independent variable and to derive g from (30).

It is now seen, from the ratio of the two parts of the expression for τ, that H is the more important for absorption, the smaller the value of P, *i.e.* the smaller the value of g. The physical explanation is obvious. For a decrease in P means an increase in the degree of ionisation of X. Hence, in order to get a sufficient number of neutral atoms to give the required optical depth, we must go deeper into the atmosphere. But in so doing we include more hydrogen atoms, and in fact, at a certain stage, sufficient to affect the general absorption. When this happens, of course, a smaller number of X atoms are required. This explains at the same time why here, and also in the preceding case, N_0 increases with decreasing P, and further why this effect should become less pronounced when H begins to count in the general absorption. *In these cases X shows a negative absolute magnitude effect,* i.e. M_0 *decreases with decreasing* g; *H continues to*

show a positive absolute magnitude effect, tending, however, to become less marked.

These physical phenomena persist through a further range of temperature in which the approximations (28) are no longer valid. The quantity K has now become of the same magnitude as P. So the device employed is to set P equal to some definite multiple of K, then to get numerical approximations to N_0, M_0 in terms of K, and finally to substitute in (27) to find the appropriate g value. It was

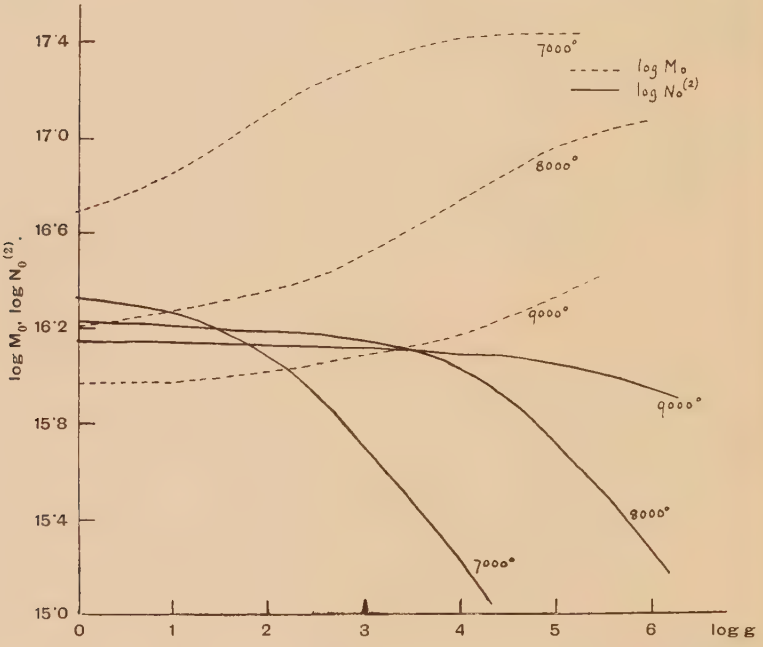

Fig. 1.—Numbers of X-atoms (M_0) and excited H atoms ($N_0^{(2)}$) for different values of g and T. $\eta = \frac{3}{4}$, $\epsilon = \frac{1}{4}$.

found possible to deal with this range by taking the cases P = 4K, P = K, P = $\frac{1}{4}$K. The work is rather lengthy, and there would be no object in giving all the formulæ employed.

In the final range of temperature we have P<<K<<L, and we find the approximate formulæ

$$N_0 g_H = \eta P^2/K \qquad M_0 g_H = \epsilon P^2/L \quad . \quad . \quad (31)$$

$$\tau = \frac{P^2}{g}\left(\eta\frac{\bar{k}}{K} + \epsilon\frac{\bar{l}}{L}\right) \quad . \quad . \quad . \quad . \quad (32)$$

It follows from (32) that $P^2 \propto g$ for given temperature, and hence from (31) that N_0, M_0 are independent of g for given temperature. *In*

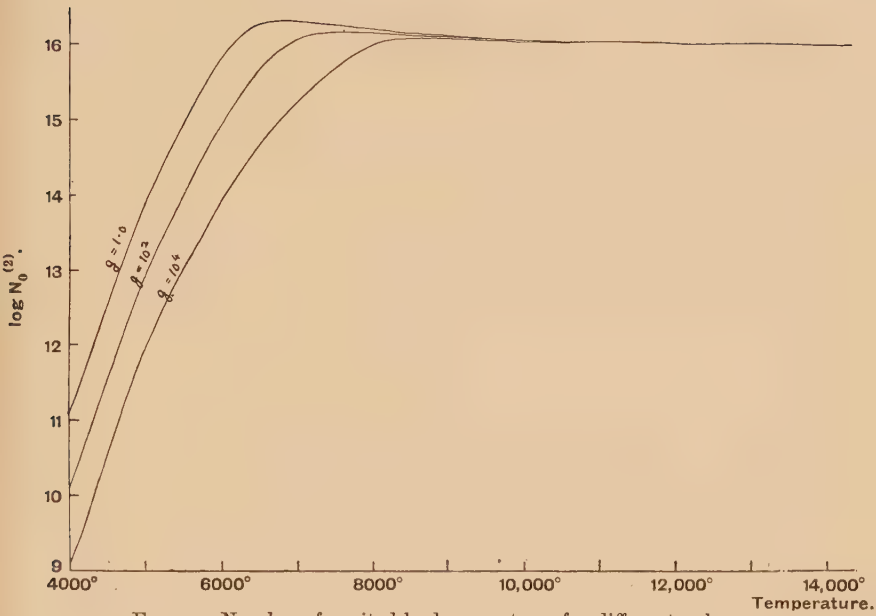

FIG. 2.—Number of excited hydrogen atoms for different values of T and g. $\eta = \frac{3}{4}$, $\epsilon = \frac{1}{4}$.

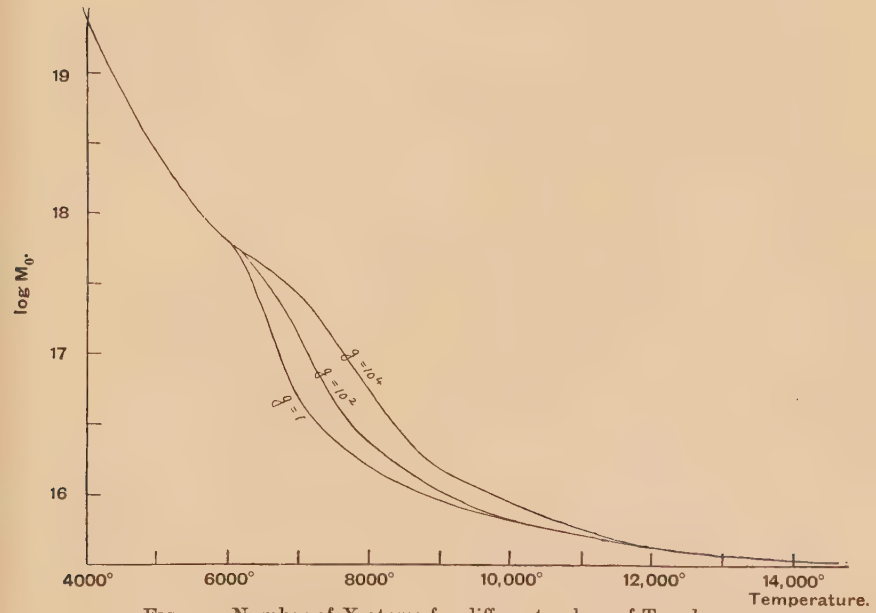

FIG. 3.—Number of X-atoms for different values of T and g. $\eta = \frac{3}{4}$, $\epsilon = \frac{1}{4}$.

these cases neither gas shows any absolute magnitude effect. We may notice too that the contributions of H and X to general absorption are in the ratio $\eta\frac{\bar{k}}{K}\Big/\epsilon\frac{\bar{l}}{L}$, which from formulæ (13), (14), and (16) is seen to be merely $\frac{\eta}{\epsilon}\left(\frac{1+0{\cdot}03185T^*}{1+0{\cdot}08621T^*}\right)$, which is independent of g and varies only slowly with T^*.

One further point requires attention. A hydrogen-like gas X will have a first excitation potential 3·75 volts, and so its *principal* lines will be those observed, and their intensity will depend on M_0 itself. For hydrogen, on the other hand, the Balmer lines are those observed, and these depend on the number $N_0^{(2)}$ of 2-quantum atoms given by

$$N_0^{(2)} = 4N_0e^{-11{\cdot}78/T^*} \quad . \quad . \quad . \quad (33)$$

This is therefore the number we have to study for the *temperature* effects. The agencies so far discussed tend on the whole to make N_0 decrease with increasing T, but the exponential factor in (33) increases with increasing T. There is thus the possibility of a maximum occurring in $N_0^{(2)}$, which turns out actually to be the case.

7. *Numerical Results.*—We first treat the case $\eta = \frac{3}{4}$, $\epsilon = \frac{1}{4}$. The values of log $N_0^{(2)}$ and log M_0 are plotted against log g for various values of T in the critical range in which the H-absorption becomes important, giving the curves shown in fig. 1. From these curves we read off the values for g = 1, 10, 10^2, 10^3, 10^4, 10^5. Some of these results are collected with those for the other ranges of T in Tables II. These show also the values of P and of σ, the ratio of the absorption due to H to that due to X, down to $\tau = \frac{2}{3}$. Figs. 2, 3 show the values of log $N_0^{(2)}$ and log M_0 respectively, plotted against T for various values of g. The phenomena described qualitatively in § 6 are now exhibited quantitatively.

TABLE II.

Depth of Reversing Layer taken as $\tau = \frac{2}{3}$.

	$\eta=\frac{3}{4}$, $\epsilon=\frac{1}{4}$; $g=1{\cdot}0$.					$\eta=\frac{3}{4}$, $\epsilon=\frac{1}{4}$; $g=10^2$.				
T^*.	log P.	log N_0.	log $N_0^{(2)}$.	log M_0.	σ.	log P.	log N_0.	log $N_0^{(2)}$.	log M_0.	σ.
0·4	$\bar{2}$·91	23·27	11·08	19·37	·00	$\bar{1}$·91	22·27	10·08	19·37	·00
0·5	$\bar{1}$·17	23·53	13·91	18·40	·00	0·17	22·53	12·91	18·40	·00
0·6	$\bar{1}$·39	23·75	15·83	17·79	·16	0·39	22·75	14·83	17·79	·00
0·7	$\bar{1}$·46	23·02	16·32	16·68	4·1	0·50	22·77	16·08	17·12	·79
0·8	$\bar{1}$·56	22·02	16·23	16·20	7·8	0·65	21·98	16·19	16·36	4·0
0·9	$\bar{1}$·70	21·22	16·14	15·96	7·8	0·75	21·21	16·13	16·02	6·0
1·0	$\bar{1}$·83	20·60	16·09	15·82	7·8	0·83	20·60	16·09	15·82	7·8
1·2	0·04	19·70	16·04	15·64	7·6	1·04	19·70	16·04	15·64	7·6
1·4	0·22	19·09	16·04	15·54	7·6	1·22	19·09	16·04	15·54	7·6
1·6	0·38	18·65	16·05	15·48	7·6	1·38	18·65	16·05	15·48	7·6

TABLE II.—*continued.*

$\eta=\frac{3}{4}$, $\epsilon=\frac{1}{4}$; $g=10^4$.

T*.	log P.	log N_0.	log $N_0^{(2)}$.	log M_0.	σ.
0·4	0·91	21·27	9·08	19·37	·00
0·5	1·17	21·53	11·91	18·40	·00
0·6	1·39	22·75	13·83	17·79	·00
0·7	1·58	21·93	15·24	17·41	·03
0·8	1·68	21·82	16·03	16·74	1·0
0·9	1·73	21·18	16·10	16·18	4·3
1·0	1·86	20·58	16·07	15·96	7·8
1·2	2·04	19·70	16·04	15·64	7·6
1·4	2·22	19·09	16·04	15·54	7·6
1·6	2·38	18·65	16·05	15·48	7·6

$\eta=\frac{1}{2}$, $\epsilon=\frac{1}{2}$; $g=1\cdot0$.

T*.	log P.	log N_0.	log $N_0^{(2)}$.	log M_0.	σ.
0·4	$\bar{2}$·91	22·87	10·69	19·37	·00
0·5	$\bar{1}$·18	23·12	13·50	18·40	·00
0·6	$\bar{1}$·39	23·35	15·43	17·79	·06
0·7	$\bar{1}$·50	22·87	16·18	17·02	1·3
0·8	$\bar{1}$·60	21·93	16·14	16·56	2·6
0·9	$\bar{1}$·75	21·13	16·05	16·36	2·6
1·0	$\bar{1}$·87	20·51	16·00	16·21	2·6
1·2	0·09	19·61	15·97	16·03	2·6
1·4	0·27	19·00	15·95	15·92	2·5
1·6	0·43	18·56	15·96	15·87	2·5

$\eta=\frac{1}{2}$, $\epsilon=\frac{1}{2}$; $g=10^2$.

T*.	log P.	log N_0.	log $N_0^{(2)}$.	log M_0.	σ.
0·4	$\bar{1}$·91	21·87	9·69	19·37	·00
0·5	0·18	22·12	12·50	18·40	·00
0·6	0·39	22·35	14·43	17·79	·00
0·7	0·54	22·48	15·79	17·29	·27
0·8	0·63	21·85	16·06	16·70	1·6
0·9	0·77	21·10	16·02	16·37	2·3
1·0	0·87	20·51	16·00	16·21	2·6
1·2	1·09	19·61	15·97	16·03	2·6
1·4	1·27	19·00	15·95	15·92	2·5
1·6	1·43	18·56	15·96	15·87	2·5

$\eta=\frac{1}{2}$, $\epsilon=\frac{1}{2}$; $g=10^4$.

T*.	log P.	log N_0.	log $N_0^{(2)}$.	log M_0.	σ.
0·4	0·91	20·87	8·69	19·37	·00
0·5	1·18	21·12	11·50	18·40	·00
0·6	1·39	21·35	13·43	17·79	·00
0·7	1·56	21·54	14·85	17·41	·01
0·8	1·67	21·52	15·73	16·90	·43
0·9	1·81	20·98	15·90	16·51	1·5
1·0	1·88	20·49	15·98	16·26	2·1
1·2	2·09	19·61	15·97	16·03	2·6
1·4	2·27	19·00	15·95	15·92	2·5
1·6	2·43	18·56	15·96	15·87	2·5

The first thing to notice is that our curves for H are very like those calculated by Milne * for hydrogen. We insist, however, that our results are not strictly applicable to hydrogen in any real star, but intended rather to show the general behaviour of the lines of an excited atom of relatively high ionisation potential. So regarded, *i.e.* apart from any "hydrogen anomaly," the values of $N_0^{(2)}$ are of quite the right order of magnitude. Thus our model stars, which, be it remembered, are constructed without any astronomical data, would look more or less like real stars as far as the strength of the lines is concerned. Had they failed badly in this respect they would have been of little use for further discussion. We notice too that the values of P range about those derived by other methods. This also is satisfactory, for, since X at least is always highly ionised and provides an important fraction of the total number of atoms, P must give a good measure also of the total pressure. The latter therefore turns out to be of the kind we expect in real stars.

* E. A. Milne, *Phil. Trans.*, *loc. cit.*, fig. 3.

We observe next that the general behaviour of $N_0^{(2)}$, the existence of the maximum and the "positive" absolute magnitude effect on the low temperature side, again mimics the behaviour in real stars. It fails to do so, however, on the high temperature side when the real stars are known to exhibit a negative absolute magnitude effect.* Milne discusses the same point, and finds that his first law for the absorption coefficient $\kappa = 0{\cdot}85P/T^{*9{\cdot}2}$ fails to reproduce this phenomenon. He finds, however, that the law $\kappa = \text{const.}$ would give this type of magnitude effect at high temperatures, but no magnitude effect at all on the low temperature side. The law $\kappa = \text{const.}$ has, however, as Milne points out, no basis in physical theory. But now we have at one point in the present work come upon a negative absolute magnitude effect whose significance we have to examine.

The curves for M_0, at any rate in the greater part of the temperature range, show again the right order of magnitude for observable spectra. Throughout the range, M_0 decreases with increasing T. The chief peculiarity is that in the range where X is changing from being predominant in the absorption to contributing its final, nearly constant, fraction of the optical thickness, it exhibits a negative absolute magnitude effect. This effect is not large, but should be just appreciable in our case. For example, at 7000° M_0 increases about sixfold in going from $g = 1$ to $g = 10^4$. But for other gases in other circumstances the effect might well be somewhat greater. The point is that we have here a factor which, on a purely physical theory of the absorption coefficient, may under favourable circumstances give rise to a negative absolute magnitude effect. In fact, wherever a gas is predominant in absorption in one range of T, and then begins at higher values of T to give place to another, as we expect, less easily ionised gas, there must be a tendency towards such an effect. For example, if hydrogen is contributing largely to general absorption in the neighbourhood of its maximum, and then if some other gas like helium with a higher ionisation potential begins to take a share, the relative positions of hydrogen and helium would be like those of X and H respectively in our models. In such circumstances we might expect the kind of magnitude effect under discussion.

This may be the explanation of the observed phenomenon. At any rate it seems that no other known physical theory will account for it. Nevertheless, even if the present one should prove correct, much more refined calculations based on a more detailed theory of the absorption coefficient and a better knowledge of the chemical composition of stellar atmospheres would be needed to establish it.

8. *Other Values of* η, ϵ.—Our reason for giving the above discussion before giving the remaining results was not to confuse the issues by too much detail. Table II. gives also the results for $\eta = \frac{1}{2}$, $\epsilon = \frac{1}{2}$. Their general behaviour is the same as before. The main difference is that the magnitude effect for M_0 is still less pronounced. This is due to the fact that its contribution to the absorption does not vary

* Y. Öhman, *Nova Acta Uppsala* (IV.), 7 (1930), No. 3. This paper gives very full observational data on the intensities of the hydrogen lines in stellar spectra.

so much as in the previous case. This holds to a still greater extent for $\eta = \frac{1}{4}$, $\epsilon = \frac{3}{4}$, where, instead of giving a complete table, the following results are given as typical :—

$\eta = \frac{1}{4}$, $\epsilon = \frac{3}{4}$; $T^* = c{\cdot}8$.

log g.	log P.	log N_0.	log $N_0^{(2)}$.	log M_0.	σ.
·00	$\bar{1}{\cdot}66$	21·74	15·95	16·84	0·87
4·57	2·00	20·98	15·19	17·07	0·09

$T^* = 0{\cdot}9$.

·00	$\bar{1}{\cdot}80$	20·94	15·96	16·64	0·87
4·03	1·83	20·81	15·73	16·73	0·51

These additional calculations show little more than the otherwise evident result that if a gas is so abundant that it always contributes a large part to the general optical thickness, then it cannot show important magnitude effects. It is just interesting to show the quantitative results.

9. *One-constituent Atmospheres.*—If only one component, say H, is present, then $\eta = 1$, $\epsilon = 0$, and equations (25), (27) reduce to

$$N_0 = P^2/g\text{H}K \quad . \quad . \quad . \quad . \quad (25')$$

$$\tau = \text{H}kN_0 \quad . \quad . \quad . \quad . \quad (27').$$

Thus from (27′) N_0 is merely proportional to the inverse of $\bar{k}$ and is *independent of* g. This result continues to hold if other atoms are present without contributing to the general absorption. This conclusion, that were any single gas solely responsible for the general absorption it could not show absolute magnitude effects, was noticed by Professor Milne at an early stage of the work. The author had been testing the hypothesis that hydrogen, owing to its abundance, might provide effectively the whole general opacity of stellar atmospheres. Professor Milne's argument shows at once that this is untenable, at any rate for M-type stars, in which the hydrogen lines show such a marked dependence on absolute magnitude.

10. *Hydrogen Atmospheres.*—In spite of the foregoing conclusion it may not be out of place to put on record a brief summary of the results obtained for 100 per cent. hydrogen atmospheres. They serve to show the kind of effect produced in the spectral energy curve by a dependence of the absorption coefficient on wave-length, and in particular the distortion at the head of the Balmer series. They show further the main features in the continuous spectrum that would result from an excess of hydrogen, and how they would affect deductions of the effective temperature.

Since only one gas is involved, it is now less impracticable to use the more correct Rosseland mean a of $a(\nu)$ defined by

$$\frac{1}{a} = \int_0^\infty \frac{1}{a(\nu)} \frac{\partial \text{I}_\nu}{\partial \text{T}} d\nu \Big/ \int_0^\infty \frac{\partial \text{I}_\nu}{\partial \text{T}} d\nu \quad . \quad . \quad . \quad (34)$$

We write $x = h\nu/k\mathrm{T}, \quad x_\lambda = h\nu_\lambda/k\mathrm{T}$ (35)

In (8) we may replace the factor $(1 - e^{-h\nu/k\mathrm{T}})$ by unity, without introducing a large error, and obtain

$$a(\nu) = p_\lambda/\nu^3 \quad \text{for} \quad x_{\lambda-1} > x > x_\lambda. \qquad (36)$$

where p_λ is a coefficient depending on T but not on x. Making these substitutions in (34) we find

$$\frac{1}{a} = \frac{\left(\frac{k\mathrm{T}}{h}\right)^3}{\int_0^\infty \frac{x^4 e^x}{(e^x-1)^2}dx}\left[\frac{1}{p_1}\int_{x_1}^{\infty}\frac{x^7 e^x dx}{(e^x-1)^2} + \frac{1}{p_2}\int_{x_2}^{x_1} + \ldots + \frac{1}{p_\lambda}\int_{x_\lambda}^{x_{\lambda-1}} + \ldots\right] \qquad (37)$$

The integrals were evaluated by Simpson's rule. Eddington * has shown that the radiation of frequency ν may be taken as having an effective temperature T_ν given by

$$\mathrm{T}_\nu^4 = \tfrac{1}{2}(1 + a/a(\nu))\mathrm{T}_e^4 \qquad (38)$$

where T_e is the star's effective temperature. A suitable mean value of the ratio $a/a(\nu)$, which is a function † of T and so of τ, is its value for temperature T_e. Spectral energy curves for various values of T_e were computed by use of equation (38).

Results.—Absorption at the Head of the Balmer Series.—Extensive observations of the continuous spectrum of stars in the neighbourhood of the head of the Balmer series have been made by Chi'ng-Sung Yü.‡ He exhibits his results in a series of curves which he compares with Planck curves in order to derive effective temperatures. He has, of course, no absolute scale of intensity.

In figs. 4–7 the calculated curves for the region λ3000 to λ6000 for various temperatures are compared with some of Yü's curves. The latter have been copied from his figures (he does not give tables of his results) on such a scale that two typical points coincide with the comparison curves. We indicate the temperature obtained by Yü. The numbers VI*a*, etc., refer to the figures in his paper.

The theoretical curves show a sharp peak at the head of the Balmer series, with a vertical drop where the extra absorption sets in. But Yü's results and others § show that actually the absorption sets in gradually some distance on the long wave-length side of the series head. This, no doubt, is some kind of "pressure effect," and if it could be allowed for theoretically would round off the sharp peak and do away with the subsequent absolutely vertical drop in intensity.

Apart from this, we see that the theoretical curves show quite the right amount of absorption at the series head. This being so, it would

* Eddington, *Internal Constitution of the Stars* (1926), p. 330.

† It is to be remembered that in § 5 we supposed T constant through the reversing layer.

‡ Chi'ng-Sung Yü, *Lick Obs. Bull.*, **12** (1926), 104.

§ See Wright, *Nature*, **109** (1922), 810; Nicholson, *M.N.*, **85** (1925), 253; Davidson, Minnaert, Ornstein, and Stratton, *M.N.*, **88** (1928), 536.

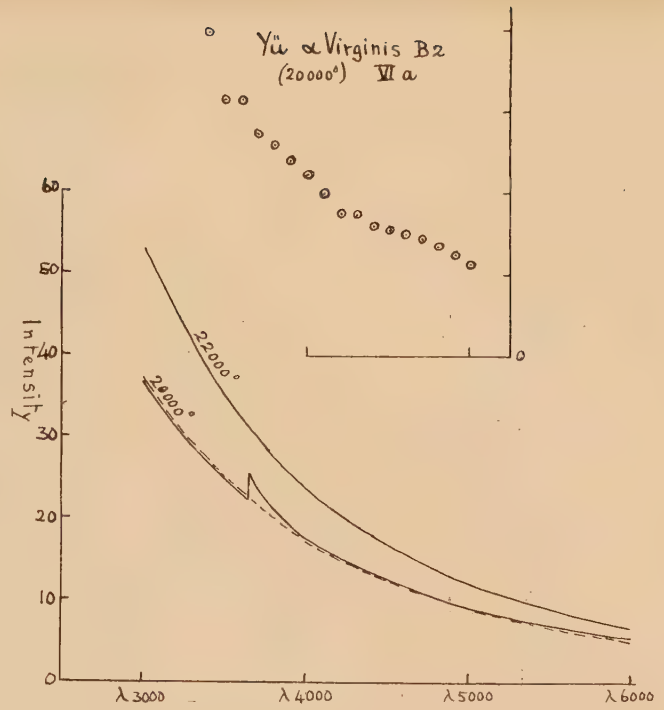

FIG. 4.—Comparison of theoretical curve for hydrogen star with black-body curves and with Yü's observed curve for α Virginis.

—— (Upper) = Black-body curve for T_e = 22,000° (absolute units).
—— (Lower) = Theoretical curve for T_e = 22,000°.
- - - - = Black-body curve for T_e = 20,000° (relative units).

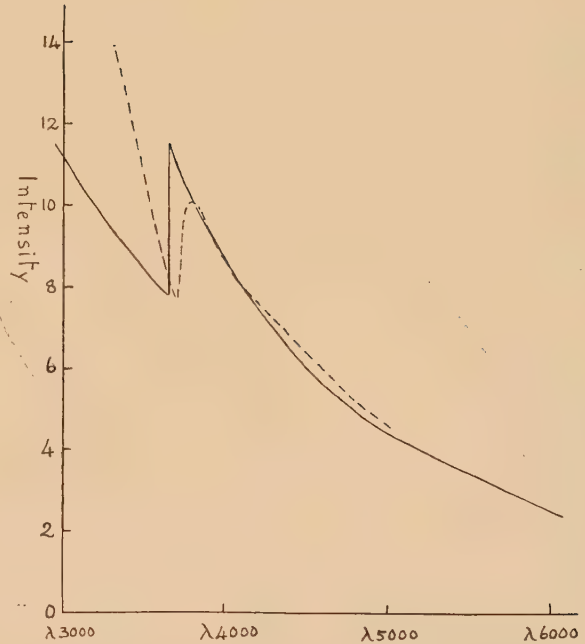

FIG. 5.—Comparison of theoretical curve for hydrogen star with Yü's observed curve for ι Herculis.

—— = Theoretical curve for T_e = 15,000°.
- - - - = Yü ι Herculis, B3 (18,000°) VIII *b*.

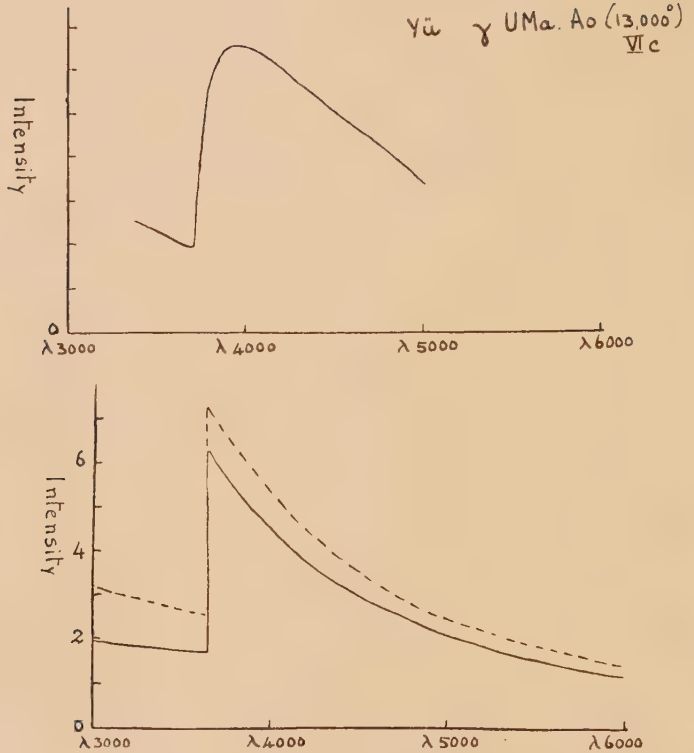

Fig. 6.—Comparison of theoretical curves for hydrogen star with Yü's observed curve for γ UM*a*

—— Theoretical curve for T_e = 10,000°.
- - - - Theoretical curve for T_e = 11,000°.

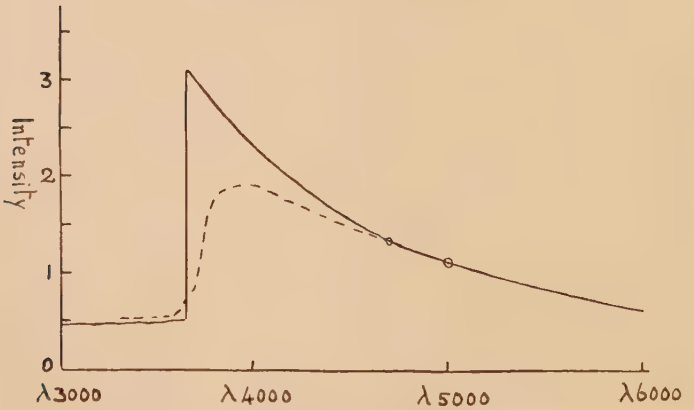

Fig. 7.—Comparison of theoretical curves for hydrogen star with Yü's observed curve for δ Geminorum.

—— Theoretical curve for T_e = 8000°.
- - - - Yü, δ Gem, Fo (12,000°) VI *g*.

seem better to derive an effective temperature by comparison with curves such as these than with ordinary Planck curves. The general

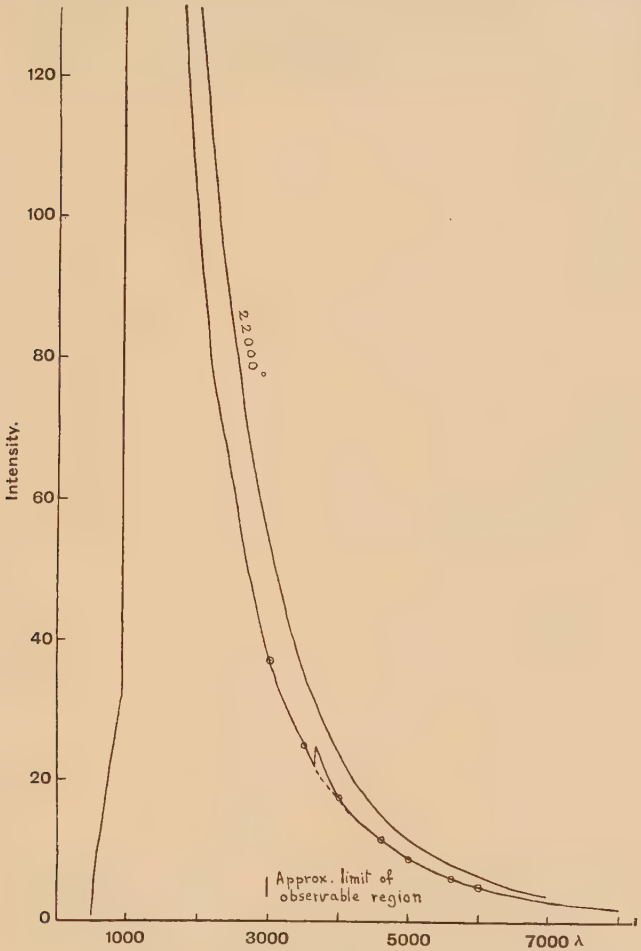

FIG. 8.—Comparison of theoretical curve for hydrogen atmosphere with black-body curves.

———— Theoretical curve for T_e = 22,000°.
⊙ - - - ⊙ Black-body curve for 20,000° (relative units).
22,000° Black-body curve for 22,000° (absolute units).

indication is that comparison with Planck curves tends to give too high effective temperatures.

Theoretical Spectral Energy Curves.—A comparison of computed curves with the corresponding Planck curves for the corresponding value of T_e on the same scale is given in figs. 8–11. In each case a

second Planck curve is given, which, on a suitable scale, agrees well with the theoretical curve on the redward side of λ4000. We may notice that (*a*) the theoretical curve is very different from the corresponding black-body curve. This is especially the case in the ultra-violet, and shows that if the absorption varies much with wave-length, the com-

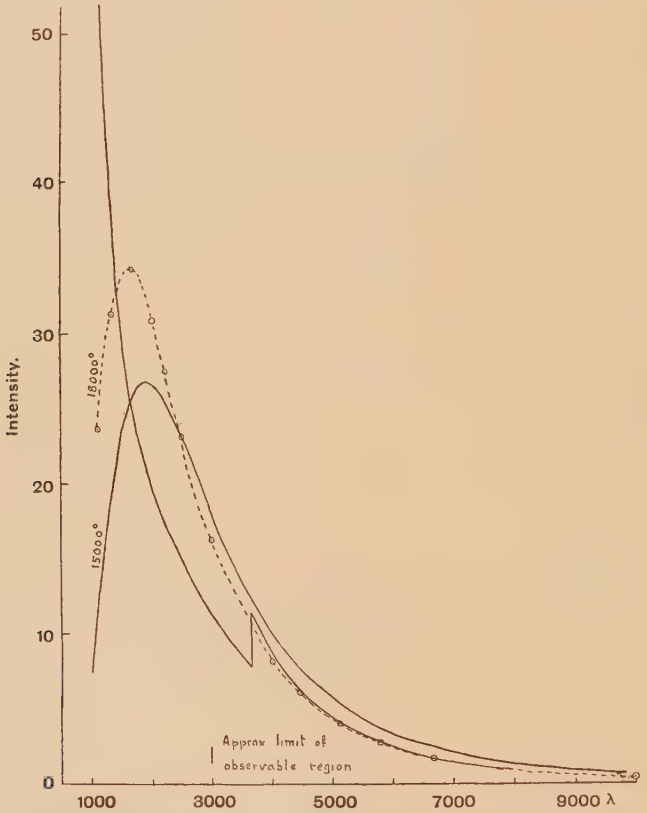

Fig. 9.—Comparison of theoretical curve for hydrogen atmosphere (T_e = 15,000°) with black-body curves for 15,000° (absolute units) (15,000°) and 18,000° (relative units) (18,000°).

plete energy curve of a star may be nothing like an ordinary Planck curve. (*b*) At high temperatures the absorption at the head of the Balmer series becomes small, and at sufficiently high temperatures would not be observed even in a 100 per cent. hydrogen atmosphere. (*c*) In all cases it is possible to choose another black-body curve whose *shape* fits well the theoretical curve up to the head of the Balmer series (especially if allowance is made for the "rounding-off" mentioned above). For values of T_e about 20,000°, this curve corresponds to temperatures somewhat below T_e, while for lower values of T_e this

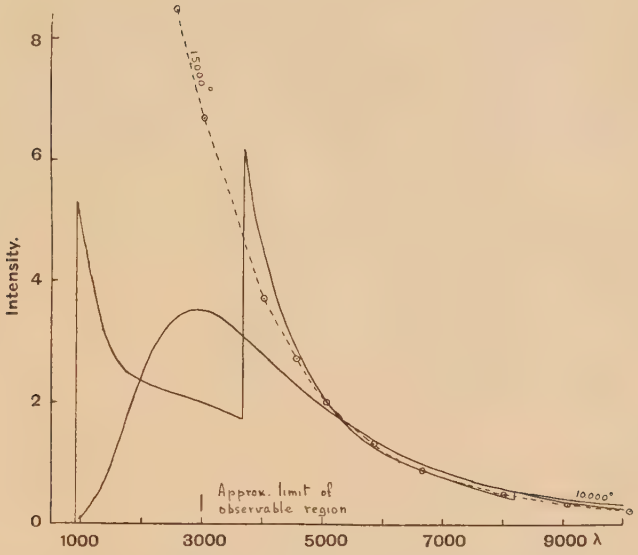

FIG. 10.—Comparison of theoretical curves for hydrogen atmosphere (T_e = 10,000°) with black-body curves for 10,000° (absolute units) (10,000°) and 15,000° (relative units) (15,000°).

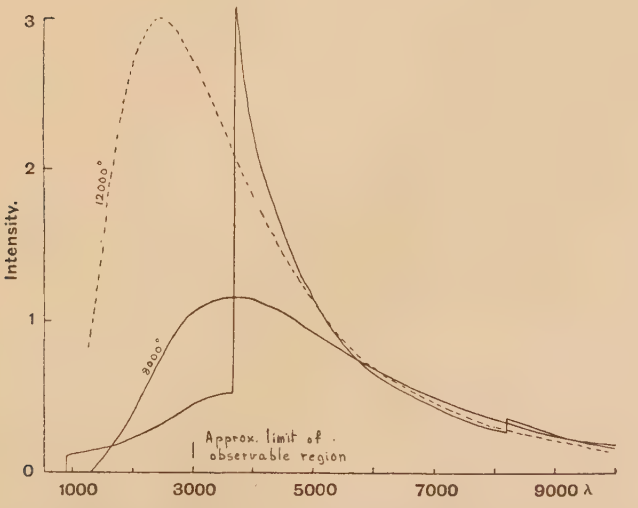

FIG. 11.—Comparison of theoretical curve for hydrogen atmosphere (T_e = 8000°) with black-body curves for 8000° (absolute units) (8000°) and 12,000° (relative units) (12,000°).

curve corresponds to temperatures somewhat above T_e. These curves should be compared with a figure given by Abbot,* when it will be seen that our fitting of a second Planck curve to the theoretical curve is definitely like his fitting of a Planck curve to the observed curve. If this has any significance, it means that, except for the hottest stars, the effective temperatures derived will be too high. This would

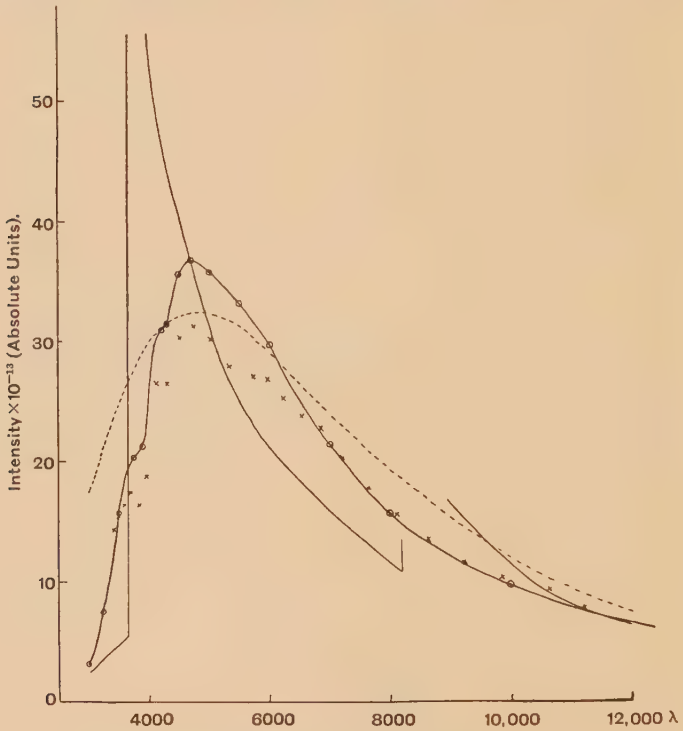

FIG. 12.—Spectral energy curves for the sun.

——— The full curve represents $T_e = 5740°$ throughout. It is shown for not quite all wave-lengths λ.
○—○ Abbot's observed curve (1903–10).
× × ,, ,, ,, (1920–22).
- - - - - Black-body curve for 6000°.

explain why these temperatures lead to values of the stellar radii smaller than those obtained by other methods.

The Sun.—It is of some interest to see what a hydrogen star of the same effective temperature as the sun would look like. This is indicated in fig. 12 where the theoretical curve for $T_e = 5740°$ is compared, on an absolute scale, with Abbot's † observations and with a Planck curve

* Abbot, *Astrophys. Journal*, **60** (1924), 87, see fig. 5, p. 102.

† Abbot and colleagues, *Ann. Smith. Inst.*, 1913, iii; 1922, iv; *Smith. Misc. Coll.*, 1923, **74**, No. 7.

for 6000°. The crude comparison is a little absurd, but one cannot help inferring that the tendency of an abundance of hydrogen would be to shift the maximum towards the violet and to depress the curve in the ultra-violet. This tempts one to suppose that an explanation of the main features in which the observed curve differs from a Planck curve may lie in this direction.

While Professor Milne's argument shows definitely that hydrogen cannot, in general, be responsible for most of the atmospheric opacity, we do seem to have found indications that it is of importance in some stars in some parts of their spectra. Such indications suggest that it would be worth while to investigate the dependence of the general absorption coefficient on wave-length, and to use this to calculate spectral energy curves which would provide standards of comparison. In this way it should be possible to derive more significant effective temperatures than the ordinarily used " colour temperatures."

Mathematical Department,
University of Edinburgh :
1931 *June.*

The Absorption Coefficient of a Degenerate Gas.

By Bertha Swirles, Ph.D.

(*Communicated by E. A. Milne.*)

§ 1. The recent work of Milne * on stellar structure suggests that the material of the central regions of a star is an ideal gas of very high density consisting of stripped nuclei and free electrons in a " degenerate " state. In the present paper an expression is obtained for the mean absorption coefficient of such a gas when the electrons alone are degenerate. It is found that this mean absorption coefficient varies with the inverse square of the temperature. The writer hopes shortly to investigate a model of a star, with the use of this formula.

An investigation of the mean absorption coefficient for a non-degenerate gas was made by Milne.† This was based on Kramers's correspondence principle argument, which has now been superseded by the very full calculations of Gaunt ‡ on the lines of quantum mechanics. Absorption of radiation takes place in two ways, (1) by a free electron in an encounter with a positive nucleus, (2) by an electron bound to the nucleus. We shall show that for a degenerate gas the contribution to the absorption from (2) is much less than that from (1). The method used in evaluating the mean is that suitable for astronomical applications, as suggested by Rosseland.§

§ 2. *Absorption Due to " Free-free " Electron Transitions.*—Let one electron with energy E encounter a positive charge Ze per unit time, in

* E. A. Milne, *M.N.*, **91**, 4, 1930. Referred to as MI.

† E. A. Milne, *M.N.*, **85**, 750, 1925. Referred to as MII.

‡ J. A. Gaunt, *Phil. Trans.*, A, **229**, 163, 1930. Referred to as GI. *Roy. Soc. Proc.*, A, **126**, 654, 1930. Referred to as GII.

§ S. Rosseland, *M.N.*, **84**, 524, 1924.

the presence of radiation of unit intensity of frequency ν. Let the probability of a transition to an unoccupied cell of energy $E'(=E+h\nu)$ per unit time, *i.e.* per encounter, be $a_1(E,\nu)$. To obtain the probability of a transition to a state of energy E', we must multiply $a_1(E,\nu)$ by the probability that a cell of energy E' is unoccupied.

Now the number of electrons per unit volume with energies in the range $(E', E'+dE')$ is

$$\frac{1}{e^{\alpha+E'/kT}+1}\cdot\frac{4\pi p'^2dp'}{h^3} \quad . \quad . \quad . \quad (1)$$

where

$$\frac{p'^2}{2m}=E' \quad . \quad . \quad . \quad . \quad (2)$$

and α will be defined later.
The corresponding number of cells is

$$\frac{4\pi p'^2dp'}{h^3} \quad . \quad . \quad . \quad . \quad (3)$$

Therefore the probability that a cell is occupied is

$$\frac{1}{e^{\alpha+E'/kT}+1} \quad . \quad . \quad . \quad . \quad (4)$$

and the probability that it is empty is therefore

$$1-\frac{1}{e^{\alpha+E'/kT}+1}=\frac{e^{\alpha+E'/kT}}{e^{\alpha+E'/kT}+1} \quad . \quad . \quad (5)$$

The intensity of black-body radiation of frequency ν is

$$I(\nu)=\frac{C\nu^3}{e^{h\nu/kT}-1} \quad . \quad . \quad . \quad . \quad (6)$$

where

$$C=8\pi h/c^2.$$

Therefore the rate of absorption of energy from radiation of frequency ν by electrons with energies in the range $(E, E+dE)$ is, per unit volume,

$$a_1(E,\nu)\,I(\nu)\times\left(\begin{array}{c}\text{number of electrons per unit}\\ \text{volume with energies } (E, E+dE)\end{array}\right)\times\left(\begin{array}{c}\text{probability that cell}\\ \text{of energy } E' \text{ is empty}\end{array}\right)$$

$$=a_1(E,\nu)\cdot\frac{C\nu^3}{e^{h\nu/kT}-1}\cdot\frac{1}{e^{\alpha+E/kT}+1}\cdot\frac{4\pi p^2dp}{h^3}\cdot\frac{e^{\alpha+E'/kT}}{e^{\alpha+E'/kT}+1} \quad . \quad (7)$$

and the rate of absorption per unit intensity $a_1(\nu)$ is obtained by dividing by $I(\nu)$ and integrating with respect to E.

It is worth while in passing to verify that the absorption balances the emission. Let the probability of a *stimulated* transition of an electron with energy E' to an unoccupied cell of energy E be $b_1(E',\nu)$. Then the total rate of emission of radiation of frequency ν by electrons of energies $(E', E'+dE')$ is

$$b_1(E',\nu)\cdot(I(\nu)+C\nu^3)\cdot\frac{1}{e^{\alpha+E'/kT}+1}\cdot\frac{4\pi p'^2dp'}{h^3}\cdot\frac{e^{\alpha+E/kT}}{e^{\alpha+E/kT}+1} \quad . \quad (8)$$

It is easy to see from GI, pp. 192–4, in particular equation (5.24), that

$$p'b_1(\mathrm{E}', \nu) = pa_1(\mathrm{E}, \nu).$$

Also,

$$p'dp' = mdE' = mdE = pdp.$$

Therefore (8) becomes

$$a_1(\mathrm{E}, \nu) \cdot \frac{C\nu^3 e^{h\nu/k\mathrm{T}}}{e^{h\nu/k\mathrm{T}} - 1} \cdot \frac{1}{e^{\alpha+\mathrm{E}'/k\mathrm{T}} + 1} \cdot \frac{4\pi p^2 dp}{h^3} \cdot \frac{e^{\alpha+\mathrm{E}/k\mathrm{T}}}{e^{\alpha+\mathrm{E}/k\mathrm{T}} + 1} \cdot \quad (9)$$

which is identical with (7) since

$$\mathrm{E} + h\nu = \mathrm{E}'.$$

According to Gaunt *

$$a_1(\mathrm{E}, \nu) = \frac{4\pi Z^2 e^6}{3\sqrt{3}hcmp\nu^3} \cdot g \quad . \quad . \quad . \quad (10)$$

where $g \to 1$ when $\mathrm{E}, \mathrm{E}' \to 0$. It appears also that $g \to 1$ when E alone $\to 0$. For the present we shall assume $g = 1$ for all E and ν, although further investigation of the validity of this is necessary. Then

$$a_1(\nu) = \frac{16\pi^2 Z^2 e^6}{3\sqrt{3}h^4 c\nu^3} \int_0^\infty \frac{e^{\alpha+(\mathrm{E}+h\nu)/k\mathrm{T}}}{(e^{\alpha+\mathrm{E}/k\mathrm{T}} + 1)(e^{\alpha+(\mathrm{E}+h\nu)/k\mathrm{T}} + 1)} d\mathrm{E} \quad . \quad (11)$$

$$= \frac{Ak\mathrm{T}}{\nu^3} \int_{e^\alpha}^\infty \frac{dx}{(x+1)(x+e^{-h\nu/k\mathrm{T}})} \quad . \quad . \quad . \quad . \quad (12)$$

where

$$\mathrm{A} = \frac{16\pi^2 Z^2 e^6}{3\sqrt{3}h^4 c}.$$

(12) is found to be

$$\frac{\mathrm{A}}{\nu^3(1 - e^{-h\nu/k\mathrm{T}})} \left\{ h\nu + k\mathrm{T} \log \left(\frac{e^\alpha + 1}{e^{\alpha+h\nu/k\mathrm{T}} + 1} \right) \right\} \quad . \quad . \quad (13)$$

We now consider approximations to (13), (1) when α is large and positive, corresponding to classical statistics, (2) when α is large and negative, corresponding to complete degeneracy.

If α is large and positive

$$a_1(\nu) \simeq \frac{\mathrm{A}}{\nu^3(1 - e^{-h\nu/k\mathrm{T}})} \left\{ h\nu + k\mathrm{T} \left(-\frac{h\nu}{k\mathrm{T}} + e^{-\alpha}(1 - e^{-h\nu/k\mathrm{T}}) + \ldots \right) \right\}$$

and

$$e^{-\alpha} \simeq \frac{h^3 \mathrm{N}}{(2\pi mk\mathrm{T})^{\frac{3}{2}}} \quad . \quad . \quad . \quad . \quad (14)$$

where N is the number of electrons per unit volume.

Then

$$a_1(\nu) \sim \frac{Ak\mathrm{T}}{\nu^3} e^{-\alpha} \quad . \quad . \quad . \quad . \quad (15)$$

* GI, p. 200; GII, p. 657. We use a_1 for Gaunt's a_0.

If α is large and negative and $\alpha + h\nu/k\mathrm{T} < 0$

$$a_1(\nu) \simeq \frac{\mathrm{A}}{\nu^3(1 - e^{-h\nu/k\mathrm{T}})}\{h\nu + k\mathrm{T}e^{\alpha}(1 + e^{h\nu/k\mathrm{T}}) + \ldots\} \quad . \quad (16)$$

$$\simeq \frac{\mathrm{A}h}{\nu^2(1 - e^{-h\nu/k\mathrm{T}})} \quad . \quad . \quad . \quad . \quad . \quad . \quad (17)$$

If α is large and negative but $\alpha + h\nu/k\mathrm{T} > 0$

$$a_1(\nu) \simeq \frac{\mathrm{A}}{\nu^3(1 - e^{-h\nu/k\mathrm{T}})}\left[h\nu + k\mathrm{T}\left\{-\left(\alpha + \frac{h\nu}{k\mathrm{T}}\right) + e^{\alpha} - e^{-(\alpha + h\nu/k\mathrm{T})} + \ldots\right\}\right] \quad (18)$$

$$\simeq \frac{-\mathrm{A}\alpha k\mathrm{T}}{\nu^3(1 - e^{-h\nu/k\mathrm{T}})} \quad . \quad . \quad . \quad . \quad . \quad . \quad . \quad . \quad . \quad (19)$$

where *

$$-\alpha \simeq \frac{h^2}{2mk\mathrm{T}}\left(\frac{3\mathrm{N}}{4\pi}\right)^{\frac{2}{3}}.$$

§ 3. *Effect of "Bound-free" Transitions.*—The energy E of an electron bound in an orbit of principal quantum number n to a nucleus of charge Ze is given by

$$\mathrm{E} = -\frac{2\pi^2 mZ^2e^4}{h^2n^2} = -\frac{\mathrm{R}hZ^2}{n^2} \quad . \quad . \quad . \quad (20)$$

if we neglect interactions with other bound electrons. If $\nu > |\mathrm{E}|$, the electron may make a transition to a state of positive energy E′. Let the probability of such a transition to an unoccupied cell be $a_2(\mathrm{E}, \nu)$. Then if n is large,

$$a_2(\mathrm{E}, \nu) \simeq \frac{1}{n^3} \cdot \frac{16\pi^2Z^2e^6}{3\sqrt{3}h^4c\nu^3} \cdot \frac{4\pi^2mZ^2e^4}{h^2n^2} \quad . \quad . \quad (21)$$

Gaunt shows that this formula is a fair approximation even when n is small if $\mathrm{E}' \simeq 0$. Then the contribution to the absorption coefficient due to transitions from levels with principal quantum number n is

$$\frac{4\mathrm{AR}hZ^2}{n^3\nu^3} \cdot \frac{e^{\alpha + \mathrm{E}'/k\mathrm{T}}}{e^{\alpha + \mathrm{E}'/k\mathrm{T}} + 1} \quad . \quad . \quad . \quad (22)$$

If α is large and positive this tends to

$$\frac{4\mathrm{AR}hZ^2}{n^3\nu^3} \quad . \quad . \quad . \quad . \quad . \quad (23)$$

$\mathrm{R}hZ^2$ is of the order of $k\mathrm{T}$ and (23) is larger than (15). A full investigation of the photo-electric absorption, similar to that of Milne,† is then necessary.

If, however, α is large and negative, (22) becomes approximately

$$\frac{4\mathrm{AR}hZ^2}{n^3\nu^3} e^{\alpha + \mathrm{E}'/k\mathrm{T}} \quad . \quad . \quad . \quad . \quad (24)$$

* L. Brillouin, *Statistiques Quantiques* (1930), p. 146.
† MII, p. 753.

if

$$\alpha + \mathrm{E}'/k\mathrm{T} < 0$$

which will hold for values of ν for which (21) is valid. (24) may therefore be neglected compared with (17). Further justification is necessary, but we shall assume that this is true for all values of ν.

§ 4. *The Mean Absorption Coefficient of a Degenerate Gas.*—We have now to evaluate the mean value a_1 of $a_1(\nu)$ when α is large and negative. According to Rosseland * the correct mean for astronomical applications is given by

$$\frac{1}{a_1} = \frac{\int_0^\infty \frac{1}{a_1(\nu)} \frac{\partial \mathrm{I}(\nu)}{\partial \mathrm{T}} d\nu}{\int_0^\infty \frac{\partial \mathrm{I}(\nu)}{\partial \mathrm{T}} d\nu} \quad . \quad . \quad . \quad (25)$$

Then from (17) and (19)

$$\frac{1}{a_1} \simeq \frac{\frac{1}{\mathrm{A}}\int_0^{-ak\mathrm{T}/h} \frac{\nu^2(1-e^{-h\nu/k\mathrm{T}})}{h} \frac{\partial}{\partial \mathrm{T}}\left(\frac{\nu^3}{e^{h\nu/k\mathrm{T}}-1}\right)d\nu - \frac{1}{\mathrm{A}ak\mathrm{T}}\int_{-ak\mathrm{T}/h}^\infty \nu^3(1-e^{-h\nu/k\mathrm{T}})\frac{\partial}{\partial \mathrm{T}}\left(\frac{\nu^3}{e^{h\nu/k\mathrm{T}}-1}\right)d\nu}{\int_0^\infty \frac{\partial}{\partial \mathrm{T}}\left(\frac{\nu^3}{e^{h\nu/k\mathrm{T}}-1}\right)d\nu} \quad (26)$$

It is easy to verify that when $\alpha \to -\infty$ the second integral in the numerator tends to zero. Therefore,

$$\frac{1}{a_1} \simeq \frac{\frac{k^6\mathrm{T}^5}{\mathrm{A}h^7}\int_0^\infty \frac{x^6}{e^x-1}dx}{\frac{k^4\mathrm{T}^3}{h^4}\int_0^\infty \frac{x^4e^x}{(e^x-1)^2}dx} \quad . \quad . \quad . \quad . \quad (27)$$

$$= \frac{k^2\mathrm{T}^2}{\mathrm{A}h^3} \cdot \frac{6\,!\,(1+2^{-7}+3^{-7}+\ldots)}{4\,!\,(1+2^{-4}+3^{-4}+\ldots)} \quad . \quad . \quad (28)$$

Therefore, substituting for A,

$$a_1 \simeq \frac{8\pi^2\mathrm{Z}^2e^6\lambda}{45\sqrt{3}hc} \cdot \frac{1}{k^2\mathrm{T}^2} \quad . \quad . \quad . \quad . \quad (29)$$

where λ is a factor very nearly equal to unity. This formula evaluates the absorption coefficient of a degenerate gas.

It is of interest to compare (29) with the mean of a_1 for the non-degenerate gas, for which α is large and positive. This is approximately

$$\frac{8\pi^2}{315\sqrt{3}} \frac{\mathrm{Z}^2e^6h^2\lambda}{c(2\pi m)^{\frac{3}{2}}} \cdot \frac{\mathrm{N}}{(k\mathrm{T})^{\frac{7}{2}}} \quad . \quad . \quad . \quad (30)$$

where N is the number of electrons per unit volume. The ratio of (29) to (30) is, apart from a numerical factor,

$$\frac{(2\pi mk\mathrm{T})^{\frac{3}{2}}}{h^3\mathrm{N}} \quad . \quad . \quad . \quad . \quad (31)$$

* S. Rosseland, *loc. cit.*

For a highly degenerate system for which (29) is appropriate, (31) is very much less than unity. If the photo-electric absorption is considered as well, (30) may have to be multiplied by a considerable numerical factor. (31) is, however, sufficient to indicate that the theoretical value of the mean absorption coefficient is much smaller when the degeneracy is taken into account. The consequences of this cannot be deduced until an investigation has been made of a stellar model with a mean absorption coefficient given by the new formula.*

Note on the Hartmann Test for Parabolic and Hyperbolic Mirrors.
By Prof. R. A. Sampson, F.R.S.

The interesting method published by Mr. Hindle † for testing a hyperbolic mirror with the help of a spherical mirror is a great improvement on other practice. Except in regard to publication it can hardly be called new, as some of us will be aware. Identically the same method was communicated to me by Mr. J. A. Armstrong of Sir Howard Grubb, Parsons & Co., in connection with testing the secondary mirror of the 36-inch Edinburgh reflector. I was struck with its neatness, but of course I was not at liberty to publish it. The first letter I find referring to it bears the date 1929 January 19. However, my purpose in sending this note is not to deal with the question of priority, in which matter any credit for making it generally available is due to Mr. Hindle, but to add a certain improvement upon its application to the Hartmann test, which was put into practice at the Walker Gate works for the hyperbolic mirror and before that for the main parabolic mirror. To begin with the parabolic mirror, this is usually tested at its centre of curvature. It is astigmatic at this point, but the aberrational corrections to be applied for the various zones are well known. But the difficulty arises that, in order to secure good images, the artificial star, as well as the camera, ought to be on the axis of the mirror, which they cannot be if they are to be at the same distance away. To interpose a reflecting device, carrying the image away to the side, is not unobjectionable. But if the artificial star is put, say, half-way between the centre of curvature and the principal focus, the centre of the camera will be twice as far away, and a comfortable distance will be left for disposing the indispensable accessories. Just the same plan may be adopted for testing a hyperbolic mirror with the help of a spherical mirror. It is only necessary to assign the aberrational corrections to be applied to the measured points of intersection with the axis of the rays from the various zones. These are as follows :—

Fig. 1. For a ray issuing from P, striking the mirror at M and meeting the axis at Q, a correct parabola throws Q out beyond a standard point Q_0 by the amount

$$\tfrac{1}{2}FQ \cdot AM^2/AF^2.$$

---

* See MI.

† *M.N.*, **91**, 592, 1931.

Fig. 1.

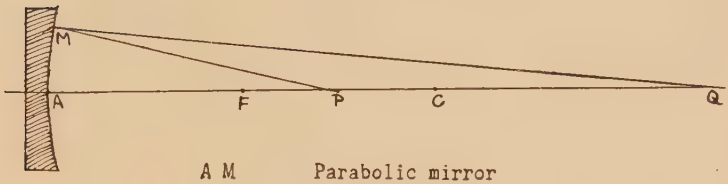

A M Parabolic mirror
F Principal focus
C Centre of curvature

Fig. 2.

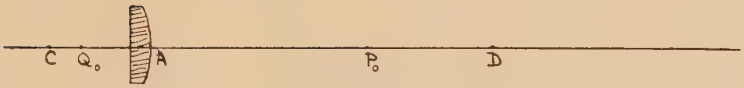

$P_0A = u_0$, $DA = U$, $AQ_0 = v_0$, $AC = V$

Fig. 3.

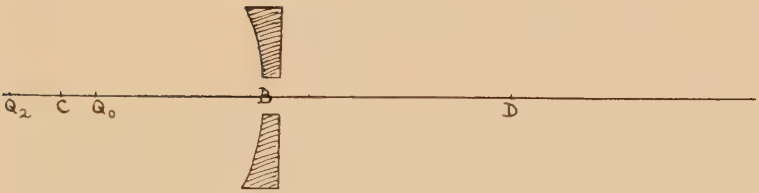

$Q_0B = u_2$, $BQ_2 = v_2$

Fig. 4.

$Q_2A = u_4$, $AQ_4 = v_4$

Figs. 2, 3, 4. Axial rays issue from an artificial star at P_0, strike the hyperbolic mirror (A), and are returned as from Q_0; they then strike the spherical mirror (B) and are converged to Q_2; on the way they strike the hyperbolic mirror (A) again and are converged finally to Q_4. But a ray originating from P_0 at an angle α_0 to the axis is brought to a point nearer to the surfaces than Q_4 by the amount

$$\tfrac{1}{2}\alpha_0^2(v_2/u_2)^2(v_4/u_4)^2(u_0+v_0)\left[\frac{u_0v_0}{UV}-1\right],$$

$$+\alpha_0^2(u_0/v_0)^2(v_4/u_4)^2\frac{v_2^2}{r}\left(\frac{u_2}{r}-1\right)^2,$$

$$+\tfrac{1}{2}\alpha_0^2(u_2/v_2)^2(u_0/v_0)^2(u_4+v_4)\left[\frac{u_4v_4}{UV}-1\right].$$

In this expression U, V denote the values taken by u_0, v_0 (or u_4, v_4) when P_0, Q_0 (or Q_4, Q_2) are at the foci C, D of the hyperbola. The expression $\frac{u_0v_0}{UV}-1$ is negative, $\frac{u_4v_4}{UV}-1$ is positive. Further, we have u_0 positive, v_0 negative, u_0+v_0 positive, and v_4 positive, u_4 negative, u_4+v_4 positive. r is the radius of the spherical mirror and is taken as positive, as are also u_2 and v_2. The first and third terms are accordingly of opposite signs, and if P_0 is not too far from P they will be found nearly to cancel one another.

Interlocking of Triplets of Absorption Lines.

By R. v. d. R. Woolley, Ph.D.

In a previous paper the present writer * has discussed a case of two interlocked absorption lines. A direct solution was made of the simultaneous differential equations, obtained by making simplifying approximations as nearly as possible similar to those ordinarily made in the treatment of principal lines, and it was found that the widths of the lines were not appreciably affected by the interlocking.

In the present paper we consider the case of a triplet (or doublet) of lines, having the same upper state, and lower states which are not themselves the upper states of strong lines. (These conditions are fulfilled by $n^3S - 2^3P$ triplets of the alkali earths, and by $2^2P - 2^2S$ doublets of the alkali metals.)

The interlocking of one member of a multiplet with the other members may be regarded in the following way. The formation of any one line at any point in the atmosphere is governed by the number of atoms per c.c. of the atmosphere at that point in the two atomic states connected with the line. The atmosphere is not exactly in thermodynamical equilibrium with radiation, and the number of atoms in any state will depend on the intensities of those lines involving

* Woolley, *M.N.*, **90**, 779, 1930.

transitions in which it is the upper state, the equilibrium condition being that the total number of transitions, per c.c. per sec., into the state must equal the number of transitions away from it, since there can be no secular increase in the number of atoms in any particular state. There is not, however, detailed balancing in each of the separate transitions.

Fig. 1 shows the scheme of energy levels for the Mg triplet, at 5167A, 5173A, and 5184A, taken from Grotrian.* There are no other transitions connected with the 2^3S state. The 2^3P_1 and 2^3P_3 states are not the upper states of any transitions, but 2^3P_2 is the upper state of a fairly weak line $1^1S - 2^3P_2$ at 4571A. We here suppose that this line does not appreciably disturb the number of atoms in the 2^3P_2 state.

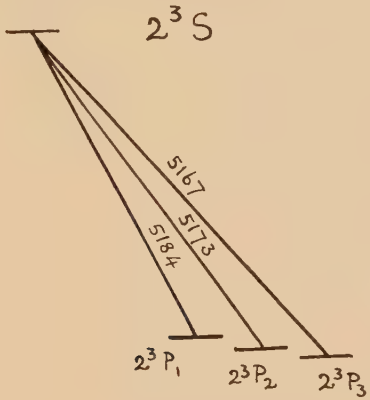

Fig. 1.

The number of atoms per c.c. in the 2^3S state depends on the intensities of the three lines in the triplet.

It is known from observation of the Mg triplet in the sun † that the lines have very closely the relative intensities given by the theory which neglects interlocking. This fact suggests a method of successive approximation for the mathematical treatment of the problem. We take as a first approximation the theory which neglects interlocking, and calculate on this basis the number of atoms per c.c. in the 2^3S state at any particular optical depth. With this number we proceed to calculate the second approximation to the contour of the line.

In the ordinary theory of the formation of a principal line it is assumed that each frequency within the line can be considered independently of the line as a whole; ‡ if we suppose that absorption in the wings of a line is due to a finite width of the energy levels, then we must suppose that when an atom has absorbed a quantum in the wings of a line it re-emits a quantum of exactly the same frequency.

* *Handbuch der Astrophysik.*, Bd. III, 2, 3, p. 533.
† Minnaert, *Zeitschrift für Astrophysik.*, **1**, 192, 1930.
‡ Eddington, *M.N.*, **89**, 621, 1929.

The atom must be supposed to have some sort of " memory " of the exact position in the lower energy level from which the upward transition came. This hypothesis is rather improbable, but may be approximately correct in the case of wide lines.*

The generalisation of this assumption to the case of a triplet is as follows : if the central frequencies of the three lines are ν_1, ν_2, and ν_3, then the frequencies $\nu_1 + \Delta\nu$, $\nu_2 + \Delta\nu$, and $\nu_3 + \Delta\nu$ are interlocked with each other but are independent of all other frequencies. The physical picture is that these three frequencies arise from transitions between a common, slightly displaced upper state and three equally displaced (or undisplaced) lower states, and the atom in the upper state " remembers " the displacement of the lower state from which it came, and reproduces this displacement in the downward transition.

We retain this hypothesis in the present paper, which is concerned with comparing triplet lines with non-interlocked lines, so that we must make the same assumptions for the triplet lines as are made in the case of principal lines.

The general method of calculating the contour of an absorption line when the number of atoms in the upper state has been disturbed by interlocking has been given by Eddington. †

Considering one line at a time :

Let k be the coefficient of continuous absorption,
l_ν the coefficient of line absorption,
$J_\nu'(\theta)d\nu$ the flow of radiation of frequency ν to $\nu + d\nu$ within the line in a direction making an angle θ with the outward direction,
$J(\theta)d\nu$ the corresponding flow just outside the line,
$d\omega$ the element of solid angle.

$$J = \frac{1}{4\pi}\int J(\theta)d\omega \quad \text{and} \quad H = \frac{1}{4\pi}\int J(\theta)\cos\theta d\omega$$

$$J_\nu' = \frac{1}{4\pi}\int J_\nu'(\theta)d\omega \quad \text{and} \quad H_\nu' = \frac{1}{4\pi}\int J_\nu'(\theta)\cos\theta d\omega$$

$$T = -\int \kappa\rho dr \qquad \eta = l_\nu/k.$$

Let n' be the ratio of the number of atoms in the upper state to the number in the lower state, and n the corresponding ratio for thermodynamical equilibrium, and set $n' = fn$. Superelastic collisions are neglected.

Then if we set $\sigma = (1 + n)\sqrt{3}$, the contour is given in *M.N.*, **89**, 633, equation (31),

$$\left(1 + \frac{2}{\sqrt{3}}\right)H_\nu' = \int_0^\infty (1 + fn)e^{-\sigma\tau}J_T d\tau,$$

* Woolley, *Mt. Wilson Contr.*, No. 421 ; *Ap. J.*, **73**, 201, 1931.
† *M.N.*, **89**, 633, 1929.

and since $J_T = H(2 + 3\tau)$ we have

$$\frac{H_\nu'}{H} = \frac{1}{1 + \frac{2}{\sqrt{3}}} \int_0^\infty (1 + fn) e^{-\sigma\tau} (2 + 3\tau) d\tau \quad . \quad . \quad (1)$$

Let N_s be the number of atoms per c.c in the upper state, and let the numbers in the three lower states be $\chi_1 N_P$, $\chi_2 N_P$, and $\chi_3 N_P$. χ_1, χ_2, and χ_3 are the statistical weights of the states. Let f_1, f_2, and f_3 be the oscillator strengths of the three lines, and M be the mass of the atom.

Let the atomic absorption coefficients for the three frequencies $\nu_1 + \Delta\nu$, $\nu_2 + \Delta\nu$, and $\nu_3 + \Delta\nu$ be $f_1 s_{\Delta\nu}$, $f_2 s_{\Delta\nu}$, and $f_3 s_{\Delta\nu}$ respectively. Then the number of transitions into state S per c.c. per second is

$$N_P M s_{\Delta\nu} \{ f_1 \chi_1 J_{\nu_1}' + f_2 \chi_2 J_{\nu_2}' + f_3 \chi_3 J_{\nu_3}' \}.$$

The number of downward transitions per second from a given number of atoms in the upper state is an atomic constant. Consideration of detailed balancing under thermodynamical equilibrium shows that if N_{ST} is the number of atoms per c.c. in state S when the substance is in thermodynamical equilibrium with matter at a temperature T, and a_{SP} the probability of a downward transition in one second,

$$\begin{aligned} N_{ST} a_{SP} &= N_P M s_{\Delta\nu} \{ f_1 \chi_1 J_T + f_2 \chi_2 J_T + f_3 \chi_3 J_T \} \\ &= N_P M s_{\Delta\nu} J_T \end{aligned}$$

since

$$\sum_{r=1,\,2,\,3} f_r \chi_r = 1.$$

The number of downward transitions per c.c. per second at any point in the actual atmosphere is therefore

$$N_S a_{SP} = \frac{N_S}{N_{ST}} \cdot N_P M s_{\Delta\nu} J_T.$$

If we ignore the effect of collisions in regulating the value of N_S, the value will be determined by the condition that the total number of transitions into the state per second is equal to the total number out of it.

Hence

$$\frac{N_S}{N_{ST}} \cdot N_P M s_{\Delta\nu} J_T = N_P \cdot M s_{\Delta\nu} \sum_{r=1,\,2,\,3} f_r \chi_r J_{\nu_r}'$$

$$\frac{N_S}{N_{ST}} = \sum_{r=1,\,2,\,3} f_r \chi_r \frac{J_{\nu_r}'}{J_T}.$$

The quantity N_S/N_{ST} is the factor f in equation (1) (not to be confused with the oscillator strengths f_r). We calculate f at every point by taking the values of J_{ν_r}' from our first approximation, which is the theory which neglects interlocking. Then, from a well-known equation,*

$$J_{\nu_r}' = J_T - \frac{2H\eta_r}{1 + \eta_r + \frac{2}{3} q_r} e^{-q_r \tau}$$

where $q_r^2 = 3(1 + \eta_r)$ and $\eta_r = l_\nu/\kappa$ for the r^{th} line ($r = 1$, 2, or 3).

* Eddington, *loc. cit.*, equations (14), (16), with $\varepsilon = 0$.

Using the relation $J_T = H(2 + 3\tau)$, we get

$$f = \sum_{r=1,\,2,\,3} \chi_r f_r \left(1 - \frac{\eta_r}{1 + \eta_r + \frac{2}{3}q_r} \frac{e^{-q_r\tau}}{1 + \frac{3}{2}\tau}\right) . \quad . \quad (2)$$

Substituting this value of f in equation (1)

$$\left(1 + \frac{2}{\sqrt{3}}\right)\frac{H_{\nu_1}'}{H} = \frac{1 + \frac{2}{\sqrt{3}}(1 + \eta_1)}{1 + \eta_1} - 2\eta_1 \sum_{r=1,\,2,\,3} \frac{\chi_r f_r \eta_r}{(1 + \eta_r + \frac{2}{3}q_r)(q_r + \sqrt{3}\cdot(1 + \eta_r))} \quad (3$$

With only one lower state the summation disappears and $\chi_r f_r = 1$ (3) gives the same results as the ordinary formula

$$\frac{H_\nu'}{H} = \frac{1 + \frac{2}{3}q}{1 + \eta + \frac{2}{3}q} \quad . \quad . \quad . \quad . \quad (4)$$

In the case of a doublet there are, of course, only two terms to be summed.

Table I. shows values of H_ν'/H calculated for a triplet for which the values of $\chi_r f_r$ are $\frac{1}{9}$, $\frac{3}{9}$, and $\frac{5}{9}$ respectively. The values in parenthesis are calculated from formula (4), as if the lines were not interlocked.

TABLE I.

Values of H_ν'/H for a Triplet of Interlocked Lines.

η.	$\frac{1}{5}$.	$\frac{2}{5}$.	1.	$\frac{1}{3}$.	1.	$\frac{5}{3}$.	1.	3.	5.
H_ν'/H	·92	·80	·73	·87	·73	·63	·73	·53	·41
	(·92)	(·80)	(·73)	(·87)	(·73)	(·63)	(·73)	(·53)	(·43)

η.	$\frac{5}{3}$.	5.	$\frac{25}{3}$.	5.	15.	25.	10.	30.	50.
H_ν'/H	·66	·45	·31	·52	·29	·10	·47	·23	·01
	(·63)	(·43)	(·35)	(·43)	(·27)	(·18)	(·32)	(·20)	(·16)

This table shows that the interlocking process does not appreciably affect that part of the contour which lies above the ordinate $H_\nu'/H = \frac{7}{10}$. Measurements of line width made at points such that $H_\nu'/H > \frac{7}{10}$ are to be interpreted exactly as if the lines were not interlocked with each other. Further, the closeness of the values found to the values in parenthesis, which are the same as those of the first approximation, shows that the successive approximations are highly convergent here.

The central portions of the line exhibit striking interlocking effects, and the approximate method is probably valueless in the last case given in the table (η = 10, 30, 50). In any case, superelastic collisions should be taken into account when considering the centres of the lines, and we have neglected them.

It is also to be noticed that the effect of interlocking is in the reverse sense to that hitherto expected—that is to say, the strongest line is strengthened and the weak line partly filled up. The argument usually

given * is as follows : since the strongest line is the blackest line, there will be relatively fewer upward transitions in this frequency than in the other frequencies leading to the same upper state. The downward transitions, however, take place in a constant ratio among all the lines, this ratio being an atomic constant. The strongest line is accordingly filled up at the expense of the weaker ones.

This argument, however, only applies to the uppermost layer of the atmosphere. In the interior the values of J_ν'/J_T all tend to unity, and the recovery is quicker in the case of the stronger of two lines,

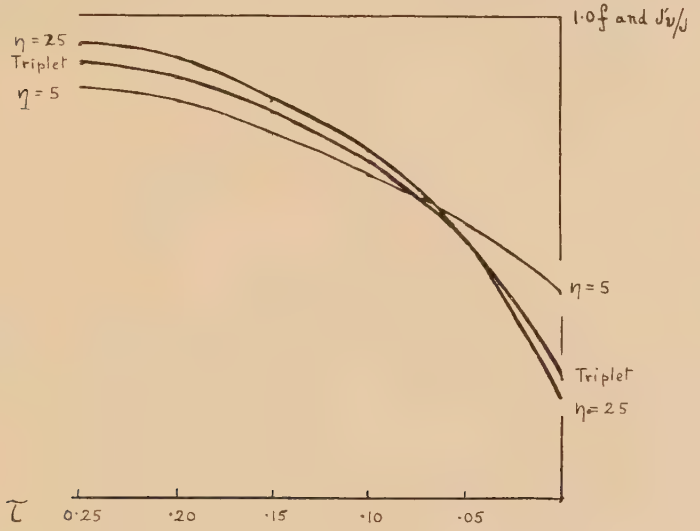

Fig. 2.

so that at a small optical depth this becomes the weaker of the two, judging intensities by the quantity $1 - J_\nu'/J_T$. Calculations shown in Table II. and illustrated in fig. 2 demonstrate this point.

Table II.

The Factor f as a Function of the Optical Depth τ.

τ.	*f*.	J_ν'/J.		
	η=5, 15, 25.	η=5.	15.	25.
0	0·25	·43	·27	·21
0·05	·53	·57	·53	·53
·10	·70	·67	·68	·72
·15	·80	·75	·79	·81
·20	·88	·81	·86	·90
·25	·90	·85	·90	·94

* Woolley, *Ap. J.*, **73**, 200, 1931.

The values of f, calculated for a triplet at a point where the three values of η are 5, 15, and 25, are shown. The values of J_ν'/J are given for three non-interlocked lines at $\eta = 5$, 15, and 25. f is plotted against τ in fig. 2, and the values of J_ν'/J are shown for the two lines $\eta = 5$ and $\eta = 25$. From the figure, the line ($\eta = 25$) which is blacker at the top of the atmosphere is weaker for all depths greater than τ. Below this depth the interlocking effect is reversed, *i.e.* tends to strengthen the stronger line. The calculations shown in Table I. show that this effect predominates.

We repeat our principal conclusion, that measurements of line width made at points such that $H_\nu'/H > {}_1{}^7{}_0$ can be interpreted exactly as if the lines were not interlocked with each other.

Gonville and Caius College, Cambridge:
1931 *May* 25.

The Formation of the Magnesium b Lines in the Solar Atmosphere.

By H. H. Plaskett.

Introduction.—A prerequisite to the physical interpretation of stellar spectra is a knowledge of the method by which absorption lines are formed in the atmosphere of the star. This fact was recognized by Schwarzschild * as early as 1914, and in a classical paper he gave the mathematical details of two idealized models for the origin of such lines, a model of pure absorption and one of pure scattering (Schuster). At the same time he pointed out that it was possible to test these models by comparing the observed behaviour of the absorption lines across the disc of the sun with the behaviour predicted by the idealized model at various angles of emergence, and, fully as important, he made such a test by measuring the contours of the H and K lines at the centre of the sun and at a point twelve seconds of arc from the limb. From his measures Schwarzschild concluded, since the lines did not completely disappear at the limb as predicted by the model of pure absorption, that scattering played an essential part in the formation of these lines. The next step in the development of such models was taken by Eddington † who suggested a model atmosphere in which atoms excited by the absorption of radiation become de-excited, in part by collisions of the second kind (absorption), and in part by re-emission of the same frequency (scattering). The mathematical and physical consequences of this model have been greatly developed as a result of further investigations by Milne ‡ and by Eddington.§

In view of both the importance of the problem and the development of a third model since Schwarzschild's investigation, it seems appropriate

* K. Schwarzschild, *Sitz. d. Preuss. Akad.*, p. 1183, 1914.
† A. S. Eddington, *Internal Constitution of the Stars*, p. 337, 1926.
‡ E. A. Milne, *Monthly Notices*, **88**, 493, 1928; **89**, 3, 1928.
§ A. S. Eddington, *ibid.*, **89**, 620, 1929.

at the present time to study anew the behaviour of absorption lines across the solar disc. Two of the three models, however, namely, those of Schuster and Eddington, presuppose in the first place that the absorption line being studied wholly determines the number of atoms in the excited state, and, in the second place, if de-excitation takes place

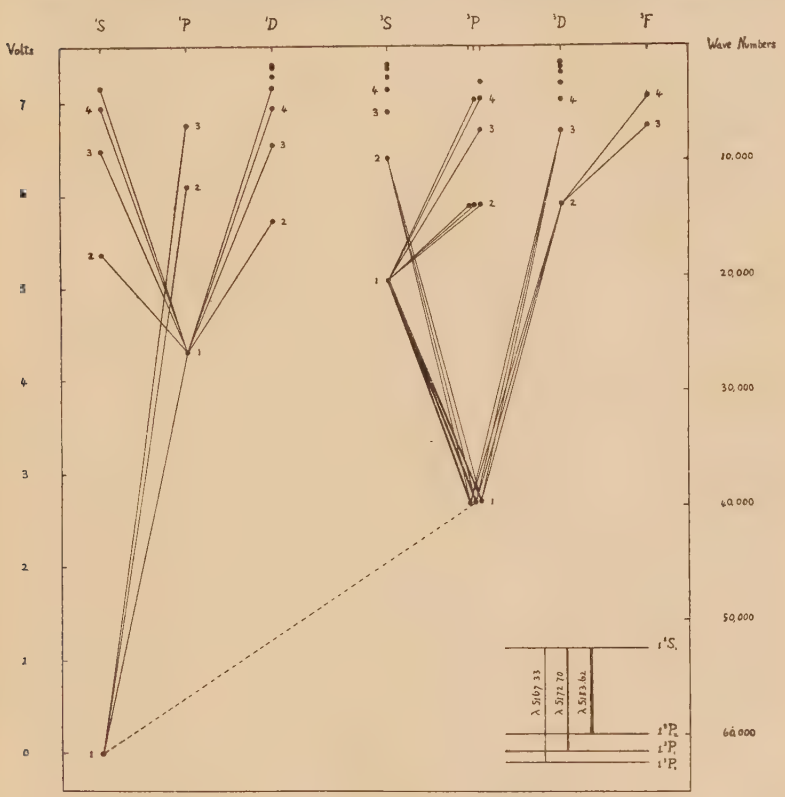

FIG. 1.—Grotrian diagram for magnesium.

by emission, that the emitted radiation has the same frequency as the absorption line. These two conditions are satisfied by relatively few solar absorption lines; thus none of the Balmer lines fulfils either condition, and even so-called resonance lines, such as H and K, do not meet the first requirement. Of the strong lines in the solar spectrum in regions relatively free from foreign lines, these two conditions are probably most satisfactorily met by the transitions $1^3P - 1^3S$ in magnesium. These transitions, which give rise to the solar *b* group, are shown as heavy lines in the Grotrian diagram in fig. 1. On account of the weakness of the inter-system combinations (only $1^1S_0 - 1^3P_1$ is observed) it may safely be assumed that there is no way either into or out of 1^3S by transitions from the singlet system. In the triplet system

only ^3P terms can combine with 1^3S, and the states involved outside of 1^3P are 2^3P, with an excitation potential of 5·8 volts, 3^3P with 6·7 volts, and so on. The numbers of atoms with such high excitation potentials must be relatively small, and such additions as these make to the population of 1^3S will be balanced, partially at least, by absorptions to these states out of 1^3S; indeed the absorption line $1^3S - 3^3P$ (λ7657·60) occurs in the solar spectrum. In short, the number of atoms in 1^3S is determined almost wholly by absorption from 1^3P, and emissions from 1^3S can take place only back to 1^3P. The *Mg b* lines thus fulfil both conditions satisfactorily.

What is true for the *Mg b* lines regarded as a unit, may not, however, be valid for the individual lines of this triplet. At the outset it is clear that an individual atom which absorbs one member of the triplet does not necessarily re-emit the same line, otherwise in the recent experiments of Frisch and Pringsheim * on the corresponding triplet in mercury, an absorption of λ5461 ($1^3P_2 - 1^3S_1$) would have been accompanied by a re-emission of λ5461 alone, not of the whole triplet. While the two necessary conditions are not fulfilled if a single line of the triplet is absorbed, it can be shown,† for absorption of all lines of the triplet, that there is an exact balance between absorption and emission over a space element in the gas. Laboratory measures ‡ of the intensities in emission of the $1^3P - 1^3S$ multiplet for *Mg*, and the corresponding triplets in other elements, have shown an intensity ratio 5 : 3 : 1 for the lines ending in the terms 1^3P_2, 1^3P_1, and 1^3P_0 respectively (the sum rule). Since these emission lines start from a common upper state, this intensity ratio means, neglecting very small differences of frequency, that the Einstein coefficients $A_{21}\left(= \frac{q_1}{q_2}\frac{8\pi h\nu^3}{c^3}B_{12}\right)$ for these lines are in the ratio 5 : 3 : 1. Further, since the statistical weights q_1 for the lower states are as 5 : 3 : 1, it follows that the transition coefficients B_{12} for these lines are identical. Consequently in an assemblage of atoms, illuminated by continuous radiation of constant intensity over the small wave-length interval $\lambda\lambda$5167–5184, where the 1^3P atoms are distributed in accordance with the statistical weights of the substates, the transitions up will be as the number of atoms in the sub-states, that is as 5 : 3 : 1, and the transitions down as the transition probabilities A_{21}, or also as 5 : 3 : 1. In the case of high temperature radiation, or continuous radiation crossed by the absorption lines under investigation, which latter, as Woolley § points out, is the case for atoms high up in the solar atmosphere, then atoms, subject to this non-uniform radiation and distributed among the 1^3P states in accordance with the statistical weights, will no longer show transitions up in the ratio 5 : 3 : 1. In these circumstances, however, the atoms immediately redistribute themselves among the 1^3P sub-states, and the balance of up and down transitions is restored. In short, the required space average balancing

* R. Frisch and P. Pringsheim, *Zeitschr. f. Phys.*, **67**, 169, 1931.
† L. S. Ornstein, *Proc. Phys. Soc. London*, **37**, 334, 1925.
‡ H. Dorgelo, *Phys. Zeitschr.*, **26**, 756, 1925.
§ R. V. d. R. Woolley, *Astroph. Journ.*, **73**, 194, 1931.

holds, and the *Mg b* lines not only as a group but also as individual lines satisfactorily meet the conditions necessary for an adequate test of theories of line formation.

The present paper contains an observational investigation of the behaviour of these *Mg b* lines across the solar disc, and a comparison of the observed behaviour with that predicted by the three models of line formation. The first three sections of the paper deal with the observational problems; a discussion of the spectrophotometric problems involved appears in the first section, measurement of plates and results in the second, and in the third a very full discussion is given of all sources of error in the investigation, with special reference to the effect of finite resolving power. These observed contours with a satisfactorily small error are discussed in comparison with the predictions of theory in the fourth section, and this comparison shows that the Eddington model gives the best representation of observation. Finally, in the fifth section some physical and astrophysical consequences of the results of this comparison are discussed, as well as those consequences which necessarily follow the adoption of the Eddington model.

Section 1.—Observational Methods.

1.1. The observational problem, that of finding the contours of the *Mg b* lines at various points on the solar disc, demands for its solution three essential features of technique. These are that the spectra be photographed with apparatus of high resolving power, that the spectra refer to definite and known points on the solar disc, and finally that an adequate method of spectrophotometry be used. For the opportunity of meeting these first two requirements I am greatly indebted to Mr. R. M. Stewart, Director, and to Dr. R. E. DeLury, of the Dominion Observatory, Ottawa, for permission to use the exceptionally fine solar equipment of that institution for some ten days in 1928. The third, and by no means the least important requirement, is secured by an application of the wedge method.

1.2. *The Ottawa Solar Spectroscope and Telescope.*—The Ottawa spectroscope, full descriptions of which have been given elsewhere,* is of the Littrow form with a collimating camera lens of 15 cm. (6 inches) aperture and of 696 cm. (22 feet 10 inches) focal length. The grating, made by Anderson in 1911, has a ruled surface 12·7 cm. (5 inches) in width by 9·8 cm. ($3\frac{7}{8}$ inches) in height, with 5900 lines to the cm. (15,000 to the inch). Astigmatism, due to crooked lines, is removed by diaphragming off three-fifths of the height of the ruling. This is accomplished by placing a central rectangular diaphragm 12·7 by 3·9 cm. (5 by 1·55 inch) on the collimating lens with the grating so placed in its cell that only the straight part of the ruling is illuminated. Fortunately the full width of the ruling may be used, with a consequent theoretical resolving power in the first order of 75,000.

This Anderson grating was selected in 1911 after comparative tests

* R. E. DeLury, *Report of Chief Astronomer, Canada*, p. 251, 1909; p. 254, 1911; J. S. Plaskett and R. E. DeLury, *Trans. Roy. Soc. Canada*, **5**, 107, 1911.

with two excellent Michelson gratings. Of these Michelson gratings, one, with a serial number 43, was the grating used by Gale and Lemon * in their study of the fine structure of the mercury lines, and was characterized by a remarkable freedom from ghosts. On account of slightly poorer definition in the second and third orders, smaller dispersion and lower brightness, it was rejected in favour of Michelson grating 55. This grating suitably diaphragmed gave very bright spectra with satisfactory definition. The Anderson grating (serial number not known), which in turn was substituted for Michelson 55, is described as giving definition of the same high quality with a remarkable freedom from diffuse light. With the facilities and time at my disposal it was impossible to test the performance of this grating on terrestrial sources, but it is clear from the foregoing comparisons made by J. S. Plaskett and R. E. DeLury, to say nothing of the known good quality of all early Anderson rulings,† that this grating is characterized not only by excellent definition but by a remarkable freedom from ghosts.

The grating and the collimating lens, adjustable for angle and focus respectively, are mounted in a carefully milled iron casting which forms the back end of the spectroscope. The front end, carrying the slit of adjustable width and 2·5 cm. clear height, the plate-holder, and the guide-plate, is a brass casting. These two metal parts of the spectroscope are united by a heavy wooden box firmly screwed to them, and externally braced. This box, around the grating, is double walled to minimize temperature changes, and the whole box is lined with black felt and internally diaphragmed to reduce scattered light. Light reflected from the components of the collimating lens is thrown below the level of the plate-holder by slightly tilting the lens.

The spectroscope is mounted at an angle of $3\frac{1}{2}°$ to the horizontal in the basement of the observatory. A concave mirror 46 cm. (18 inches) in diameter and of 2440 cm. (80 feet) focal length, illuminated by a 51 cm. cœlostat mirror with an auxiliary flat, forms an image of the sun some 227 mm. (about 9 inches) in diameter on the guide-plate of the spectroscope. The definition given by this solar telescope, in spite of the well-known disadvantages of a horizontal mounting, is on the whole good; this is in part accounted for by the exceedingly well ventilated shelter which covers the whole equipment. Changes of mirror focus during exposure were minimized by blowing air with an electric fan over the surface of the cœlostat, and in between exposures all surfaces were protected from the sun by a blind.

1.3. *Wedge Method of Spectrophotometry.*—Given such equipment for securing spectra, the final problem is the conversion of the measurable blackening on the photographic plate in terms of the intensity of the incident radiation which produces this blackening. In exact spectrophotometry this conversion is made by the substitution method of Hartmann ‡; radiation from two sources within the same small

* H. G. Gale and H. B. Lemon, *Astroph. Journ.*, **31**, 78, 1910.
† W. F. Meggers and C. C. Kiess, *Journ. Opt. Soc. America*, **6**, 417, 1922.
‡ J. Hartmann, *Zeitschr. f. Instrumentk.*, **19**, 97, 1899.

wave-length interval have the same intensities if, and only if, equal blackenings are produced on the same photographic plate after exposures of equal duration. This requirement has been satisfied in the present investigation by an application of the wedge method.

A small wedge (W. iv *) some 6 mm. in height and made of neutral tint glass, backed with a piece of transparent glass of the same angle and refractive index to avoid refraction and dispersion, is mounted in contact with and parallel to the spectroscope slit. If $I_\lambda(o)$ be the radiation within the wave-length interval λ to $\lambda + d\lambda$ incident on the wedge, and $I_\lambda(h)$ the radiation in the same wave-length interval transmitted by the wedge at the height h, then we may put

$$I_\lambda(h) = I_\lambda(o) \cdot \phi_\lambda(h) \cdot \quad . \quad . \quad . \quad . \quad (1)$$

where $\phi_\lambda(h)$ is the transmission of the wedge as a function of height and wave-length (since the glass of the wedge is not strictly neutral), and is a quantity which has to be found from a calibration (see § 1.5). The resulting wedge spectrum is one in which the blackening on the plate shades off from a maximum at a point on the plate corresponding to the thin edge of the wedge, where $\phi_\lambda(h)$ is a maximum, to a very small value at a point corresponding to the thick end of the wedge where the transmission is small. Provided the transmission of the wedge is known, and provided that the exposure times of the wedge spectrum and the spectrum under investigation are the same, then the ratio of intensity r_λ in the line to that in the adjacent continuous spectrum is from Hartmann's criterion given by

$$r_\lambda = \phi_\lambda(h')/\phi_\lambda(h'') \quad . \quad . \quad . \quad . \quad (2)$$

where h' and h'' are the corresponding heights on the wedge at which the blackenings in the wedge spectrum are the same as those observed in the line and in the adjacent continuous spectrum respectively.

1.4. *Details of the Exposures.*—After some preliminary experiments and very careful spectroscopic focus tests during the last few days of June, the plates on which the present investigation is based were exposed on 1928 July 1. The spectroscope was used in the second order; this gave ample dispersion (1·16 A. per mm.) and resolving power (150,000) for the problem, and at the same time reduced still further the already small chance of distortion by grating ghosts. To minimize scattered light in the spectroscope, already small on account of the felt lining and internal diaphragms, and to eliminate overlapping third order ultra-violet spectrum, a yellow filter (equivalent to Wratten K3, opaque to the violet at λ4500) was mounted permanently some 80 cm. in front of the spectroscope slit. Details of the exposures made under these conditions on July 1 are given in Table I. In successive columns appear the plate number, the slit width in mm., the diameter of the solar image in mm., the position of the sun on the slit, the position of the wedge in front of the slit, and the times of exposure.

* H. H. Plaskett, *Pub. Dom. Astroph. Obs. Victoria*, **2**, 213, 1923.

TABLE I.

Details of Exposures on 1928 July 1.

Plate.	Slit. mm.	Solar Diameter. mm.	Sun.	Wedge.	Exposure E.S.T. h m s m s
L 4155	·036	227·2	Centre	Erect	13 50 00–53 00
			N. Limb		13 55 10–58 10
			Centre	Rever.	14 01 00–04 00
L 4156	·036	227·0	Centre	Erect	15 21 00–25 00
			N. Limb		15 27 10–31 10
			Centre	Rever	15 34 10–38 10
L 4157	·036	227·0	Centre	Erect	16 10 45–14 45
			N. Limb		16 16 40–20 40
			Centre	Rever.	16 23 00–27 00

The first and last of the three exposures of equal duration on each plate were spectra of the centre of the sun made through the neutral tint wedge (W. iv.). In the first of these the wedge was erect (thin edge down) and the thick edge just below the centre of the slit, and in the last the wedge was reversed with thin edge up and just below the centre of the slit. This particular arrangement was chosen in order that the wedge erect and reverse spectra together (see Wedge Method,* p. 219) should effectively eliminate non-uniformity of illumination over the height of the wedge, which arises from occulting of light in the spectroscope and from the falling off of intensity away from the centre of the solar image. These wedge spectra, in addition to giving the necessary standardization for conversion of photographic blackenings into incident intensities, also served to give spectra of the solar centre comparable in intensity (by virtue of absorption in the wedge) with the spectrum of the limb.

The middle exposure on each plate, of exactly the same exposure time as that for the two wedge spectra, was made with the slit radial to and set on the northern limb of the sun. This showed the exact position of the limb, and gave a spectrum within the limb to a distance of some 17 mm. This is the method used by Unsöld;† it has the advantage that any desired portion of the limb spectrum within the above limits, corresponding to a cosine of the angle of emergence from 0·00 to 0·50, may be measured for line contour. In order to secure this advantage, however, several essential precautions must be observed. In the first place the solar image should be focussed on the slit for the wave-length region being photographed; secondly, the image should be carefully guided on the slit; thirdly, the sky should be transparent and free from haze to avoid distortion of the limb spectrum by light scattered from the brighter central portions of the sun; and finally the definition should be good. These requirements were satisfied

* H. H. Plaskett, *Pub. Dom. Astroph. Obs. Victoria*, **2**, 213, 1923.
† A Unsöld, *Zeitschr. f. Phys.*, **46**, 765, 1928.

in the present investigation. The strictly achromatic image of large size formed by the Ottawa solar telescope was clearly a great advantage in meeting the first requirement; the position of this image on the slit and guide-plate of the spectroscope could be adjusted by means of controls, so that irregularities in drive and atmospheric refraction could be easily compensated in order to meet the second requirement. Finally, the plates were all taken on a day, July 1, exceptionally free from haze, when the solar definition was moderately good, in order to satisfy the two remaining conditions.

The exposures, detailed in Table I., were made on unbacked Cramer Iso Process Plates. This emulsion gives a clean working plate of fine grain which is very suitable for spectrophotometric investigations in the green and yellow. The plates so obtained were developed with a Parkhurst developer * with hydroquinone and potassium carbonate as an accelerator. By the courtesy of R. M. Motherwell, this development, and the subsequent careful fixing and washing, were carried out in his dark-room, which is specially designed for photographic photometry. The resulting plates proved to be exceptionally clean and free from the slightest trace of fog.

1.5. *Calibration of Wedge.*—The accuracy of this spectrophotometric investigation depends upon the accuracy with which the transmission $\phi_\lambda(h)$ of the wedge is determined. Although the wedge (W. iv.) used in this investigation had previously been calibrated,† it was decided, in view of the possibility of several improvements in technique, to repeat the calibration at Cambridge (Mass.) with a Hilger laboratory spectroscope. The arrangement of apparatus was as follows: A seasoned, standardized Nela ribbon filament lamp burning off a storage battery, with two resistances in parallel and an ammeter in the circuit, was used at fixed current (20·3 amperes) as a constant source of intensity. An image of this lamp filament, wider and longer than the spectroscope slit, was formed on the slit by means of a Cooke anastigmat lens of 4·5 cm. aperture and 20 cm. focal length. The aperture ratio of the beam forming the image on the slit was f/7·6 and of the spectroscope collimator f/9; consequently the collimator was more than filled for all positions of the image on the slit. The spectroscope was a Hilger Constant Deviation Instrument (Model B260) with an achromatic collimating lens, single element camera lens, long slit and dense prism. This prism, which was not large enough to accept the full beam from the collimator, was adjusted not only for minimum deviation but also to take the median portion of the parallel pencil emerging from the collimator. The spectroscope and the Cooke lens were carefully collimated, and secured firmly to a heavy table in a fully darkened room of the Astronomical Laboratory.

The wedge was mounted in a cell, so that it could be placed in either an erect or a reversed position in front of and in contact with the spectroscope slit. If $I_\lambda(h)$ is the radiation from the lamp incident on the wedge at the height h, then from (1) the radiation transmitted by the wedge is

* R. M. Motherwell, *Pub. Dom. Obs. Ottawa*, **8**, 121, 1925.

† H. H. Plaskett, *Pub. Dom. Astroph. Obs. Victoria*, **2**, 213, 1923.

$I_\lambda(h) \cdot \phi_\lambda(h)$. Now remove the wedge and reduce the intensity by some known factor k, so that the incident intensity at the same point on the slit, that is at the height h, is $k \cdot I_\lambda(h)$. If now a wedge and a non-wedge spectrum be made on the same plate with the same exposure time under the above conditions, and if at the same height h in each spectrum the photographic blackening is the same, then from Hartmann's criterion

$$\phi_\lambda(h) = k \quad . \quad . \quad . \quad . \quad . \quad (3)$$

and we have determined the wedge transmission for this wave-length and height. The actual measurement of the spectra is carried out by trial and error until a height h' is found in the wedge spectrum, where the photographic blackening is exactly the same as that in the non-wedge spectrum at the same height h'. The height h' on the plate is transferred to the equivalent height h on the wedge or slit when the spectroscope magnification is known ; this latter is precisely determined by measuring the distance between two narrow white lines at top and bottom of the wedge spectrum, which are due to narrow strips of occulting matter in the wedge separated by a known distance.

The great advantage of this procedure is that we do not have to secure uniformity of illumination over the height of the wedge. This is obvious from the fact that the comparison is between the radiation transmitted by the wedge at the height h on the slit on the one hand, and the radiation reduced by a known factor k at the same point on the slit, that is at the height h, on the other ; no matter how the illumination may vary from point to point along the height of the slit, provided the distribution does not change between the two exposures, the resulting wedge transmission is unaffected. Undoubtedly non-uniformity of illumination over the height of the slit has been one of the most fruitful sources of error in the wedge method and the similar Utrecht methods of spectrophotometry. Even when the illumination incident on the slit is uniform the spectroscope itself introduces non-uniformity, partly by occulting of the collimator,* unless certain precautions are taken, and partly from the fact that only light from the centre of the slit, lying on the optical axis, passes through a principal plane of the prism. Light from any other part of the slit passes obliquely through the prism, and suffers not only greater dispersion, indicated by the curvature of spectral lines, but also greater absorption. There does not seem to be any simple way of avoiding this type of non-uniformity produced by the prism spectroscope, and it is therefore important to have a method of wedge calibration, such as the present one, which is independent of this difficulty.

The final requirement in this calibration is a method for the reduction of the intensity by a known amount k. This has been accomplished by diaphragming the collimator—a suggestion which followed from Lloyd A. Jones's method of spectrophotometry.† Seven diaphragms were constructed with a slot and stop, so that each fitted in exactly the same way on a cap with a large circular opening placed over the

* H. H. Plaskett, *Pub. Dom. Astroph. Obs. Victoria*, **4**, 140, 1928.
† L. A. Jones, *Journ. Opt. Soc. America*, **10**, 561, 1925.

collimating lens. In each of these diaphragms were bored twenty-one similarly placed holes; these holes were truly circular and of exactly the same size in any one diaphragm. One diaphragm differed from another only in the diameter of the holes bored in it, not in the number of the holes, nor in their distribution over the collimator when placed in the spectroscope. I am indebted to H. L. Mann of Cambridge (Mass.) for devising means of meeting these specifications mechanically. The exact identity in the positions of the holes was secured by fixing each diaphragm in turn, by means of its slot and stop, to a master plate on which the hole pattern was marked and from which it could be transferred to the diaphragm. The exact identity in diameter of holes for a given diaphragm, and their circularity, was secured by first boring the holes, whose position had been marked as above, with a twist drill of smaller gauge than the diameter finally required. The diaphragm was then given a coat of a hard, dead black paint, and placed in a lathe where each hole was turned out by a special tool of the required size. The final result was that each diaphragm was dead black up to the edge of the holes, and that within the errors of measurement each hole was truly circular and of the same diameter.

The mean diameter of the holes in each of these diaphragms, measured in mm., was: Dia. 1, 3·637; Dia. 2, 2·734; Dia. 3, 2·129; Dia. 4, 1·707; Dia. 5, 1·290; Dia. 6, 1·038; Dia. 7, 0·866. The standard deviation for the measurement of a single hole in any diaphragm was $\pm$ 0·01 mm. Diaphragm 1 was always used with the wedge spectrum, and the other diaphragms with the non-wedge spectrum. Since the light emerging from the collimator is parallel, and since the diaphragm holes are exactly similarly placed so that prism and lens absorption is the same for each diaphragm, it follows that the value of k for a given diaphragm is given by the ratio of the area of the holes in it to the area of the holes in diaphragm 1. Thus for the second diaphragm

$$k = (2{\cdot}734/3{\cdot}637)^2 = 0{\cdot}565,$$

for the third diaphragm

$$k = (2{\cdot}129/3{\cdot}637)^2 = 0{\cdot}343,$$

and so on. In order to ensure that the light beam suffered no obstruction in the spectroscope, due, for example, to the small size of the prism, all but the seven central holes of the twenty-one in each diaphragm were masked off. It may be noted that the only other effect of the introduction of such diaphragms, outside of the desired change in spectroscope transmission, is to increase the diffractional spread around a point image. Since we are working with a continuous source this introduces no photometric error.

With a procedure as outlined above, sixteen plates (Ilford Special Rapid Panchromatic) were exposed. On each of these there was one wedge spectrum, made with diaphragm 1, and three non-wedge spectra made with other diaphragms. All four exposures on each plate were made of course with exactly the same lamp current and exactly the same exposure time (of the order of one minute). These exposures

on the various plates were made in all possible orders of wedge and non-wedge spectra with the various diaphragms. From the sixteen plates there were finally eight non-wedge exposures for each diaphragm from which to find the wedge transmission by means of (3). The plates so obtained, with the red end of the spectrum masked off in spectroscope, were developed with Rodinal 1/20.

These plates were measured by the indicated method of trial and error from tracings made, in a direction parallel to the h co-ordinate at the desired wave-length, with the Moll microphotometer (see § 2.2). The results are given in Table II. The successive columns of this table contain the diaphragm number, the value of log k (base 10), and the values of h in half mm. units above the thin edge of the wedge at which log $\phi_\lambda(h)$ is equal to log k in the second column. These values of h are means of the eight pairs of exposures for each diaphragm; the attached errors are the standard deviations for a single pair of exposures. The three columns of these mean values of h are for the wave-lengths 4800 A., 5200 A., and 5600 A. respectively.

Table II.

The Transmission of the Wedge W. iv.

Diaphragm.	$\log_{10} k$.	Values of h in half-mm. units.		
		λ4800.	λ5200.	λ5600.
2	−0·248	1·70±·17	1·68±·33	1·89±·46
3	−0·465	3·72 ·19	3·95 ·25	4·12 ·28
4	−0·654	5·08 ·24	5·44 ·25	5·85 ·28
5	−0·900	7·36 ·14	7·74 ·19	8·01 ·21
6	−1·089	9·07 ·20	9·59 ·17	10·06 ·22
7	−1·246	10·34 ·30		

The results of this wedge calibration, given numerically in Table II., are shown graphically in fig. 2. The ordinate in this figure is log $\phi_\lambda(h)$, and the abscissa is h; a different origin for h is chosen for each of the three wave-lengths in order to avoid confusion. From the run of the observed points, taken directly from Table II., it is clear that the log of the wedge transmission is a linear function of height on the wedge—a result usually assumed in the calibration of neutral tint glass wedges, and here shown to be true for this particular wedge W. iv.

The results of this calibration may therefore be represented by a formula

$$\log \phi_\lambda(h) = -h\sigma_\lambda + \log b_\lambda$$

or

$$\phi_\lambda(h) = b_\lambda 10^{-h\sigma_\lambda} \quad . \quad . \quad . \quad . \quad (4)$$

In this equation σ_λ is the so-called wedge constant, and $1 - b_\lambda$, a constant over the small wave-length region investigated, is the fraction of light reflected from the front and back surfaces of the wedge. The values of these unknowns may be most conveniently found by making a least squares solution of (4) in its logarithmic form; at λ4800 six

observation equations may be formed from the numerical data in Table II., and for the other two wave-lengths five equations each. The solution of the resulting normal equations leads to the results :—

$$\lambda 4800 : \sigma_\lambda = 0{\cdot}116 \pm {\cdot}002 : \log b_\lambda = -0{\cdot}049 \pm {\cdot}013$$
$$\lambda 5200 : \quad = 0{\cdot}108 \pm {\cdot}002 : \quad = -0{\cdot}059 \pm {\cdot}015$$
$$\lambda 5600 : \quad = 0{\cdot}105 \pm {\cdot}002 : \quad = -0{\cdot}043 \pm {\cdot}016$$

The insertion of these values in the logarithmic form of (4) leads to the straight lines shown graphically in fig. 2.

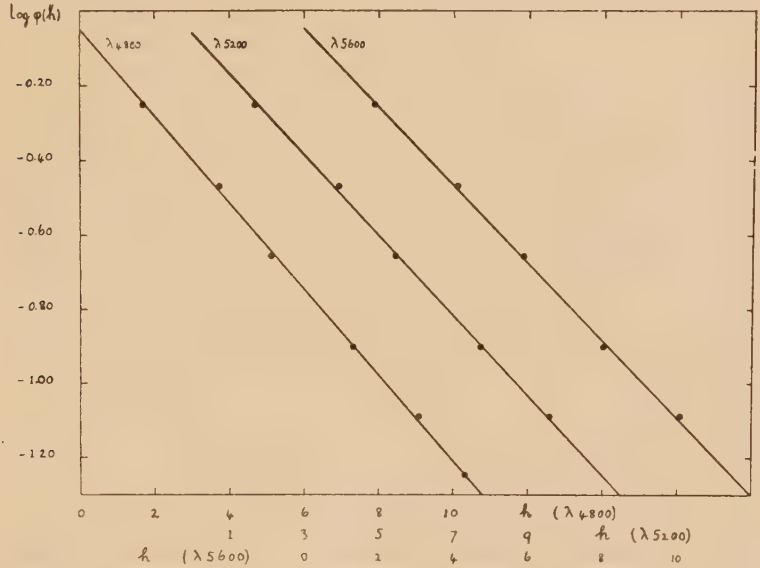

FIG. 2.—Logarithm of wedge transmission (ordinate) as a function of height on wedge (abscissa) in half mm. units.

These values of the wedge constant may be compared with those found in the previous calibration.* At the same three wave-lengths the previously found values of σ_λ were $0{\cdot}113 \pm {\cdot}002$, $0{\cdot}110 \pm {\cdot}002$, and $0{\cdot}109 \pm {\cdot}002$. The results of the old and new calibrations are therefore just barely in agreement within the limiting errors, but there can be no doubt, in view of the precautions adopted, that the results of the new calibration are considerably more free from systematic error. Using these new results it is clear that the wedge constant σ_λ may be treated as independent of wave-length over the interval required for the investigation of the *Mg b* lines. Its value is

$$\sigma_\lambda = 0{\cdot}108 \pm {\cdot}002.$$

Section 2.—Plate Measurement and Results.

2.1. The plates obtained, as listed in Table I., carry a spectrum of the solar limb and, with exactly the same exposure time, two wedge

* H. H. Plaskett, *Pub. Dom. Astroph. Obs. Victoria*, **2**, 213, 1923.

spectra of the centre of the solar disc. From these plates we wish to find at given points on the disc and at various wave-lengths across the *Mg b* lines, the ratio of intensity in the line to the intensity in the adjacent continuous spectrum. If we measure the blackness at the required wave-length in the line and the corresponding blackness in the adjacent continuous spectrum, then we may find the desired intensity ratio r at this wave-length by finding the heights h' and h'' in the wedge spectra at which these blacknesses for line and continuous spectrum respectively appear. From (2) and (4) the required intensity ratio is

$$r = \phi(h')/\phi(h'') = 10^{-(h'-h'')\sigma} \quad . \quad . \quad . \quad (5)$$

where $\sigma = 0{\cdot}108$ is known from our wedge calibration.

The only outstanding problem then lies in the measurement of the blackness or opacity of the photographic plate at the required positions. In Schwarzschild's investigation * such measurement was carried out on a Hartmann microphotometer; in the hands of an experienced measurer this instrument is both consistent and rapid, and, which is more important, its sources of systematic error, thanks to Hartmann and Schwarzschild,† are known and easily eliminated. Such an instrument was not available for the present investigation, and consequently it was necessary to use the Moll microphotometer of the Harvard College Observatory. Before discussing the measurement of tracings made with this machine, it will be necessary briefly to indicate one or two of its characteristics.

2.2. *The Moll Microphotometer.*—Complete descriptions of this microphotometer have been given elsewhere ‡ and need not be repeated here. It suffices to say that throughout this investigation the size of the illuminated patch on the photographic plate, the transmission of which was indicated by the thermocouple and galvanometer, remained constant at 0·033 by 0·986 mm. In order that the lag in response of the thermocouple and galvanometer (of the order of two seconds) should not distort the registered galvanometer deflections, the plate was driven past the illuminated patch at 2·27 cm. per hour, or, in other words, a given point on the plate required 5·2 seconds to cross the illuminated area. For the great majority of the tracings of galvanometer deflections, the magnification of the tracing over that of the original plate was 27·2; for the remainder it was 6·8. In the use of this instrument it has proved necessary to note three peculiarities, namely, the amount of transmission by infra-red light, collimation difficulties, and asymmetrical registration.

Since the thermocouple is an equal energy receiver, and since the colour temperature of the small spiral filament lamp used as a source does not exceed 2800° K, it is clear that the greater part of the radiation transmitted by the plate and registered by the thermocouple has a wave-length greater than 7000 A., with a maximum energy some-

* K. Schwarzschild, *Sitz. d. Preuss. Akad.*, p. 1183, 1914.

† K. Schwarzschild and W. Villiger, *Astroph. Journ.*, **23**, 284, 1906.

‡ W. J. H. Moll, *Proc. Phys. Soc. London*, **33**, 207, 1921; W. J. H. Moll and H. C. Burger, *Phil. Mag.*, **50**, 618, 1925.

where around 10,000 A. Thus the introduction in the light beam of a 10 per cent. aqueous solution of copper sulphate, 1 cm. thick, which absorbs everything to the red of λ7000, reduces the galvanometer deflection by over 90 per cent. This fact has two consequences. In the first place, by virtue of the optical arrangement of the instrument, the transmissions which it measures are for directed, not diffuse, radiation; consequently light scattering greatly influences the measured transmissions. Light scattering, however, reaches a maximum when the particles doing the scattering are comparable in size with the wavelength of the light.* Since the silver grains are of the order of one micron in diameter, it can be readily seen that a comparatively small deposit of silver on the plate will greatly reduce the measured transmission. This accounts for the well-known insensitivity of the Moll microphotometer to moderately dense deposits of silver, which are, on the other hand, well measurable visually with a Hartmann microphotometer. In the second place, the illuminated patch on the photographic plate is focussed there by the eye with a visually corrected microscope objective. In infra-red light this patch will be larger and its edges not well defined. In more recent models this difficulty has been overcome by the use of apochromatic objectives corrected for infra-red and visual radiation. In the present investigation, since such objectives were not available, the width of the illuminated patch in visual light, namely 0·033 mm., was chosen as small as was consistent with securing measurable transmissions.

Unless the lamp filament, condensing lens, slit, and two microscope objectives are carefully collimated, the image of the illuminated patch on the thermocouple is surrounded by an unsymmetrical halo which distorts the measured transmissions. This halo arises from images, more or less in focus, of the illuminated objective surfaces. Lack of collimation may arise from two sources; on the one hand the lamp filament may not be on the optical axis of the condensing lens, and on the other the microscope objectives (unfortunately mounted on the ways through which the plate carriage passes) may shift during the registration of the plate. The first difficulty was eliminated by providing adjusting screws for the lamp in its housing, and the second by testing collimation before and after each tracing, with a rejection of all tracings where the collimation became defective.

Plates with artificial spectrum lines, known to be symmetrical, were found to give asymmetrical tracings when run through the microphotometer. After an investigation of various possible sources of this asymmetry, it was finally found that the slit and cylindrical lens, which limited and focussed the beam of light thrown by the galvanometer mirror, were not parallel to the axis of the drum carrying the bromide paper, on which the tracing of the mirror movement was made. The tracing, consequently, was made with respect to an oblique system of co-ordinates, and such a tracing, measured with a rectangular system of co-ordinates, appeared asymmetrical. This lack of parallelism of the slit arose from warping of the wooden cover which both

* H. N. Russell, *Proc. Nat. Acad. Science*, **8**, 115, 1922.

carried it and protected the bromide paper from stray light. Unfortunately when this trouble was located tracings had been made of all the spectra, and it was impossible to tell from the tracings themselves what the slit slope, known to vary with humidity, had been. Consequently after an adjustment of the slit slope had been made, the tracings were all repeated; as a precaution the position of the slit was marked on each tracing by allowing the mirror image to trace a line on the bromide paper with the drum stationary.

2.3. *Measurement of Tracings.*—Consider first the tracings made with the motion of the plate parallel to the wave-length direction. Of each plate three such tracings were made, one at a point 3·6 mm. from the apparent limb corresponding to the emergence of radiation making an angle of 75° 31′ with the radial direction outwards, one at 9·5 mm. with a corresponding angle of 66° 25′, and finally one of a wedge reversed spectrum of the solar centre where the angle of emergence is zero. These positions were marked on the plate by ruling

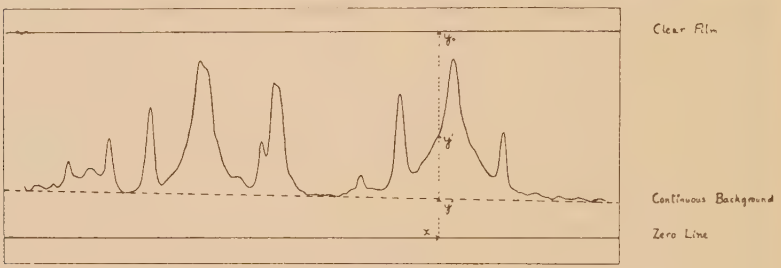

Fig. 3.—Portion of microphotometer tracing of plate L4157 at $\cos\theta = 0{\cdot}25$.

lines 2·6 and 4·6 mm. for the first case, and 8·5 and 10·5 mm. for the second, from the apparent limb; the plate itself was adjusted in the microphotometer until the illuminated patch (0·986 mm. high) moved parallel to these pairs of lines and midway between them. In the case of the solar centre the illuminated patch was adjusted until the illuminated patch moved parallel to the thin edge of the wedge spectrum in a region of suitable blackening. On account of imperfect seeing and guiding, this apparent limb, from which these positions are measured in the first two instances, is not perfectly sharp, and it is subsequently necessary (see §2.41), from intensity measures across the limb, to determine both its mean position and the true position of these ruled lines with respect to it. This will give a revised value of the angles of emergence; in the meantime we shall use the above provisional values whose cosines are 0·25, 0·40, and 1·00.

A portion of one such tracing (plate L 4157, $\cos\theta = 0{\cdot}25$) is reproduced in fig. 3. The x co-ordinate of this tracing is closely a linear function of wave-length on the plate, and the y co-ordinate, measured from the zero line (light completely cut off from thermocouple), is the galvanometer deflection which is linearly proportional to the transmission of the plate. These x and y co-ordinates, for all desired points on the tracing, may be directly read off from a sheet of transparent

mm. cross-section linen, which is placed over the whole tracing and held fast with respect to it whilst the measurement is carried out.

The measured x co-ordinate is converted to wave-length after multiplication by a factor $(\lambda_2 - \lambda_1)/(x_2 - x_1)$ where λ_1, λ_2 are the wave-lengths of a pair of known lines, and x_1, x_2 are their corresponding x co-ordinates on the tracing. The use of such a linear relation assumes that the grating gives a normal spectrum and that there is no distortion in registration, due either to lost motion in the train of gears, or to shrinkage or expansion of the bromide paper after registration and before measurement. None of these assumptions is true, but we may correct these computed wave-lengths for the errors so introduced, by the construction, in the usual way, of an O − C curve as a function of wave-length ; in this curve we use the observed (true) and computed wave-lengths of all lines which appear on the tracing. From the smoothness of these O − C curves it is evident that the wave-lengths, obtained by an application of this correction, are accurate to within a hundredth of an angstrom—a very satisfactory precision.

The y co-ordinate, measured from the zero lines, is the deflection of the galvanometer, which is directly proportional to the current generated in the thermocouple by the light transmitted by the plate. The actual plate transmission will be given by this measured y co-ordinate divided by the galvanometer deflection when no plate is interposed, or preferably by the deflection for an adjacent unexposed portion of the same plate, called the clear film. This latter deflection is put on each tracing, and its ordinate we shall denote by y_0. The ratio y/y_0 is the plate transmission, its reciprocal is the opacity, and the logarithm of this opacity is the plate density. Any of these quantities is a convenient measure of plate blackness ; in what follows we shall use the plate transmission y/y_0.

At each wave-length we require y/y_0 not only for the line but also for the adjacent continuous spectrum. We must therefore decide what the blackness of the continuous spectrum would be if the absorption line were not present. Over such short wave-length intervals, both the intensity distribution in the continuous solar spectrum incident on the plate, and the photographic sensitivity, will change so slowly and uniformly with wave-length that the plate transmission of the observed continuous spectrum may be assumed to vary linearly. Two regions are therefore selected, on either side of the line in question, where there is reasonable evidence from the run of y/y_0 that no effect of the absorption line remains. These two regions are joined by a straight line continuous with the background outside the zone of influence of the absorption line ; this is shown as a dotted line in fig. 3, where it is called the continuous background. On account of the large magnification (27·2), only about fifteen angstroms are included on each tracing, and it is sometimes difficult to be certain that this continuous background line joins on to the continuous spectrum at regions outside of all possible influence by the absorption line. In order to have an independent estimate of the continuous background, uninfluenced by this possibility, tracings were repeated of all the plates

with a magnification of 6·8, and the background drawn in on them by the same method.

2.31. We now have for various wave-lengths, at given positions on the disc, measures of plate transmission y/y_0 in line and adjacent continuous spectrum. To convert these measures to the desired intensity ratio r by means of (5), we must find the heights h' and h'' in the wedge spectra at which these same two plates' transmissions occur. In order to find these heights, tracings are made in the continuous spectrum, undistorted by absorption lines, at $\lambda 5170$ for the plate region $\lambda\lambda 5165$–5176, and at $\lambda 5187$ for the plate region $\lambda\lambda 5177$–5190. These tracings are made by orienting the plate in the microphotometer so that its direction of travel is perpendicular to the wave-length co-ordinate—that is, parallel to the h co-ordinate in the wedge spectrum. In making such tracings one wedge spectrum traverses the illuminated patch from high light transmission, corresponding to the thick end of the wedge, to low light transmission (thin edge), and the other wedge spectrum, since it is reversed on the plate, makes its traverse in the opposite direction. The resulting tracings, measured as before, now have an x co-ordinate which may be directly converted to half-mm. units on the wedge itself; this follows since the plate for a Littrow spectroscope has unit magnification over the slit, and since the magnification of the tracing over the plate is exactly known. The quantity y/y_0 measures as in an ordinary tracing the plate transmission. These transmissions are then plotted as a function of height on the wedge; typical results for the plate L4157 at $\lambda 5170$ are shown in fig. 4, where the ordinate is y/y_0 and the abcissa is h, the height in half-mm. units on the wedge. In this figure the results from the wedge-erect spectrum are shown by circles with vertical bars, and those for the wedge-reversed spectrum by circles with horizontal bars; it will be noted that there is a systematic difference between the two spectra, in the sense that the wedge-erect values show a greater plate transmission at the thin edge. This difference is the anticipated effect due to occulting of light in the Littrow spectroscope; the resulting non-uniformity of illumination over the wedge, since it is not centrally symmetrical, is completely eliminated by drawing a smooth curve, as shown in fig. 4, between the two sets of values. This curve (fig. 4) may be immediately used to find the wedge heights corresponding to given transmissions measured on plate L4157 in the wave-length interval $\lambda\lambda 5165$–5176 for the spectra at $\cos\theta = 0{\cdot}25$ and $0{\cdot}40$.

In the case of the spectrum at $\cos\theta = 1{\cdot}00$, in which the transmissions for line and continuous spectrum have been determined from the tracing of a wedge reversed spectrum, a slightly different procedure is necessary. In making the tracing of this wedge spectrum with the plate motion parallel to the wave-length co-ordinate, the illuminated patch as usual has stretched over a height of 0·986 mm.; in this height the plate transmission y/y_0 is varying because the deposit of silver in a wedge spectrum necessarily varies with height. The plate transmission measured by the microphotometer is therefore the average over the height 0·986 mm. of this smoothly varying transmission. Now when

we come to find the relation between plate transmission and wedge height for this spectrum at $\cos\theta = 1{\cdot}00$, that is to run the wedge spectra through the microphotometer parallel to the h co-ordinate, we should also use a slit of 0·986 mm. length in the h direction to obtain a similar average. Actually, however, the slit has only extended over 0·033 mm. in the h direction in making the curve reproduced in fig. 4. Instead of repeating the tracing with the new slit extension, it is more simple and as accurate to calculate, in the way first described by Lord

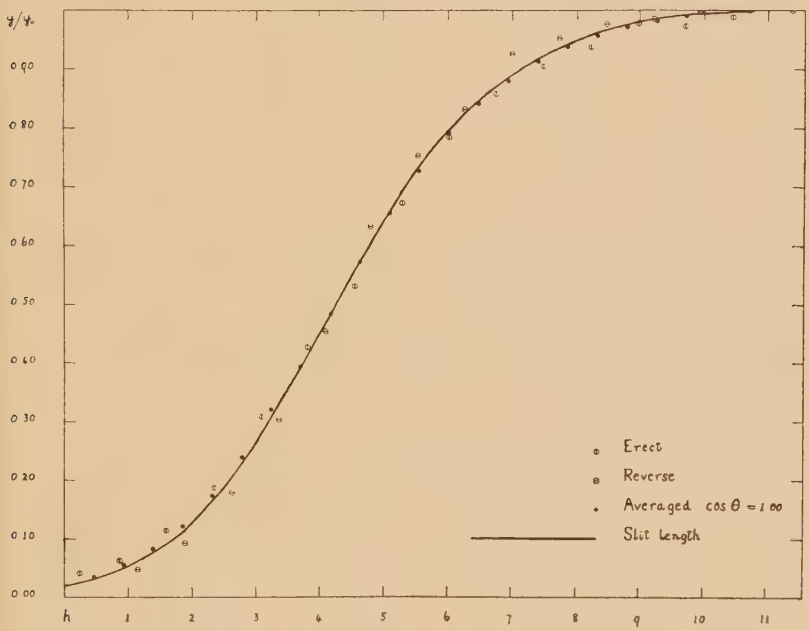

FIG. 4.—Characteristic curve for plate L4157 at $\lambda 5170$. Ordinates are y/y_0, the plate transmission, and abscissæ are wedge heights in half-mm. units.

Rayleigh,* the shape of the averaged curve from the true curve given in fig. 4. The horizontal line, in the lower right-hand corner of fig. 4, shows the length in the direction of the wedge height over which we must average (namely, 1·972 half-mm. units), and the small filled circles show the run of this averaged curve calculated by Rayleigh's method. Similar directly measured characteristic curves for positions $\cos\theta = 0{\cdot}25$ and 0·40, and calculated averaged curves for $\cos\theta = 1{\cdot}00$ have been determined from the two wedge spectra, at each of the two wave-lengths and on each of the three plates. There is, therefore, for each plate and each wave-length region, an appropriate characteristic curve from which to determine wedge height h corresponding to measured plate transmission y/y_0.

2.4. *Reduction of Measures and Final Results.*—A typical set of

* Lord Rayleigh, *Scientific Papers*, **1**, 135, 1871.

reduction of measures is shown in Table III. for the plate L4157 at $\cos\theta = 0{\cdot}25$, the plate for which a tracing and a characteristic curve have already been given. The first three columns of this table give

TABLE III.

Portion of Reduction for L4157, cos θ=0·25.

x.	Comp. λ.	Obs. λ.	y'/y_0.	y''/y_0.	h'.	h''.	log r.
87·0	6·044	6·036	·245	·219	2·85	2·69	−0·017
88·0	6·087	6·079	·278	·218	3·04	2·68	−0·039
89·0	6·129	6·121	·322	·218	3·30	2·68	−0·067
89·5	6·151	6·142	·348	·218	3·44	2·68	−0·082
90·0	6·172	6·163	·390	·217	3·68	2·68	−0·108
90·5	6·193	6·184	·431	·217	3·91	2·68	−0·133
91·1	6·219	6·210	·498	·217	4·20	2·68	−0·164

the x co-ordinate in mm. (arbitrary origin), the computed wave-length, (516) 6·044, and the corrected wave-length, the last two derived from x in the manner described in § 2.3. The fourth column contains y'/y_0 for the line, the fifth y''/y_0 for the adjacent continuous spectrum, and the sixth and seventh columns the values of h corresponding to these plate transmissions read off from the continuous line in fig. 4. The last column gives log r, which from (5) is given by $-(h'-h'')\sigma$, where, from § 1.5, $\sigma = 0{\cdot}108$.

Proceeding in this way, values of log r at a great number of wave-lengths were found for the three positions on the solar disc from the three plates. In order to find, for a given position on the disc, the mean value of log r from all three plates, the following procedure was adopted. For a given position on the sun, the value of log r from both the high and the low magnification tracings for one plate was plotted on a single sheet of cross-section paper on a large scale. A smooth curve was drawn through the points in such a way that, where the two tracings differed, the high magnification tracing was given a weight of two against one for the low magnification tracing. From this smooth curve, at a number of predetermined wave-lengths the value of log r for this particular plate at the given position on the solar disc was read off, and this value with that of r entered in a table. Similarly values of log r and r were found for the other two plates at this particular position on the solar disc. The mean of these values of r was then taken in the following way. For $\cos\theta = 0{\cdot}25$ and 1·00 a straight mean was taken of r; for $\cos\theta = 0{\cdot}40$, where the continuous background was so dense in plates L4155, 4156 as to make plate transmissions and corresponding heights in the wedge spectra very uncertain, a weighted mean was taken with the two mentioned plates having a weight unity and L4157 a weight of one and a half.

In view of possible future applications of this material a selection of the mean values from this complete table is given in Table IV. The first column contains the wave-length to the hundredth of an angstrom, thus (51)65·80, the second the mean intensity ratio r at this wave-

TABLE IV.

Mean Values of r.

λ.	cos θ.		
	·238.	·391.	1·00.
65·80	·987	·986	·985
65·96	·952	·968	·965
66·04	·942	·949	·948
66·12	·870	·872	·858
66·20	·707	·705	·671
66·24	·592	·609	·525
66·29	·544	·545	·472
66·32	·568	·586	·519
66·40	·813	·799	·802
66·48	·918	·911	·908
66·52	·923	·920	·916
66·64	·886	·882	·880
66·80	·846	·824	·809
67·04	·719	·686	·561
67·16	·611	·595	·433
67·24	·497	·489	·327
67·30	·395	·391	·254
67·34	·375	·360	·234
67·40	·394	·379	·258
67·44	·411	·396	·268
67·48	·414	·397	·268
67·52	·430	·406	·288
67·56	·485	·464	·346
67·64	·645	·621	·497
67·72	·718	·683	·593
67·88	·831	·799	·766
68·00	·873	·849	·834
68·08	·882	·861	·856
68·16	·868	·852	·845
68·28	·909	·877	·886
68·40	·930	·941	·921
68·48	·921	·941	·909
68·56	·837	·822	·791
68·64	·702	·683	·604
68·66	·691	·671	·589
68·72	·745	·716	·661
68·76	·769	·752	·709
68·80	·726	·721	·661
68·88	·517	·519	·401
68·94	·472	·457	·337
68·98	·480	·460	·329
69·04	·489	·458	·335
69·12	·606	·559	·501
69·20	·803	·768	·752
69·32	·880	·867	·858
69·60	·961	·962	·958
70·00	·984	·982	·983
70·40	·968	·977	·967
70·60	·930	·932	·935
70·72	·865	·843	·821
70·77	·832	·793	·765
70·84	·890	·863	·849
70·92	·926	·927	·924
71·20	·930	·940	·928
71·28	·923	·926	·913
71·36	·895	·883	·886
71·48	·750	·713	·684
71·56	·543	·499	·425
71·61	·485	·467	·364
71·66	·530	·522	·413
71·76	·756	·727	·691
71·84	·820	·805	·762
72·00	·802	·777	·710
72·16	·742	·702	·601
72·24	·714	·671	·542
72·32	·681	·642	·487
72·40	·640	·607	·436
72·48	·594	·559	·378
72·56	·518	·497	·324
72·60	·461	·458	·289
72·66	·368	·363	·230
72·70	·356	·340	·216
72·76	·381	·372	·243
72·80	·450	·425	·291
72·84	·521	·488	·335
72·92	·603	·566	·399
73·00	·653	·609	·446
73·12	·704	·668	·531
73·28	·770	·729	·646
73·44	·820	·787	·741
73·56	·828	·809	·785
73·64	·788	·779	·773
73·72	·634	·624	·617
73·75	·612	·598	·547
73·78	·630	·641	·544
73·84	·790	·774	·685
73·92	·903	·867	·857
74·20	·914	·920	·925
74·80	·967	·970	·961
75·20	·987	·987	·977
79·50	·986	..	·975
80·80	·951	·944	·926
81·00	·940	·937	·909
81·20	·910	·881	·872
81·28	·876	·851	·825
81·33	·866	·839	·801
81·41	·885	·865	·844
81·50	·900	·892	·887
81·60	·913	·913	·888
81·80	·889	·887	·848
81·90	·882	·873	·831
82·00	·885	·878	·844
82·20	·881	·858	·832
82·40	·847	·822	·792
82·60	·817	·785	·735

TABLE IV.—*continued.*

λ.	cos θ. ·238.	·391.	1·00.	λ.	cos θ. ·238.	·391.	1·00.	λ.	cos θ. ·238.	·391.	1·00.
82·80	·775	·735	·658	84·28	·638	·595	·450	85·88	·705	·677	·628
83·00	·728	·674	·551	84·32	·672	·632	·488	85·91	·676	·650	·576
83·20	·661	·614	·438	84·36	·718	·674	·574	85·94	·701	·672	·629
83·32	·619	·574	·378	84·44	·755	·721	·633	85·98	·783	·777	·777
83·40	·573	·541	·337	84·48	·744	·717	·624	86·04	·906	·922	·884
83·48	·490	·481	·288	84·52	·710	·684	·578	86·12	·944	·957	·930
83·56	·366	·368	·229	84·56	·686	·653	·540	86·24	·936	..	·920
83·62	·339	·333	·186	84·62	·719	·701	·627	86·32	·914	..	·907
83·68	·375	·361	·211	84·66	·782	·753	·693	86·40	·915	..	·921
83·76	·497	·470	·289	84·82	·849	·810	·789	86·48	·913	..	·907
83·80	·538	·505	·311	85·10	·888	·867	·851	86·56	·876	..	·846
83·88	·599	·559	·359	85·30	·906	·905	·883	86·64	·917	..	·910
83·96	·639	·587	·404	85·50	·916	·935	·902	86·76	·962	..	·954
84·04	·668	·611	·441	85·66	·932	·941	·918	86·80	·965	..	·959
84·12	·681	·625	·469	85·74	·916	·921	·890	87·00	·977	·966	·974
84·20	·670	·617	·468	85·82	·848	·819	·801	87·20	·981	·968	·976
84·24	·652	·606	·457	85·86	·760	·710	·685	87·40	·987	·976	·992

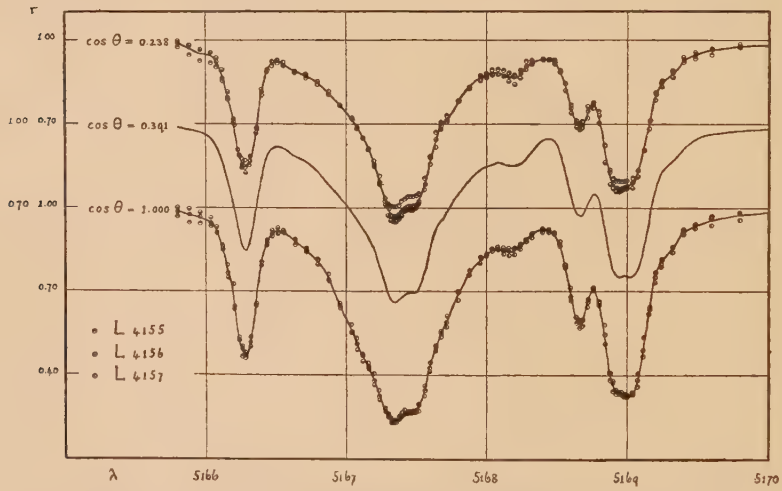

FIG. 5.—Values of r (ratio of intensity in line to that in adjacent continuous spectrum) for *Mg* $1^3P_0-1^3S_1$, λ5167·33 at cos θ=0·238, 0·391, and 1·00. The other lines appearing conspicuously in the figure are λ5166·29 (*Fe I*), λ5167·51 (*Fe I*), λ5168·19 (no identification), λ5168·66 (*Ni I*), λ5168·91 (*Fe I*), and λ5169·05 (*Fe II*). The heavy curves are the mean values of r; the individual values of r for each of the three plates are shown at cos θ=0·238 and 1·00 by differently half-filled circles.

length for $\cos\theta = 0{\cdot}25$, the third the same ratio for $\cos\theta = 0{\cdot}40$, and the last column the same ratio for $\cos\theta = 1{\cdot}00$. These observed mean intensity ratios r (from the complete table) are shown as smooth

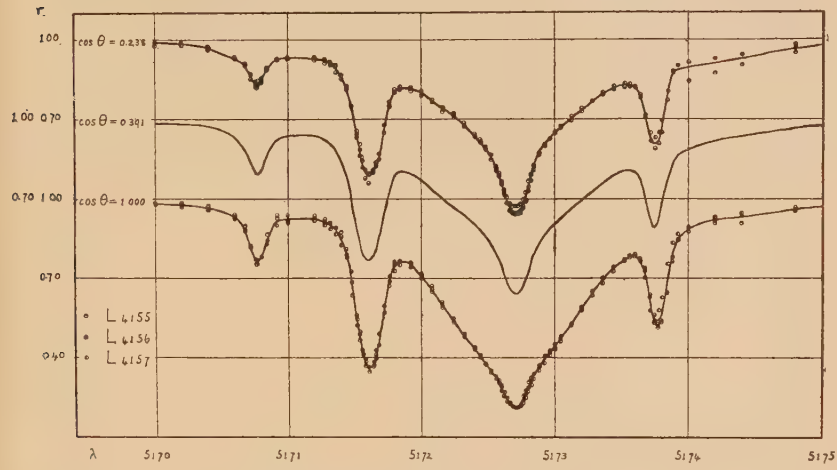

FIG. 6.—Values of r for the *Mg* line $1^3P_1-1^3S_1$, $\lambda 5172{\cdot}70$ at $\cos\theta = 0{\cdot}238$, $0{\cdot}391$, and $1{\cdot}00$. The other conspicuous lines in the figure are $\lambda 5170{\cdot}77$ (*Fe I*), $\lambda 5171{\cdot}61$ (*Fe I*), and $\lambda 5173{\cdot}75$ (*Ti I*). Compare also fig. 5.

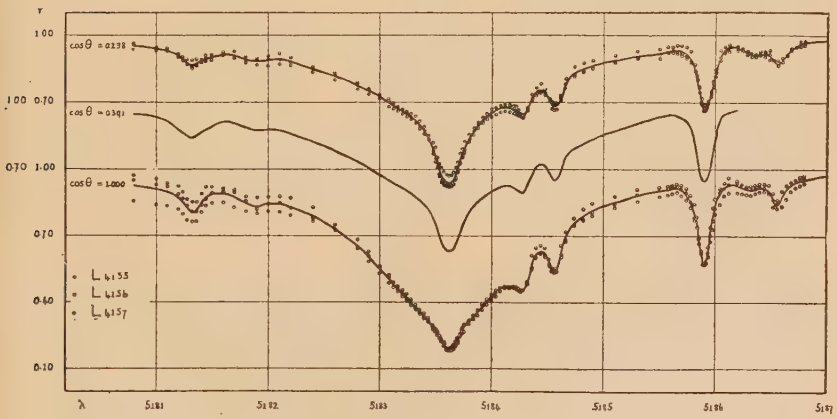

FIG. 7.—Values of r for the *Mg* line $1^3P_2-1^3S_1$, $\lambda 5183{\cdot}62$ at $\cos\theta = 0{\cdot}238$, $0{\cdot}391$, and $1{\cdot}00$. The other conspicuous lines in the figure are $\lambda 5181{\cdot}33$ (no identification), $\lambda 5184{\cdot}28$ (*Fe I*), $\lambda 5184{\cdot}56$ (*Ni I*, *Cr I*, *Fe I*), $\lambda 5185{\cdot}91$ (*Ti II*), $\lambda 5186{\cdot}33$ (*Ti I*), and $\lambda 5186{\cdot}55$ (no identification). Compare also fig. 5.

curves in figs. 5, 6, and 7. The uppermost curve in each figure is for $\cos\theta = 0{\cdot}25$, the middle curve for $\cos\theta = 0{\cdot}40$, and the bottom curve for $\cos\theta = 1{\cdot}00$. In the top and bottom curves the actual individual intensity ratios from the three plates are entered separately in order to give some idea of the scatter of these individual values. The

scatter for cos θ = 0·40, for which the individual values have not been entered in order to avoid confusion, is about twice as large as for the other two positions; this greater scatter is due to the higher density of the continuous background at cos θ = 0·40.

2.41. From the beginning of § 2.3 it will be recalled that, on account of diffuseness of the solar limb, there was some uncertainty as to the exact position on the disc at which the above values of r have been found. To remove this uncertainty microphotometer tracings have been made of the limb-spectrum parallel to the spectrum lines, that is radial to the limb, and from these and the appropriate characteristic

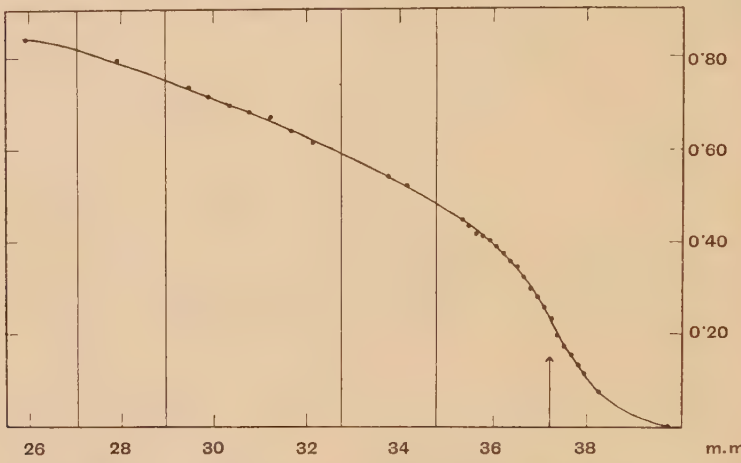

Fig. 8.—Intensity distribution across the solar limb as measured on plate L4157. Ordinates are intensities on an arbitrary scale, and abscissæ are distances in mm. from an arbitrary origin on the solar image. The two pairs of vertical lines represent the positions on plate at which the microphotometer was run. The point of inflection—that is, the mean position of the limb—is shown by an arrow.

curves the intensity distribution across the limb has been determined. Such an intensity curve for plate L4157 is plotted in fig. 8, with intensities on an arbitrary scale as ordinates, and positions on the solar disc in mm. with arbitrary origin as abscissæ. For this particular plate the values of r have been determined midway between each pair of vertical lines drawn in on diagram—that is, at positions intended to be such that cos θ = 0·25 and 0·40. The problem is now on this, and similar figures for the other plates, to find the mean position of the solar limb and hence, from the distance of the vertical lines from this point, the actual values of cos θ.

If I(x) is the true intensity distribution across the solar disc, $i(x)$ the observed intensity distribution, and $f(x)$ the fraction of time that the solar image has its centre at x, then

$$i(x) = \int_{x-R}^{x+R} I(x-\xi) f(\xi) d\xi \quad . \quad . \quad . \quad (6),$$

where the origin of x is at the mean position of the solar centre, the radius of the solar disc is R, and the limits of integration are the limits within which $I(x - \xi)$ is not equal to zero. Knowing $I(x)$ empirically from Abbot's observations, and assuming that $f(x)$ is of the form $e^{-k^2x^2}$, it would be possible to integrate (6) graphically, and by comparison with observation, to find k and the mean position of the solar limb at $x = R$. Instead of adopting this laborious procedure, scarcely justified in view of the implicit assumption in (6) that the intensity measured on the plate is proportional to the incident intensity multiplied by the length of exposure, we note that, if $I(x)$ is constant (no darkening towards the solar limb), then $i(x)$ has a point of inflection exactly at $x = R$. If $I(x)$ is of the form $a - mx$ (limb darkening linearly proportional to distance from the centre), then

$$i(x) = \frac{1}{k}\left[(a - mx)\{\text{erf } k(x + R) - \text{erf } k(x - R)\} + \frac{m}{2k}\{e^{-k^2(x-R)^2} - e^{-k^2(x+R)^2}\}\right] \quad (7)$$

and the mean value of limb position occurs nearer the centre of the solar image than the point of inflection. By an appropriate choice of a, m, and k it is possible to represent the observed intensity just outside the limb quite closely by (7). It is then found that the point of inflection in this theoretical curve, within the uncertainty of its determination, falls again at $x = R$. If, then, in the actually observed intensity distribution, we assume that the mean position of the solar limb occurs exactly at the point of inflection, we shall make a systematic error of the same order as the uncertainty of finding this point.

Measuring from the point of inflection, it is possible to find on fig. 8 and the similar diagrams for the other two plates, the exact position inside the limb at which the line contours have been determined, and therefore the corresponding value of $\cos\theta$. The results of this operation are :

	L4155.	L4156.	L4157.	Mean.
$\cos\theta$ =	0·239	0·232	0·243	0·238
$\cos\theta$ =	0·392	0·386	0·394	0·391.

These mean values are therefore adopted as the positions at which the mean values of r in Table IV have been determined, and are inserted at the heads of the columns in that table. At the centre of the sun's disc this difficulty of course does not occur, and the corresponding value of $\cos\theta$ there is exactly unity.

Section 3.—Errors of Investigation.

3.1. The values of r, the ratio of intensity in the line to that in the adjacent continuous spectrum, found in this investigation and summarized in Table IV., have resulted from an accurate and careful piece of first order spectrophotometry. These results, nevertheless, are subject to certain errors, and the amount of these must be assessed in order to know the probable accuracy of the final results. These errors are in part accidental and in part systematic ; the latter class arises

from errors in wedge calibration, from limitations of the photographic plate in the registration of incident light intensity over small regions, from averaging by the microphotometer, and finally from the finite resolving power of the spectroscope. These various sources of error are considered in turn, and the results summarized in § 3.7.

3.2. *Accidental Error.*—The accidental error of the determination may be found from the dispersion among the individual values of r for the three plates. The standard deviation of the residuals from the mean r, a selection of values of which have been given in Table IV., was computed for each mean r and expressed as a percentage of it. To save space these individual values have not been quoted, but their mean for each of the three positions on the solar disc has been taken; these mean values are:

$\cos\theta = 0{\cdot}238$ $\quad \pm 2{\cdot}25$ per cent.
$\cos\theta = 0{\cdot}391$ $\quad \pm 5{\cdot}53$,,
$\cos\theta = 1{\cdot}00$ $\quad \pm 2{\cdot}62$,,

These quantities are a measure of the accidental error for a single determination of r on one plate. In view of the fact that r is a ratio of intensities, it follows that the accidental errors of a single intensity determination for the above three regions are $\pm$ 1·6, $\pm$ 3·9, $\pm$ 1·9 per cent. respectively. The accidental error of an intensity determination has thus been exceptionally small, even if we include the higher value for $\cos\theta = 0{\cdot}391$ (the standard deviation of an observation of weight unity), where the low plate transmission for the continuous background has made the determination of the ratio r much more uncertain. Finally we may note that the standard deviation, not of a single determination of r, but of the mean value of r, as given in Table IV., is for the three regions $\pm$ 1·30, $\pm$ 2·95, and $\pm$ 1·51 per cent. respectively.

3.3. *Systematic Error in Wedge Constant.*—The systematic error in r due to the inaccuracy in the wedge constant may be readily evaluated. Differentiating (5) we have

$$\frac{\delta r}{r} = \frac{\delta\sigma}{\sigma} \cdot \log_e r = \pm 4{\cdot}26 \log_{10} r \quad . \quad . \quad (8),$$

since from § 1.5, $\sigma = 0{\cdot}108 \pm {\cdot}002$, and therefore $\frac{\delta\sigma}{\sigma} = \pm 1{\cdot}85$ per cent. From (8) it will be seen that the smaller r is, the larger will be its systematic error arising from inaccuracy in the wedge calibration. The maximum systematic error from this source will therefore occur at the centre of the strongest line, namely $\lambda 5183{\cdot}62$, and there for the three regions $\cos\theta = 0{\cdot}238$, 0·391, and 1·00 it is $\pm$ 2·00, $\pm$ 2·04, and $\pm$ 3·11 per cent. respectively.

3.4. *Systematic Error due to Photographic Limitations.*—Owing to light scattering in the emulsion, neighbourhood development effects, and gelatine contraction the photographic plate is not an accurate photometric receiver for light incident over small plate regions. These limitations of the plate affect the measured intensity distribution in an absorption line in the following ways: First, the intense radiation in

the adjacent continuous spectrum is scattered by the silver bromide grains into the absorption line; the measured value of r in the line centre is thus made too large. Secondly, the reaction products of development, most vigorously produced in the well-exposed regions of the adjacent continuous spectrum, diffuse into the line and hinder development; the measured value of r in the line centre is thus made too small. These first two effects therefore tend to neutralize each other. Thirdly, the well-exposed continuous spectrum becomes tanned on development, dries more quickly than the adjacent absorption line, and in drying pulls the continuous spectrum in on itself, thus widening the absorption line. These three effects have been very fully investigated by numerous workers, and their results, together with new material of his own, have been summarized by Ross.* As a measure of these effects Ross finds the mutual influence of adjacent images both sensitive and convenient; his experiments and measures show errors of the order of three or four microns in the separation of a close pair of emission lines, where these three effects more or less conspire together, and errors of less than a micron for a similar pair of absorption lines, where the effects, as we have seen, tend to neutralize each other.

In order to investigate the errors arising from these photographic limitations, which from the above discussion will presumably be small, two experiments were made. In the first, an artificial spectrum in the narrow wave-length region $\lambda\lambda 5100$-5500 was photographed on a reduced scale with a Cooke f/8 lens, giving excellent definition. The "spectrum" was an opal glass, on which were placed narrow pieces of black paper to give "absorption lines" of rectangular contour; this was illuminated from behind with diffuse radiation, which had passed through a Wratten filter, No. 74. Photographs were made of this source on the same brand of plate, Cramer Iso Process, used in the present solar investigation; some of these plates were developed with the same Parkhurst developer,† and others with Rodinal 1/32. Direct measures and microphotometer tracings were made of these plates. It was found from measures of the plates, both wet and dry, that there was a gelatine contraction effect for both developers of the order of 0·01 mm.; as the effect would be a maximum for such an artificial spectrum with its hard edged lines, it is probably safe to assume that gelatine contraction effects produce errors of position well below 0·01 A. for the solar lines, a quantity which is negligibly small. For the Rodinal developed plates there was a very marked Eberhard or neighbourhood development effect, but for the plates developed with the Parkhurst developer, used in the solar investigation, no effects either of neighbourhood effect or light scattering in the emulsion, within the limits of accuracy imposed by the microphotometer (see § 3.5), could be detected.

In the second experiment a contact positive of one of the solar plates was made, with light of $\lambda 5300$, on a Cramer Iso Process plate.

* F. E. Ross, *Physics of Developed Photographic Image*, chaps. iv., v., 1924.

† R. M. Motherwell, *Pub. Dom. Obs. Ottawa*, **8**, 121, 1925.

The intensity distribution in the contour of $\lambda 5172{\cdot}70$ was determined from this positive, as well as from the original negative, by the methods described in § 2. Since the three photographic limitations will affect the contact positive to an even greater extent than the original negative (since in the positive we are dealing effectively with an emission line), the difference between the intensity distribution for positive and negative will be a measure of the errors arising from these sources. The line contours from these two plates showed no differences as large as the accidental errors from plate to plate. Especially at the line centre, where the maximum effect was to be expected, no systematic difference was found.

From these experiments, and the work of Ross, it was concluded that the limitations of the photographic plate had produced systematic errors in the line contours determined in the present investigation, which were less than the accidental errors of the investigation. A generous estimate of the amount of systematic error so introduced would be $\pm$ 2 per cent.

3.5. *Averaging by Microphotometer.*—In the determination of plate transmission by the microphotometer, it is, of course, the transmission averaged over a width of 0·033 mm. (or a slightly greater width on account of infra-red light, § 2.2) which is registered by the thermocouple and galvanometer. If there is a sharp boundary between a transparent and relatively opaque region on the plate, as was the case for the artificial spectra discussed in § 3.4, various secondary effects, in addition to the averaging, distort the measured plate transmission; these arise in part from a diffractional widening of the image of the illuminated area on the thermocouple, and in part from light reflected from the lens surfaces on to the plate. For the solar spectra, where no such sharp boundaries occur, only the averaging effect is present, and its sole effect is slightly to distort the measured plate transmission in regions where the first derivative of the transmission changes within the width of the illuminated area on the plate. Actual correction for this averaging effect by Rayleigh's method * gave values of y/y_0 for the solar spectra, either exactly the same as those given directly by the microphotometer, or differing at most by less than one per cent. Microphotometer averaging, uncorrected for in the present investigation, will therefore lead to a systematic error of less than one per cent.

3.6. *Spectroscopic Resolving Power.*—The diffraction pattern at wave-length λ in the focal plane of a spectroscope with a slit of finite width is given by

$$S(x) = \frac{ab}{\pi}\int_{\alpha_1}^{\alpha_2}\frac{\sin^2\alpha}{\alpha^2}d\alpha \qquad . \quad . \quad . \quad (9)$$

where

$$\alpha_1 = \frac{\pi a}{f\lambda}(x - s/2) \quad \text{and} \quad \alpha_2 = \frac{\pi a}{f\lambda}(x + s/2).$$

In this expression a is the width of the effective rectangular aperture

* Lord Rayleigh, *Scientific Papers*, **1**, 135, 1871.

on the camera lens, b its height, f the focal length of camera, s the projected width of slit in the focal plane, and x is a co-ordinate measured in the focal plane from the centre of the projected slit image and in a direction parallel to run of spectrum. This equation cannot be integrated directly, but from quadratures by Schuster * and Ornstein and Minnaert † it is possible to find numerical values of $S(x)$. $S(x)$, of course, is accurately represented by (9), only provided the spectroscope is optically perfect; grating ghosts obviously, and lens aberrations, as Shenstone ‡ has pointed out, result in distortion and amplification of the theoretical pattern.

If, now, there is incident on the spectroscope slit radiation with a true intensity distribution $L(x)$, the intensity distribution $I(x)$ observed in the focal plane will be

$$I(x) = \int_{-\infty}^{\infty} L(\xi) \, . \, S(x - \xi) d\xi \Big/ \int_{-\infty}^{\infty} S(\xi) d\xi \quad . \qquad . \qquad (10)$$

an integral equation probably first given by Wadsworth.§ Ornstein and Minnaert ‖ have suggested that the integration of this equation may be effected, and the value of $L(x)$ found from $I(x)$, if these two functions and $S(x)$ be expanded in terms of Hermitean functions. In the present instance we are interested in discovering the difference between $I(x)$ and $L(x)$ for some assumed form of $L(x)$; if the assumed $L(x)$ is properly chosen, so that it leads to an $I(x)$ of somewhat the same shape as the solar contours of the *Mg b* lines, then the difference $I(x) - L(x)$ will give the error in the observed contours on account of the finite resolving power of the spectroscope. Accordingly we shall assume $L(x) = 1 - ae^{-x^2/2\mu^2}$ represent the numerical values of $S(x)$ by Hermitean functions, and then integrate (10) to find the corresponding value of $I(x)$.

Since $S(x)$ is an even function, it may be expressed as a sum of the Hermitean functions

$$S(x) = \frac{e^{-x^2/2\sigma^2}}{\sigma \sqrt[4]{\pi}} \left[c_0' H_0\left(\frac{x}{\sigma}\right) + \frac{c_2'}{\sqrt{2^2 \, . \, 2!}} H_2\left(\frac{x}{\sigma}\right) + \frac{c_4'}{\sqrt{2^4 \, . \, 4!}} H_4\left(\frac{x}{\sigma}\right) + \, . \, . \, . \right] \qquad (11)$$

where σ, the standard deviation of the function $S(x)$, is given by

$$\sigma^2 = \int_0^{\infty} x^2 S(x) dx \Big/ \int_0^{\infty} S(x) dx \quad . \qquad . \qquad . \qquad (12)$$

and where the Hermitean polynomials have the values

$$H_0(x) = 1; \qquad H_2(x) = 4x^2 - 2;$$
$$H_4(x) = 16x^4 - 48x^2 + 12; \quad H_6(x) = 64x^6 - 480x^4 + 720x^2 - 120,$$

---

* A. Schuster, *Astroph. Journ.*, **21**, 206, 1905.
† L. S. Ornstein and M. Minnaert, *Zeitschr. f. Phys.*, **43**, 404, 1927.
‡ A. G. Shenstone, *Physical Review*, **34**, 726, 1929.
§ F. L. O. Wadsworth, *Astroph. Journ.*, **3**, 321, 1896.
‖ L. S. Ornstein and M. Minnaert, *Zeitschr. f. Phys.*, **43**, 404, 1927.

etc. In order to find the value of the coefficient c_{2n}' we multiply both sides of (11) by

$$H_{2n}\left(\frac{x}{\sigma}\right)e^{-x^2/2\sigma^2}/\sqrt{2^{2n}(2n)!\sqrt{\pi}},$$

and integrate term by term from $-\infty$ to $+\infty$. By virtue of the orthogonal property of the Hermitean functions,* and the fact that these functions are normalized, it follows that

$$c_{2n}' = \int_{-\infty}^{\infty} S(x) \cdot \frac{H_{2n}\left(\frac{x}{\sigma}\right) \cdot e^{-x^2/2\sigma^2}}{\sqrt{2^{2n}(2n)!\sqrt{\pi}}} dx \quad . \quad . \quad (13)$$

Consequently by graphical integration of (12) and (13) we may rather quickly find the quantities σ and c_{2n}' in (11).

The integral equation (10) now goes into the form

$$I(x)\int_{-\infty}^{\infty} S(\xi)d\xi = \int_{-\infty}^{\infty}(1 - ae^{-\xi^2/2\mu^2})\Big[c_0 + c_2H_2\Big(\frac{x-\xi}{\sigma}\Big) + c_4H_4\Big(\frac{x-\xi}{\sigma}\Big) + \ldots\Big]e^{-(x-\xi)^2/2\sigma^2}d\xi$$

where $c_{2n} = c_{2n}'/\sigma\sqrt{2^{2n}(2n)!\sqrt{\pi}}$. Now substitute on the right-hand side of this equation the new variable $y = \dfrac{x-\xi}{\sigma}$ and we have

$$I(x) = 1 - \frac{ae^{-x^2/2\mu^2}\int_{-\infty}^{\infty}[c_0 + c_2H_2(y) + c_4H_4(y) + \ldots]e^{-py^2+2qy}dy}{\int_{-\infty}^{\infty}[c_0 + c_2H_2(\xi) + c_4H_4(\xi) + \ldots]e^{-\xi^2/2}d\xi}$$

where $p = \dfrac{\sigma^2+\mu^2}{2\mu^2}$; $q = \dfrac{\sigma x}{2\mu^2}$. Collecting powers of y in the numerator we find the following typical integrals which have to be evaluated

$$\int_{-\infty}^{\infty} y^{2n}e^{-py^2+2qy}dy = \frac{1}{2^{2n-1}p}\sqrt{\frac{\pi}{p}}\frac{d^{2n-1}}{dq^{2n-1}}qe^{q^2/p}$$

$$\int_{-\infty}^{\infty} e^{-py^2+2qy}dy = \sqrt{\frac{\pi}{p}}e^{q^2/p}.$$

These values are given by Bierens de Haans.† In the denominator the typical integrals are γ functions. Carrying out the indicated integrations, (10) finally takes the form, where we limit the series expansion of $S(x)$ to its first four terms,

$$I(x) = 1 - ae^{-x^2/2(\mu^2+\sigma^2)}\sqrt{\frac{\mu^2}{\mu^2+\sigma^2}}\left[\frac{\beta_0 + \beta_2x^2 + \beta_4x^4 + \beta_6x^6}{b_0 + b_2 + 3b_4 + 15b_6}\right] \quad (14)$$

---

* R. Courant and D. Hilbert, *Methoden der Mathematischen Physik*, p. 77, 1930; F. Zernike, *Handbuch der Physik*, **3**, 448, 1928.

† Bierens de Haans, *Nouvelles Tables d'Intégrales Définies, Leiden*, Tables 100 (8), and 28 (1), 1867.

where

$$b_0 = c_0 - 2c_2 + 12c_4 - 120c_6\,; \quad \beta_0 = b_0 + \frac{b_2}{2p} + \frac{3b_4}{4p^2} + \frac{15b_6}{8p^3}$$

$$b_2 = 4c_2 - 48c_4 + 720c_6\,; \quad \beta_2 = \left(b_2 + \frac{6b_4}{2p} + \frac{45b_6}{4p^2}\right)\left(\frac{\sigma}{\sigma^2+\mu^2}\right)^2$$

$$b_4 = 16c_4 - 480c_6\,; \quad \beta_4 = \left(b_4 + \frac{15b_6}{2p}\right)\left(\frac{\sigma}{\sigma^2+\mu^2}\right)^4$$

$$b_6 = 64c_6\,; \quad \beta_6 = b_6\left(\frac{\sigma}{\sigma^2+\mu^2}\right)^6.$$

(14) therefore gives the observed line shape I(x), as produced by a spectroscope with a pattern S(x), when the incident radiation has the intensity distribution $L(x) = 1 - ae^{-x^2/2\mu^2}$.

It is instructive to compare this result with that obtained by Carroll * in his discussion of a somewhat similar problem. In Carroll's treatment the spectroscope pattern S(x) is limited to the case of an ideal grating of alternate transparent and opaque bars, used with an infinitely narrow slit; in the present treatment there is no restriction on S(x), which indeed may be an observed quantity for the spectroscope, except that it be representable by an expansion in terms of Hermitean functions. The other advantage of the present treatment is, that the observed contour, I(x), can be found directly from (14), whereas in Carroll's discussion it is necessary to make a separate quadrature for each value of x. The present discussion should therefore have a much wider range of applicability than to the present investigation; indeed it makes it possible, in a relatively simple fashion, to discover what lines for a given spectroscope may safely be investigated for contour without distortion by finite resolving power.

3.61. *Application to the Ottawa Spectroscope.*—We are now in a position to use (14) to find the systematic error in the observed values of r on account of finite resolving power of the Ottawa spectroscope. The fine quality of the Anderson grating used in this investigation with its presumable freedom from ghosts, and the excellent definition by the spectroscope, justify the representation of S(x) by (9). The numerical values required are a = 127 mm., b = 39·4 mm., f = 6960 mm., and s = 0·036 mm. The pattern S(x), which results from the numerical integration of (9) for these special values, is shown in fig. 9 as a continuous line. Following the method indicated above, S(x) may now be represented by (11). After performing graphically the integrations called for in (12) and (13), we find the following numerical values—c_0 = 0·791, c_2 = −·0762, c_4 = ·00489, c_6 = −·0000669, and σ = 0·0236 mm. It will be noted that the series is converging very rapidly, and, cutting it short at the fourth term, we obtain the representation of S(x) shown by the filled circles in fig. 9; the representation of S(x) by (11) is indeed a little better than 1 per cent. on the average.

* J. A. Carroll, *Monthly Notices*, **88**, 154, 1927.

Using these values of c_{2n} we may now evaluate (14) for any desired values of μ. The results of calculation for $\mu = 0{\cdot}05$ mm. are given in the first half of Table V., and for $\mu = 0{\cdot}20$ mm. in the second half; the first column of each half contains the wave-length in angstroms, the second column the value of $L(x)$, the third the value of $I(x)$, and the last

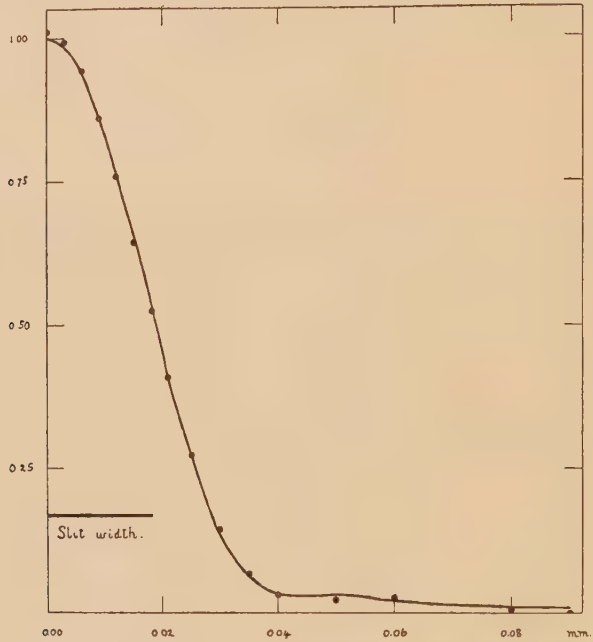

FIG. 9.—The intensity distribution, $S(x)$, in the focal plane of the Ottawa spectroscope for incident monochromatic light. Ordinates are intensities on an arbitrary scale, and abscissæ are distances in mm. on the focal plane. The half-width of the slit, projected on the focal plane, is shown by the horizontal line. The representation of $S(x)$ by the first four Hermitean functions is shown by the filled circles.

the difference, $I(x) - L(x)$, expressed as a percentage of $I(x)$. These results are shown graphically in fig. 10, where the left-hand curve refers to values in latter half of table, and the right-hand curve to first half of table. The theoretical $L(x)$ is represented by a line and the value of $I(x)$, as it would be observed by the Ottawa spectroscope, is shown by large filled circles. For purposes of comparison the actual shape of $\lambda 5183{\cdot}62$ is shown by small filled circles. Comparison of the figure and the table show that for a line ($\mu = 0{\cdot}20$ mm.), on the whole narrower than the observed *Mg b* lines, the error produced by the finite resolving power of the Ottawa spectroscope is at most 1·6 per cent. For narrower lines, however, such as $\mu = 0{\cdot}05$ mm., the error may be as much as 35 per cent. or greater. Contours of lines as narrow as this should not, of course, be determined with this instrument in this order. For the *Mg b* lines of the present investigation, however, the Ottawa spectroscope

TABLE V.

Values of L(x) *and* I(x).

λ.	L(x).	I(x).	I–L per cent.	λ.	L(x).	I(x).	I–L per cent.
·000	0·100	0·155	+35·4	·000	·180	·183	+1·6
·012	·118	·170	+30·6	·046	·197	·200	+1·5
·023	·170	·213	+20·2	·093	·243	·246	+1·2
·035	·248	·279	+11·1	·139	·316	·318	+0·6
·046	·346	·364	+ 4·9	·185	·404	·406	+0·5
·058	·444	·457	+ 2·8	·231	·502	·503	+0·2
·081	·662	·646	− 2·5	·289	·624	·624	±0·0
·104	·822	·798	− 3·0	·347	·732	·732	±0·0
·127	·920	·899	− 2·3	·405	·823	·821	−0·2
·150	·969	·956	− 1·4	·463	·889	·888	−0·1
·174	·990	·983	− 0·7	·578	·964	·963	−0·1
·197	·997	·994	− 0·3	·694	·991	·991	−0·0
·231	1·000	0·999	− 0·1	·810	·998	·998	−0·0

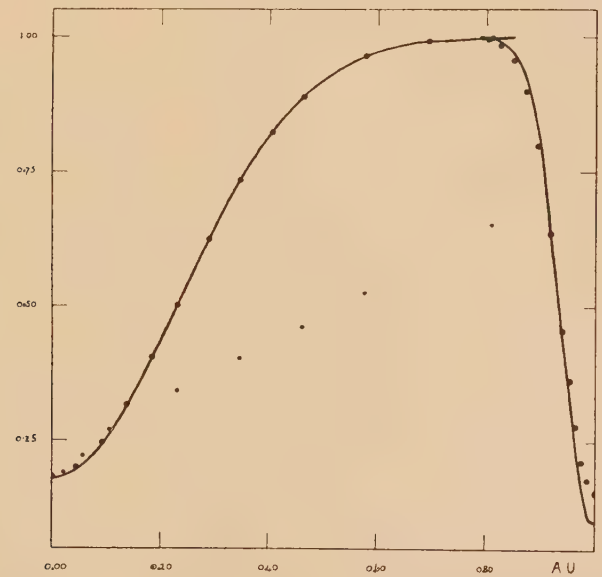

FIG. 10.—Continuous curves are $L(x)=1-0{\cdot}82e^{-x^2/0{\cdot}08}$ (left), and $1-0{\cdot}9e^{-x^2/{\cdot}005}$ (right). The large black dots show how the Ottawa spectroscope would reproduce such incident intensity distributions. For the left-hand curve, considerably narrower than the *Mg b* lines (the centre of $\lambda 5183{\cdot}62$ is shown by small black dots), the true and the observed intensity distributions differ by less than 2 per cent. Ordinates are intensity ratios, r, and abscissæ are wavelengths in A.

has sufficient resolving power, and the maximum systematic error arising from this source is not greater than 1·6 per cent.

3.7. *Total Error in Values of r.*—Summarizing the results of the discussion in this section we have :

$\cos\theta =$	0·238.	0·391.	1·00.	
Accidental error (§ 3.2)	±1·30	±2·95	±1·51	per cent.
Systematic error due to Wedge constant (§ 3.3)	±2·00	±2·04	±3·11	,,
Photographic limitations (§ 3.4)	±2	±2	±2	,,
Microphotometer (§ 3.5)	±1	±1	±1	,,
Resolving power (§ 3.6)	±1·6	±1·6	±1·6	,,

The square of the total percentage error in r will therefore be given by the sum of the squares of these errors. The resulting total errors for the three solar regions, expressed as a percentage of r, are thus :

$\cos\theta = 0{\cdot}238$ ± 3·64 per cent.
$\cos\theta = 0{\cdot}391$ ± 4·52 ,,
$\cos\theta = 1{\cdot}00$ ± 4·42 ,,

In the light of this discussion, therefore, it seems safe to assume that the total error in the values of r, given in Table IV., is less than ± 5 per cent., a satisfactorily small quantity in view of the difficulty of line contour determination.

3.8. *Other Observations.*—An interesting investigation of the contour of the *Mg b* line, λ5183·62, in the centre of the solar disc has recently been published by d'Azambuja.* Using the Meudon three-prism spectroscope of very high theoretical resolving power (over 100,000) with a linear dispersion at λ5184 of two angstroms per mm., d'Azambuja selected with a second slit strips 0·10 A. wide in the line, and with each such strip made a number of spectroheliograms of the central portion of the sun with different exposure times. The plates so obtained were measured with a photo-electric microphotometer, and the reduction to intensity followed from Schwarzschild's law using a value of $p = 0{\cdot}87$ determined from an auxiliary investigation. With such a procedure there is no question of distortion by photographic limitations (§ 3.4), microphotometer averaging (§ 3.5), nor finally by grating ghosts (§ 3.6). D'Azambuja's resulting intensity ratios r are shown in fig. 11 as filled circles, and for comparison the observed contour of the present investigation is shown as a continuous line. In view of the very different technique employed in the two investigations, each of which, therefore, will be characterized by a quite different set of systematic errors, the close agreement of the two results is very satisfactory and is good evidence of the accuracy of each.

Contours for the *Mg b* lines λλ5172·70, 5183·62 in the solar centre have also been recently published by Minnaert and Mulders.† Their results for the second of these lines are shown as open circles in fig. 11 ;

* L. d'Azambuja, *Annales de l'Observatoire de Paris*, **8**, 59, 65, 1930.
† M. Minnaert and G. F. W. Mulders, *Zeitschr. f. Astroph.*, **1**, 192, 1930.

it will immediately be noted that their values of r depart from the common results of d'Azambuja and the writer, by very much more than the limiting $\pm$ 5 per cent. total error assigned in § 3.7. It is only necessary to read the papers of Minnaert on line contours * to be convinced of the care with which his work has been performed. The

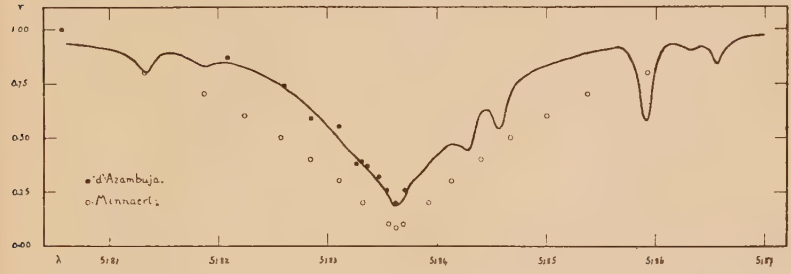

Fig. 11.—Values of r for *Mg b*, λ5183·62, at the centre of the solar disc. Continuous curve shows the mean values of r from the present investigation, the filled circles the results of d'Azambuja, and the open circles the results of Minnaert.

difference shown in fig. 11, as well as the similar differences for Minnaert's other two published contours (the K line and Hα) from the results of Schwarzschild,† Unsöld,‡ and von Klüber,§ are therefore presumably due to distortion by ghosts, which from published accounts ‖ are apparently conspicuous in the grating of the Heliophysical Institute. Fortunately, if this is the correct explanation of the above noted differences, Minnaert's valuable determination of total absorptions is unaffected.¶

* M. Minnaert, *Zeitschr. f. Phys.*, **45**, 610, 1927; M. Minnaert and B. van Assenbergh, *ibid.*, **53**, 248, 1929.

† K. Schwarzschild, *Sitz. d. Preuss. Akad.*, 1183, 1914.

‡ A. Unsöld, *Zeitschr. f. Phys.*, **46**, 765, 1928; *ibid.*, **59**, 353, 1930.

§ H. von Klüber, *ibid.*, **44**, 481, 1927.

‖ M. Minnaert, *ibid.*, **45**, 610, 1927.

¶ [Added in proof.] Since this paper was submitted to the Royal Astronomical Society, G. Righini in *Mem. d. Soc. Astronomica Italiana*, **5**, 283, 1931, has published contours for the *Mg b* lines $\lambda\lambda$5172·70, 5183·62 at the solar centre and across the disc. On fig. 11 his observations would fall (except at the line centre) about 10 per cent. below those of Minnaert and Mulders. It is difficult to tell from Righini's paper what photometric precautions he has adopted in securing his plates and in calibrating his step wedge. In the measurement of these plates, however, if I read the paper correctly, a serious error has been made. The photographic blackening across the line has been determined from tracings made with a Moll microphotometer, which from § 2.2 measures the plate transmission for infra-red light, whereas the characteristic curves have been determined by measuring the blackening of the step-wedge spectra with a Hartmann microphotometer, using visual light. Clearly a characteristic curve, which relates Hartmann blackening (plate transmission measured at, say, λ5600) with intensity incident on plate, will not serve to convert Moll blackening (plate transmission measured at, say, λ10,000) into intensity. If this has been Righini's procedure, his published contours are erroneous.

Section 4.—Comparison of Theory and Observation.

4.1. The observational investigation of the foregoing sections has yielded values of r, with a total error estimated at $\pm$ 5 per cent. for the *Mg b* lines at points on the solar disc where $\cos\theta$ = 0·238, 0·391, and 1·00. We therefore now have the material necessary to meet the purpose of the present investigation, namely, the selection of the idealized model which most accurately predicts the observed behaviour of these lines across the solar disc. Three models will be considered, one of pure absorption (Schwarzschild), one of pure scattering (Schuster), and one of combined absorption and scattering (Eddington).

4.2. *Pure Absorption.*—On this model atoms, which become excited by the absorption of radiation, are de-excited by collisions of the second kind. The radiation is therefore truly absorbed and converted into energy of thermal agitation. This is macroscopically equivalent to the transfer of radiation through an atmosphere stratified in plane parallel layers, each level of which is characterized by a mass coefficient of absorption k for the wave-length λ, an average mass coefficient of absorption $\bar{k}$ for the whole spectrum, and a density ρ. The equation of transfer is

$$\cos\theta\frac{dI(\tau,\theta)}{d\tau} = nI(\tau,\theta) - nB(\tau) \quad . \quad . \quad (15),$$

where $\tau = \int_0^x \bar{k}\rho dx$ is the optical depth, and $n = k/\bar{k}$. $I(\tau,\theta)$ is the specific intensity of radiation at the depth τ, in the wave-length interval λ to $\lambda + d\lambda$, making an angle θ with the outgoing normal (the negative direction of axis of x), and $B(\tau)$ is the specific intensity in the same wave-length interval, which would be emitted by a black body at the temperature of the depth τ. The temperature gradient in such an atmosphere, which in addition satisfies the condition of radiative equilibrium for total radiation, is given by $T^4 = T_0^4(1 + \frac{3}{2}\tau)$, and hence

$$B(\tau) = \frac{2hc^2}{\lambda^5}\left(e^{hc/R'\lambda T_0(1+\frac{3}{2}\tau)^{1/4}} - 1\right)^{-1} \quad . \quad . \quad (16)$$

As a first approximation we may expand $B(\tau)$ in a Taylor series, stopping at two terms, thus

$$B(\tau) = a + b\tau \quad . \quad . \quad . \quad . \quad (17)$$

Now integrating (15) subject to (17) we find

$$I(0,\theta) = \int_0^\infty B\left(\frac{y\cos\theta}{n}\right)e^{-y}dy = a + \frac{b}{n}\cos\theta \quad . \quad (18)$$

and in the adjacent continuous spectrum where n = 1

$$i(0,\theta) = a + b\cos\theta \quad . \quad . \quad . \quad (19)$$

This integration assumes that n is constant with optical depth, a physically reasonable assumption since both k and $\bar{k}$ depend upon pressure of free electrons, so that their ratio to a first approximation will be independent of pressure and therefore of depth. Finally from (18) and (19)

the ratio of intensity $r(\theta)$ in the line to that in the adjacent continuous spectrum, will be given for this model by

$$r(\theta) = \frac{a + \frac{b}{n}\cos\theta}{a + b\cos\theta} = \frac{1 + \frac{c}{n}\cos\theta}{1 + c\cos\theta} \quad . \quad . \quad (20)$$

where $c = b/a$.

Three consequences of this model may immediately be noted from (20). First, absorption lines disappear ($r = 1$) when $\cos\theta = 0$, that is at the limb; secondly, the minimum value of r is $1/(1 + c)$, no matter how large n may be, and, finally, $\frac{\partial r}{\partial c}$ is negative—that is, the lines increase in contrast (r becomes smaller) towards the violet end of the spectrum. In this model we see into the atmosphere to different depths depending upon the size of n; for very large values of n the radiation is said to be "saturated" and we see just to the boundary. It is therefore the boundary temperature which determines the maximum blackness of an absorption line.

We may now compare the observed behaviour of the *Mg b* lines with that predicted by (20). To make this comparison the values c and n must be found. The value of c may be found from the observed darkening towards the limb in the adjacent continuous spectrum, which by (19) is

$$\frac{i(0, \theta)}{i(0, 0)} = \frac{1 + c\cos\theta}{1 + c} \quad . \quad . \quad . \quad (21)$$

Abbot's values for the darkening, as quoted by Lindblad,* are satisfactorily fitted by (21) at $\lambda 5180$ and $\cos\theta = 0{\cdot}32$, when $c = 2{\cdot}02$. Knowing c, the value of n at any desired wave-length may be found from an application of (20) to an observed contour at a given value of $\cos\theta$, say $1{\cdot}00$. Thus without making any assumption as to the theoretical variation of n with wave-length, its value across the whole line may be found from one observed contour, on the assumption that the absorption model satisfactorily mimics actual solar conditions. We then test that assumption, and hence the validity of the model, by using the thus found values of c and n in (20) to predict the intensity ratio r at other points on the solar disc.

This comparison has been carried out for $\lambda 5183{\cdot}62$, the *Mg b* line which is most free from superposed foreign lines. Details of the comparison are given in Table VI., in which the first column contains the wave-length, thus (51)79·50, the second column the value of n computed as described above from the contour at $\cos\theta = 1{\cdot}00$, and the fourth and sixth columns contain the values of r computed from this value of n and (20) for $\cos\theta = 0{\cdot}391$ and $0{\cdot}238$ respectively. The errors attached to these computed values arise from the observational uncertainty of $\pm$ 5 per cent. in the contour at $\cos\theta = 1{\cdot}00$. If r_0 be the value of r at $\cos\theta = 1{\cdot}00$ and δr_0 this observational uncertainty, then the resulting

* B. Lindblad, *Nova Acta Reg. Soc. Sc. Upsala*, **6**, No. 1, 1923.

uncertainty in the value of r computed from (20) for any other value of $\cos\theta$ is given by differentiation of (20), that is by

$$\delta r = \frac{1+c}{\sec\theta + c}\delta r_0 \quad . \quad . \quad . \quad . \quad (22)$$

Finally, for comparison the observed values of r at these two positions on the disc are taken from Table IV. and inserted in the third and fifth columns of Table VI. These tabular values are shown graphically in fig. 12, where the continuous lines are the observed values of r for

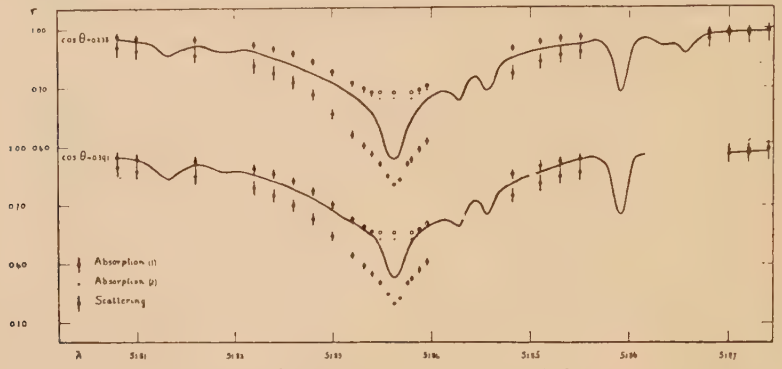

FIG. 12.—Comparison at $\cos\theta = 0{\cdot}238$ and $0{\cdot}391$ for *Mg b*, $\lambda 5183{\cdot}62$, of the values of r as observed (continuous lines), and as predicted by the model of pure absorption (open circles) and the model of pure scattering (filled circles). The predicted values have been computed from the contour at $\cos\theta = 1{\cdot}00$, and the uncertainty in the predicted values due to the ± 5 per cent. uncertainty in this contour is shown by the length of the vertical lines through the predicted circles.

$\cos\theta = 0{\cdot}238$ (upper figure in diagram) and $0{\cdot}391$, which have been taken from Table IV., and where the computed values of r for the absorption model are shown as open circles. The vertical lines through these open circles show the amount of the uncertainty in the computed value due to uncertainty in the contour at $\cos\theta = 1{\cdot}00$.

Attention may be drawn to two features of this comparison. In the line centre at $\lambda\lambda(51)83{\cdot}48$, $83{\cdot}62$, and $83{\cdot}80$ the observed values of r at $\cos\theta = 1{\cdot}00$ lead to negative values of n, which are physically meaningless. The best that can be done here is to assume $n = \infty$, and with this value (20) leads to values of r, at the other two positions on the solar disc, shown in brackets in Table VI. and as open circles *without* vertical lines in fig. 12. It will be observed that the fit is hopelessly bad at these places. In the wings, on the other hand, the line contour predicted by the model agrees moderately well with observation, though the difference between the two is slightly greater than the combined uncertainty, due to error in predicted value shown by length of vertical lines, and the $\pm$ 5 per cent. observational uncertainty in the observed contour. Further, from (22) we would have expected the fit to improve as the limb was approached, whereas, as fig. 12 shows, it gets definitely worse.

Table VI.

Values of r Computed on Absorption Model.

λ.	*n*.	cos θ=0·391.		cos θ=0·238.	
		Obs.	Comp.	Obs.	Comp.
79·50	1·04	..	·983±·032	·986	·988±·024
80·80	1·12	·944	·951 ·030	·951	·964 ·022
81·00	1·16	·937	·940 ·030	·940	·956 ·022
81·60	1·20	·913	·926 ·029	·913	·946 ·022
82·20	1·34	·858	·889 ·027	·881	·918 ·020
82·40	1·45	·822	·863 ·026	·847	·899 ·019
82·60	1·66	·785	·825 ·024	·817	·872 ·018
82·80	2·04	·735	·774 ·022	·775	·834 ·016
83·00	3·04	·674	·704 ·018	·728	·782 ·013
83·20	6·25	·614	·629 ·015	·661	·727 ·011
83·32	14·2	·574	·590 ·012	·619	·698 ·009
83·40	112	·541	·563 ·011	·573	·678 ·008
83·48	∞	·481	(·559)	·490	(·675)
83·62	∞	·333	(·559)	·339	(·675)
83·80	∞	·505	(·559)	·538	(·675)
83·88	24·0	·559	·577 ·012	·599	·689 ·009
83·96	9·17	·587	·607 ·014	·639	·710 ·010
84·82	1·46	·810	·860 ·026	·849	·897 ·019
85·10	1·29	·867	·902 ·028	·888	·928 ·021
85·30	1·21	·905	·923 ·029	·906	·943 ·022
85·50	1·17	·935	·936 ·030	·916	·953 ·022
86·80	1·06	..	·973 ·031	·965	·980 ·023
87·00	1·04	·966	·983 ·032	·977	·987 ·024
87·20	1·04	·968	·984 ·032	·981	·989 ·024
87·40	1·01	·976	·994 ·033	·987	·996 ·024

4.21. The use of (20) does not quite do full justice to the model of pure absorption, in so far as we have approximated to $B(\tau)$ by the first two terms of a Taylor expansion. In place of this expansion we may use (16), the exact value of $B(\tau)$; in this case (18) becomes

$$I(o, \theta) = KT_0^5\alpha^5\int_0^\infty \frac{e^{-y}}{e^{\alpha(1+py)^{-1/4}} - 1}dy = KT_0^5 f(\alpha, p) \quad . \quad (18'),$$

where $\alpha = \dfrac{hc}{R'\lambda T_0}$ and $p = \dfrac{3}{2}\dfrac{\cos\theta}{n}$. The integral in (18′) has been evaluated by quadratures by Lindblad * and by expansion in series

* B. Lindblad, *Uppsala Universitets Årsskrift*, **1**, 37, 1920.

by Milne;* values of $f(a, p)$ have been tabulated by the latter.† The resulting value of $r(\theta)$ is given by

$$r(\theta) = \frac{f\left(a, \frac{3}{2}\frac{\cos\theta}{n}\right)}{f\left(a, \frac{3}{2}\cos\theta\right)} \quad . \quad . \quad . \quad (20'),$$

and a may be found from the darkening towards the limb in the adjacent continuous spectrum by means of

$$\frac{i(0, \theta)}{i(0, 0)} = \frac{f(a, \frac{3}{2}\cos\theta)}{f(a, \frac{3}{2})} \quad . \quad . \quad . \quad (21')$$

A satisfactory fit with Abbot's values at $\lambda 5180$ is obtained for $a = 5{\cdot}69$. From Milne's tables a graph was then constructed on a large scale for $f(5{\cdot}69, p)$; from this graph and (20′), values of n were read off from the observed values of r at $\cos\theta = 1{\cdot}00$. Finally, using the same graph and the values of n thus obtained, the predicted values of r at $\cos\theta = 0{\cdot}391$ and $0{\cdot}238$ were found from (20′). These values, which there is no need to tabulate, are entered in fig. 12 as small open circles. Inspection of the figure shows that, while there is a slight improvement in fit in the line wings, the difference between prediction and observation in line centre is nearly as bad as before.

No further modification in the model of pure absorption appears possible. On account of the failure to predict the central line intensity we are therefore forced to reject this model, in spite of the moderately satisfactory fit in the line wings.

4.3. *Pure Scattering.*—Above a definite photospheric surface there extends, on this model, an atmosphere at low density, composed of atoms capable of existing in either one of two possible states. An atom, excited by the absorption of radiation, can, on account of the low density, only be de-excited by emission of the same frequency. Macroscopically we have a case formally equivalent to scattering, with a mass coefficient of scattering s at the wave-length λ. The equation of transfer in the wave-length interval λ to $\lambda + d\lambda$ becomes

$$\cos\theta\frac{dI(\sigma, \theta)}{d\sigma} = I(\sigma, \theta) - J(\sigma); \quad \cos\psi\frac{dI'(\sigma, \psi)}{d\sigma} = J(\sigma) - I'(\sigma, \psi) \quad (23)$$

where $\sigma = \int_0^x s\rho dx$ is the optical depth. $I(\sigma, \theta)$, $I'(\sigma, \psi)$ are the specific intensities of the out- and in-going streams of radiation, and $sJ(\sigma)$ is the specific intensity of the radiation scattered per unit of mass into the field of radiation. By definition, therefore,

$$2J(\sigma) = \int_0^{\pi/2} I(\sigma, \theta)\sin\theta d\theta + \int_0^{\pi/2} I'(\sigma, \psi)\sin\psi d\psi \quad . \quad (24)$$

This is the equation of monochromatic radiative equilibrium, and integrating (23) subject to (24) and the usual boundary condition we

* E. A. Milne, *Monthly Notices*, **81**, 375, 1921.

† E. A. Milne, *Philosophical Transactions*, A, **223**, 201, 1922.

find $J(\sigma) = \frac{1}{2}F(1 + \frac{3}{2}\sigma)$, where πF is the net flux of radiation per sq. cm. across a given plane and is constant throughout the atmosphere.

With this value of J we may now integrate (23) and obtain equations for $I(\sigma, \theta)$ and $I'(\sigma, \psi)$, in which we know everything but F. We may, however, express F in terms of the photospheric intensity $I(\sigma_1, \theta)$, where σ_1 is the total optical depth of the atmosphere above the photosphere, by using our just found values of $I(\sigma, \theta)$ and $I'(\sigma, \psi)$ to obtain an expression for the net flux πF at $\sigma = \sigma_1$. This leads to the following equation for F:

$$F(1 + \tfrac{3}{4}\sigma_1) + F\int_0^{\pi/2} (\tfrac{3}{2}\cos\psi - 1)e^{-\sigma_1 \sec\psi} \sin\psi \cos\psi d\psi = 2\int_0^{\pi/2} I(\sigma_1, \theta) \sin\theta \cos\theta d\theta \quad . \quad (25)$$

If now on the one hand we assume the optical depth σ_1 of the atmosphere to be very large, then from (25)

$$F = \frac{\int_0^{\pi/2} I(\sigma_1, \theta) \sin\theta \cos\theta d\theta}{1 + \frac{3}{4}\sigma_1} = I(\sigma_1, 0)\frac{1 + \frac{1}{3}u_1}{1 + \frac{3}{4}\sigma_1}.$$

On the extreme right-hand side of this equation we have substituted for $I(\sigma_1, \theta)$, the photospheric intensity, the quantity

$$I(\sigma_1, 0)(1 - u_1 + u_1 \cos\theta),$$

where u_1 is the so-called coefficient of darkening, in this case referring to the adjacent continuous spectrum at the wave-length λ. If now we substitute this value of F in the already known expression for $I(0, \theta)$ and divide this by $I(\sigma_1, \theta)$ we obtain our desired intensity ratio $r(\theta)$, namely,

$$r(\theta) = \frac{1}{2} \cdot \frac{1 - \frac{1}{3}u_1}{1 - u_1 + u_1 \cos\theta} \cdot \frac{1 + \frac{3}{2}\cos\theta}{1 + \frac{3}{4}\sigma_1} \quad . \quad . \quad (26),$$

which is the well-known Schuster equation. On the other hand we need restrict in no way the value of σ_1, in which case the solution of (25) for F leads to an expression involving integral logarithms, namely,

$$\frac{\int_0^{\pi/2} I(\sigma_1, \theta) \sin\theta \cos\theta d\theta}{1 + \phi(\sigma_1)} = I(\sigma_1, 0)\frac{1 - \frac{1}{3}u_1}{1 + \phi(\sigma_1)},$$

where

$$\phi(\sigma_1) = \frac{\sigma_1}{4}[3 + (1 + \sigma_1)e^{-\sigma_1} + (2\sigma_1 + \sigma_1^2)\mathrm{E}i(-\sigma_1)].$$

With this new value of F we reach, in the same way as above, a new value for $r(\theta)$, namely,

$$r(\theta) = \frac{1}{2}\frac{1 - \frac{1}{3}u_1}{1 - u_1 + u_1\cos\theta}\left[\frac{1 + \frac{3}{2}\cos\theta}{1 + \phi(\sigma_1)} + e^{-\sigma_1 \sec\theta}\left\{\frac{2(1 - u_1 + u_1\cos\theta)}{1 - \frac{1}{3}u_1} - \frac{1 + \frac{3}{2}\sigma_1 + \frac{3}{2}\cos\theta}{1 + \phi(\sigma_1)}\right\}\right] \quad (27).$$

(27) or its equivalent was first given by Unsöld,* though all the essential theory had previously been given by Milne.† It will be noted that (27) reduces to (26) for large values of σ_1, as it should.

From (27), or more simply from (26), we note the essential characteristics of absorption lines given by this model. In the first place, at $\cos\theta = 0{\cdot}00$, that is at the limb, the lines do not disappear; indeed since $\frac{\partial r}{\partial \theta} \propto \frac{(5u_1 - 3)\sin\theta}{(1 - u_1 + u_1\cos\theta)^2}$ we see that for increase of θ between 0 and $\pi/2$ the lines will actually grow stronger towards the limb if $u_1 < \frac{3}{5}$. In the second place, for a given value of θ and for sufficiently large values of σ_1 (the optical depth of the atmosphere), r can equal zero; consequently absorption lines of any desired strength are readily obtained on this model. Thirdly, for constant σ_1 and θ, r decreases with increase of u_1; but u_1, the coefficient of darkening, increases with decreasing wave-length, and hence on this model absorption lines show increasing blackness towards the violet end of the spectrum. Finally, it is to be noted that on this model there is no question of seeing to some definite depth in the atmosphere; in all cases, except where $r = 0$, we see down to the photospheric surface which underlies the scattering atmosphere.

The behaviour of absorption lines at various points on the solar disc, predicted on this model with the most complete generality by (27), may now be compared with observation. In order to simplify computation with (27), a table was drawn up giving values of $\phi(\sigma_1)$ as a function of σ_1, the value of the integral logarithm $Ei(-\sigma_1)$ being taken from Jahnke and Emde's tables; from this so prepared table a graph of $\phi(\sigma_1)$ was drawn on a large scale. From Abbot's values the coefficient u_1 has a value at the wave-length $\lambda 5180$ of 0·669. Then from this value, making use of the graph of $\phi(\sigma_1)$, values of σ_1 were computed from (27) and the observed value of r at $\cos\theta = 1{\cdot}00$. Once again it should be emphasized that this computation involves no theoretical knowledge of the variation of σ_1 with λ; (27) and the observed contour at $\cos\theta = 1{\cdot}00$ are all that are required. From these values of σ_1, values of r at $\cos\theta = 0{\cdot}238$ and 0·391 may then be computed from (27) and compared with observation.

The results are shown in Table VII., which is arranged in the same way as Table VI. The errors in the computed values of r (columns four and six), due to the $\pm$ 5 per cent. uncertainty in the observed contour at $\cos\theta = 1{\cdot}00$, were obtained with sufficient accuracy by differentiating (26), the Schuster approximation which yields

$$\frac{\delta r}{r} = \frac{\delta r_0}{r_0} \quad . \quad . \quad . \quad . \quad . \quad (28)$$

The computed values are shown in fig. 12 as filled circles, the amount of uncertainty, arising from the error in values of r at $\cos\theta = 1{\cdot}00$, being indicated by length of the vertical lines. Inspection of the figure, as well as the table, shows that the model of pure scattering fails

* A. Unsöld, *Zeitschr. f. Phys.*, **46**, 765, 1928.
† E. A. Milne, *Philosophical Transactions*, A, **223**, 201, 1922.

TABLE VII.

Values of r Computed on Scattering Model.

λ.	σ_1.	cos θ=0·391. Obs.	cos θ=0·391. Comp.	cos θ=0·238. Obs.	cos θ=0·238. Comp.
79·50	0·043	..	·964±·048	·986	·965±·048
80·80	·131	·944	·898 ·045	·951	·904 ·045
81·00	·160	·937	·879 ·044	·940	·888 ·044
81·60	·200	·913	·854 ·043	·913	·866 ·043
82·20	·314	·858	·793 ·040	·881	·813 ·041
82·40	·405	·822	·753 ·038	·847	·777 ·039
82·60	·547	·785	·700 ·035	·817	·729 ·036
82·80	0·776	·735	·631 ·032	·775	·662 ·033
83·00	1·18	·674	·540 ·027	·728	·565 ·028
83·20	1·77	·614	·443 ·022	·661	·461 ·023
83·32	2·22	·574	·389 ·019	·619	·403 ·020
83·40	2·62	·541	·350 ·018	·573	·363 ·018
83·48	3·26	·481	·302 ·015	·490	·313 ·016
83·56	4·38	·368	·243 ·012	·366	·251 ·013
83·62	5·68	·333	·198 ·010	·339	·204 ·010
83·68	4·84	·361	·225 ·011	·375	·232 ·012
83·76	3·24	·470	·303 ·015	·497	·314 ·016
83·80	2·94	·505	·324 ·016	·538	·336 ·017
83·88	2·40	·559	·372 ·019	·599	·385 ·019
83·96	2·01	·587	·412 ·021	·639	·428 ·021
84·82	0·411	·810	·749 ·037	·849	·774 ·039
85·10	·272	·867	·814 ·041	·888	·830 ·042
85·30	·210	·905	·848 ·042	·906	·860 ·043
85·50	·174	·935	·870 ·044	·916	·879 ·044
86·80	·072	..	·941 ·047	·965	·943 ·047
87·00	·045	·966	·963 ·048	·977	·963 ·048
87·20	·042	·968	·965 ·048	·981	·966 ·048
87·40	0·016	·976	·987 ·049	·987	·986 ·049

completely to predict the behaviour of the *Mg b* lines at the solar limb; indeed the O − C residuals are many times larger than the combined uncertainty due to the computed and observed contour. Here, also, just as in our discussion of the pure absorption model (§ 4.2), the use of (27) does not do full justice to the model of pure scattering, since it assumes that the darkening in the adjacent continuous spectrum can be represented by the simple cosine formula $1 - u_1 + u_1 \cos\theta$. However, we have already seen (§ 4.21) that the removal of this assumption, in the case of the model of pure absorption, has effected a negligible

improvement, and we may probably safely assume that the same result would be true for the present model. Since no further modification or improvement appears possible, we are forced to reject the model of pure scattering. Indeed, if it came to a choice between the model of pure absorption, with its complete failure to represent the line centre, and the model of pure scattering, used so frequently in astrophysical investigations in recent years, there can be little doubt that the model of pure absorption describes more satisfactorily the observed line behaviour across the solar disc.

4.4. *Combined Absorption and Scattering.*—In this model no definite photospheric surface is assumed, but the continuous radiation has its origin in all parts of the atmosphere. In this atmosphere are atoms capable of existing in either one of two states. An atom in the lower of the two states absorbs a quantum of radiation and is lifted to the upper state. De-excitation may take place from this state, either by a collision of the second kind (true absorption, since the absorbed radiation is immediately converted into thermal agitation of free electrons and atoms), or by a re-emission of the same frequency (formally equivalent to scattering). Regarded macroscopically, we have a mass coefficient of absorption k and a mass coefficient of scattering s at wave length λ in the line, and an average mass coefficient of absorption $\bar{k}$ outside the line in the adjacent continuous spectrum. Following Milne's * notation, the equation of transfer in the wave-length interval λ to $\lambda + d\lambda$, for an atmosphere stratified in plane parallel layers, takes the form

$$\cos\theta \frac{dI(x,\theta)}{\rho dx} = (k+s)I(x,\theta) - kB(x) - sJ(x) \quad . \quad (29)$$

In this equation $I(x, \theta)$ is the specific intensity at depth x making an angle θ with the outgoing normal, that is with the negative direction of x, $sJ(x)$ is the specific intensity of the radiation scattered into the beam, that is $J(x) = \int\int I(x,\theta)d\omega$, and $B(x)$ is the specific intensity of black-body radiation at a temperature appropriate to the depth x. (29) formally reduces to Eddington's † equation of transfer, if we substitute for our k Eddington's $k + \epsilon l$, and for our s Eddington's $(1 - \epsilon)l$. The condition of radiative equilibrium requires that the total radiation absorbed by a mass element be equal to the total temperature radiation emitted by the same mass element. This leads, as in § 4.2, to a temperature distribution $T^4 = T_0^4(1 + \frac{3}{2}\tau)$, where $\tau = \int_0^x \bar{k}\rho dx$, and, as in that subsection, we may express $B(\tau)$ by the first two terms of a Taylor expansion,

$$B(\tau) = a + b\tau \quad . \quad . \quad . \quad . \quad (30)$$

We have still, however, to find an expression for $J(\tau)$. If, following

* E. A. Milne, *Philosophical Transactions*, A, **228**, 421, 1929.
† A. S. Eddington, *Monthly Notices*, **89**, 620, 1929.

Eddington,* we integrate (29) over the sphere, after multiplication first by $d\omega$ and then by $\cos\theta d\omega$, and if we make the substitutions

$$n = \frac{k+s}{k}, \quad \xi^2 = \frac{k}{k+s} \quad . \quad . \quad . \quad (31),$$

where the quantities n and ξ are assumed to be constants throughout the depth of the atmosphere, we finally obtain the equation

$$\frac{1}{3}\frac{d^2(\mathrm{J}-\mathrm{B})}{d\tau^2} = n^2\xi^2(\mathrm{J}-\mathrm{B}) \quad . \quad . \quad . \quad (32)$$

The solution of (32), subject to the boundary conditions that at great depths τ, $\mathrm{J}(\tau)$, and $\mathrm{B}(\tau)$ are of the same order of magnitude, and that at $\tau = 0$ there is no ingoing radiation, leads to Milne's † equation (28), namely,

$$\mathrm{J}(\tau) = a + b\tau + \frac{\sqrt{3}}{2}\frac{\frac{2}{3}\frac{b}{n} - a}{\xi + \frac{\sqrt{3}}{2}} \cdot e^{-n\xi\tau\sqrt{3}} \quad . \quad . \quad (33)$$

We may now integrate the equation of transfer (29) to find an expression for $\mathrm{I}(0, \theta)$, substituting for $\mathrm{B}(\tau)$ and $\mathrm{J}(\tau)$ the values from (30) and (33). This value of $\mathrm{I}(0, \theta)$ will be the intensity emerging in the absorption line; the intensity $i(0, \theta)$ emerging in the adjacent continuous spectrum will be obtained by putting $n = 1$ and $\xi = 1$. The ratio of these two intensities gives the desired $r(\theta)$, namely,

$$r(\theta) = \frac{a + \frac{b}{n}\cos\theta + \frac{\sqrt{3}}{2}\frac{\frac{2}{3}\frac{b}{n} - a}{\xi + \frac{\sqrt{3}}{2}} \cdot \frac{1-\xi^2}{1+\xi\sqrt{3}\cos\theta}}{a + b\cos\theta} \quad . \quad (34)$$

The essential character of the absorption lines given by this model may be briefly noted. First, at the limb, where $\cos\theta = 0{\cdot}00$, the contrast of the lines with the adjacent continuous spectrum largely depends upon ξ. For example, if $\xi = 1$, (34) reduces to (20) and the lines disappear just as for the pure absorption model; for smaller values of ξ, and an appropriate choice of n, any desired degree of contrast may be obtained. Secondly, at any point on the disc, as small a value of r as desired may be obtained by choosing n sufficiently large and ξ sufficiently small. Finally, for a wide range of values of n and ξ, it may be shown that the lines increase in strength towards the violet. In short, at the very outset, it is seen that Eddington's model has very great flexibility, and therefore a very good chance of conforming to observation by an appropriate choice of n and ξ.

In order to make a comparison between the predictions of the

* A. S. Eddington, *Internal Constitution of the Stars*, p. 322, 1926.
† E. A. Milne, *Philosophical Transactions*, A, **228**, 421, 1929.

model and the observed behaviour of the absorption line, it is clear from (34) that $r(\theta)$ will have to be known from observation for two values of $\cos\theta$, in order to find the unknown values of n and ξ. As in the other two models no assumption is made as to the theoretical variation of n and ξ with wave-length, but these quantities are completely determined from observation at each wave-length. The test of the model then comes from using the so determined values of n and ξ to predict $r(\theta)$ at a third point on the disc.

I am greatly indebted to Professor E. A. Milne for pointing out to me that, if (34) is thrown into the form

$$r(\theta)=\frac{\xi(1+\frac{3}{2}\cos\theta)+\xi^2\frac{\sqrt{3}}{2}(1+2\cos\theta)+\frac{c}{n}\left[(1+\frac{3}{2}\cos\theta)\left(\frac{1}{\sqrt{3}}+\xi\cos\theta\right)-\xi^2\frac{1}{\sqrt{3}}(1-3\cos^2\theta)\right]}{(1+c\cos\theta)\left(\xi+\frac{\sqrt{3}}{2}\right)(1+\xi\sqrt{3}\cos\theta)} \qquad (3$$

$r(\theta)$ becomes a simple function of $1/n$, though a complicated function of ξ. Values of $r(\theta)$ at two points on the solar disc permit the determination of $1/n$ and ξ from (35), provided we know $c = b/a$. This is the same quantity c, which appeared in § 4.2, with the same value of 2·02. The method, due to Milne, of using (35) to compute $1/n$ and ξ, which from (31) have physically real values in the range zero to unity, will be made clear by reference to Tables VIII. In Table VIII*a*., which refers to $\cos\theta = 1{\cdot}00$, there appear in successive columns the wave-length, the observed r at that wave-length (from Table IV.), and the values of $1/n$, corresponding to the arbitrary values of $\xi = 0{\cdot}0$, $0{\cdot}2$, $0{\cdot}4$, $0{\cdot}6$, $0{\cdot}8$ and $1{\cdot}0$ respectively, computed by means of (35) from these ξ values and the observed r for $\cos\theta = 1{\cdot}00$, given in the second column. In Table VIII*b*., which refers to $\cos\theta = 0{\cdot}391$, there appear in successive columns the same wave-lengths, the observed values of r at these wave-lengths (from Table IV.), and in successive columns the values of r computed from (35), for $\xi = 0{\cdot}0$, $0{\cdot}2$, $0{\cdot}4$, $0{\cdot}6$, $0{\cdot}8$, and $1{\cdot}0$ respectively and the corresponding values of $1/n$ taken from Table VIII*a*. Now consider some definite wave-length, say (51)83·20. For this wave-length in Table VIII*b*. it will be noted that the computed r agrees with the observed r (in column two) for ξ between $0{\cdot}8$ and $1{\cdot}0$; graphical interpolation among the values in this table leads to $0{\cdot}928$ for ξ. Then, by graphical interpolation at this wave-length in Table VIII*a*., it is found that this particular value of ξ corresponds to $1/n = 0{\cdot}170$. Thus, by this process, the two simultaneous equations (35) for $\cos\theta = 1{\cdot}00$ and $0{\cdot}391$ are uniquely solved for $1/n$ and ξ. In successive columns of Table VIII*c*. appear the same wave-lengths, the corresponding values of ξ and $1/n$, found as just described, the computed values of r for $\cos\theta = 0{\cdot}391$, and finally in the last two columns are given for $\cos\theta = 0{\cdot}238$ the observed r (taken from Table IV.), and the value of r computed from (35) for the values of $1/n$ and ξ entered in the Table.

The value of r in the last column of Table VIII*c*. is subject to some uncertainty. This arises from the ± 5 per cent. uncertainty in the observed contours at $\cos\theta = 1{\cdot}00$ and $0{\cdot}391$, which are used with

TABLE VIII*a*.

$\cos\theta = 1{\cdot}00$.

λ.	Obs. r.	Values of $1/n$ for $\xi = 0{\cdot}0$.	$0{\cdot}2$.	$0{\cdot}4$.	$0{\cdot}6$.	$0{\cdot}8$.	$1{\cdot}0$.
79·50	·975	·875	·901	·922	·938	·951	·963
80·80	·926	·831	·848	·862	·873	·882	·889
81·00	·909	·815	·830	·841	·850	·858	·864
81·60	·888	·797	·807	·815	·822	·828	·833
82·20	·832	·746	·747	·747	·748	·748	·749
82·40	·792	·710	·704	·698	·694	·691	·689
82·60	·735	·659	·642	·629	·619	·610	·604
82·80	·658	·590	·559	·535	·516	·501	·489
83·00	·551	·494	·444	·405	·374	·349	·329
83·20	·438	·393	·322	·267	·224	·188	·160
83·32	·378	·339	·257	·194	·144	·103	·070
83·40	·337	·302	·213	·144	·089	·045	·009
83·48	·288	·258	·160	·084	·024	−·025	−·064
83·56	·229	·205	·097	·012	−·054	−·109	−·153
83·62	·186	·167	·050	−·040	−·112	−·170	−·217
83·68	·211	·189	·077	−·010	−·078	−·134	−·180
83·76	·289	·259	·162	·085	·025	−·023	−·063
83·80	·311	·279	·185	·112	·054	·008	−·030
83·88	·359	·322	·237	·171	·118	·076	·042
83·96	·404	·362	·286	·225	·178	·140	·109
84·82	·789	·708	·701	·695	·690	·687	·685
85·10	·851	·763	·767	·770	·773	·775	·777
85·30	·883	·792	·802	·809	·815	·821	·825
85·50	·902	·809	·822	·833	·841	·848	·853
86·80	·959	·860	·884	·902	·916	·929	·939
87·00	·974	·874	·900	·920	·936	·950	·961
87·20	·976	·875	·902	·923	·939	·953	·964
87·40	·992	·890	·919	·942	·960	·976	·988

(35) to compute this particular value of r. This uncertainty is evaluated as follows:—

at $\cos\theta = 1{\cdot}00$ we have $r_0 = F_0(\xi, n)$
$\cos\theta = 0{\cdot}391$ $r_1 = F_1(\xi, n)$
$\cos\theta = 0{\cdot}238$ $r_2 = F_2(\xi, n)$

Table VIIIb.

$\cos\theta = 0{\cdot}391$.

λ.	Obs. r.	Values of r for ξ=0·0.	0·2.	0·4.	0·6.	0·8.	1·0.
79·50	..	1·044	1·038	1·026	1·012	0·997	0·984
80·80	·944	0·992	0·987	0·979	0·970	·960	·951
81·00	·937	·973	·970	·963	·955	·948	·940
81·60	·913	·951	·948	·943	·937	·932	·926
82·20	·858	·890	·891	·890	·890	·889	·889
82·40	·822	·847	·849	·851	·855	·859	·863
82·60	·785	·786	·790	·797	·807	·816	·825
82·80	·735	·704	·710	·724	·740	·758	·774
83·00	·674	·590	·600	·622	·649	·677	·704
83·20	·614	·469	·483	·515	·552	·591	·629
83·32	·574	·405	·421	·458	·501	·546	·589
83·40	·541	·360	·379	·418	·466	·515	·563
83·48	·481	·308	·328	·372	·424	·477	·530
83·56	·368	·245	·268	·315	·374	·433	·491
83·62	·333	·199	·223	·275	·336	·400	·463
83·68	·361	·226	·249	·298	·358	·419	·479
83·76	·470	·309	·330	·372	·424	·478	·531
83·80	·505	·333	·352	·394	·443	·495	·545
83·88	·559	·384	·402	·440	·484	·531	·577
83·96	·587	·432	·449	·482	·523	·565	·607
84·82	·810	·845	·846	·849	·852	·857	·861
85·10	·867	·911	·910	·908	·906	·903	·901
85·30	·905	·945	·943	·938	·933	·928	·923
85·50	·935	·966	·962	·957	·950	·942	·935
86·80	..	1·026	1·022	1·011	·998	·985	·973
87·00	·966	1·043	1·037	1·025	1·011	·997	·983
87·20	·968	1·044	1·039	1·027	1·013	0·998	·984
87·40	·976	1·062	1·055	1·042	1·026	1·011	·995

and from the law of propagation of errors and these equations we have

$$\left.\begin{aligned}
\delta r_0^2 &= \left(\frac{\partial F_0}{\partial n}\right)^2 \delta n^2 + \left(\frac{\partial F_0}{\partial \xi}\right)^2 \delta \xi^2 \\
\delta r_1^2 &= \left(\frac{\partial F_1}{\partial n}\right)^2 \delta n^2 + \left(\frac{\partial F_1}{\partial \xi}\right)^2 \delta \xi^2 \\
\delta r_2^2 &= \left(\frac{\partial F_2}{\partial n}\right)^2 \delta n^2 + \left(\frac{\partial F_2}{\partial \xi}\right)^2 \delta \xi^2
\end{aligned}\right\} \quad . \quad . \quad . \quad (36)$$

TABLE VIIIc.

Values of r Computed on Model of Combined Absorption and Scattering.

λ.	ξ.	1/n.	cos θ=0·391 Comp. r.	cos θ=0·238. Obs. r.	cos θ=0·238. Comp. r.
79·50	(·000)	(·875)	(1·044)	·986	(1·081)
80·80	(·000)	(·831)	(·992)	·951	(1·026)
81·00	(·000)	(·815)	(·973)	·940	(1·006)
81·60	(·000)	(·797)	(·951)	·913	(·984)
82·20	(·000)	(·746)	(·890)	·881	(·921)
82·40	(·000)	(·710)	(·847)	·847	(·877)
82·60	·000	·659	..	·817	·814±·041
82·80	·542	·521	..	·775	·773 ·041
83·00	·780	·352	..	·728	·734 ·042
83·20	·928	·170	..	·661	·705 ·041
83·32	·926	·081	..	·619	·672 ·039
83·40	·905	·025	..	·573	·642 ·036
83·48	(·692)	(·000)	(·449)	·490	(·523)
83·56	(·431)	(·000)	(·324)	·366	(·364)
83·62	(·306)	(·000)	(·249)	·339	(·274)
83·68	(·376)	(·000)	(·290)	·375	(·325)
83·76	(·700)	(·000)	(·451)	·497	(·528)
83·80	·840	·000	..	·538	·600±·034
83·88	·918	·054	..	·599	·658 ·038
83·96	·911	·123	..	·639	·682 ·040
84·82	(·000)	(·708)	(·845)	·849	(·874)
85·10	(·000)	(·763)	(·911)	·888	(·942)
85·30	(·000)	(·792)	(·945)	·906	(·978)
85·50	(·000)	(·809)	(·966)	·916	(·999)
86·80	(·000)	(·860)	(1·026)	·965	(1·061)
87·00	(·000)	(·874)	(1·043)	·977	(1·079)
87·20	(·000)	(·875)	(1·044)	·981	(1·080)
87·40	(·000)	(·890)	(1·062)	·987	(1·099)

In these three equations the numerical values of the partial differential coefficients may be found after differentiating (35), for given corresponding pairs of values of $1/n$ and ξ. Inserting these values we may solve the first two equations of (36), in which δr_0 and δr_1 are known and arise from the ± 5 per cent. observational uncertainty, for δn^2 and $\delta \xi^2$. Entering the third equation of (36) with the now known values of δn^2 and $\delta \xi^2$, we find δr_2, the uncertainty in the computed value of r for $\cos \theta = 0{\cdot}238$. This uncertainty, which has its origin in the uncertainty in the observed contours at $\cos \theta = 1{\cdot}00$ and $0{\cdot}391$, is entered in the last column of Table VIIIc.

Reference to Table VIII*b*. shows that, for the line centre and line wings, it is impossible to solve the two equations with physically real values of $1/n$ and ξ, which from (31) must lie between zero and one. Thus in the line centre, at the wave-lengths (51)83·48 to (51)83·76 inclusive, the mathematical solution of the equations leads to negative values of $1/n$. For these five points in the line contour the smallest physically possible value of $1/n$ has been assumed, namely zero, and the corresponding value of ξ found by graphical interpolation in Table VIII*a*. In Table VIII*c*. these values appear in brackets, and from

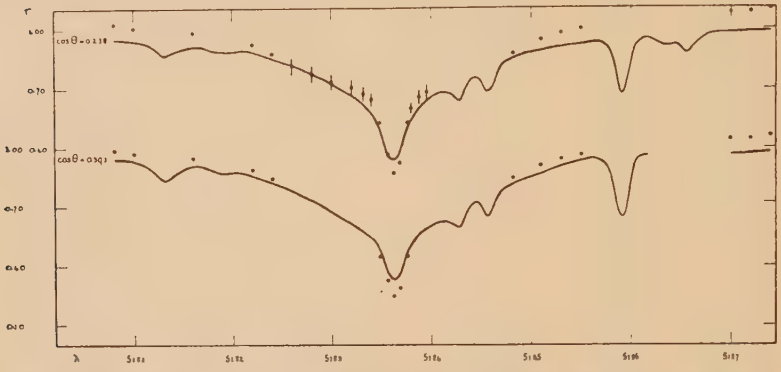

FIG. 13.—Comparison, principally at $\cos\theta = 0{\cdot}238$ for *Mg b*, $\lambda 5183{\cdot}62$, of the values of r as observed (continuous lines), and as predicted by the model of combined absorption and scattering (filled circles). The predicted values have been computed from the contours at $\cos\theta = 1{\cdot}00$ and $0{\cdot}391$, and the uncertainty in the predicted values, due to the $\pm$ 5 per cent. uncertainty in these observed contours, is shown by the lengths of the vertical lines through the predicted points.

these bracketed values have been computed r not only for $\cos\theta = 0{\cdot}238$ but also for $\cos\theta = 0{\cdot}391$. Similarly in the line wings, from $\lambda(51)82{\cdot}40$ to the red, and from $\lambda(51)84{\cdot}82$ to the violet, the mathematical solution of the equations requires (with the exception of $\lambda(51)82{\cdot}40$) values of ξ greater than unity. It will be noted, however, that in those portions of the line where the mathematical solution yields physically possible values of $1/n$ and ξ, the latter variable outside of the line core is steadily decreasing towards the line wing. Accordingly the value zero has been arbitrarily adopted for ξ, and the corresponding value of $1/n$ has been read out of Table VIII*a*. The thus found values of $1/n$ and ξ are also entered in Table VIII*c*. with brackets, and from these have been computed the values of r for $\cos\theta = 0{\cdot}238$ and $0{\cdot}391$ entered in the same table, also bracketed.

A graphical comparison of observation and theory is given in fig. 13. The observed contours (taken from Table IV.) at $\cos\theta = 0{\cdot}238$ and $0{\cdot}391$ are shown as continuous lines, and the computed values of r are shown as filled circles. Where these circles have vertical lines, the length of this line shows the uncertainty in the computed value, entered in last column of Table VIII*c*.; this uncertainty, it may be mentioned

again, is due to the observational uncertainty in the contours at $\cos\theta = 1{\cdot}00$ and $0{\cdot}391$, which are the basis of the computation. Where the circles have no vertical lines, this means that the mathematical solution of the equations has yielded a physically impossible value for either $1/n$ or ξ. Following the method described in the preceding paragraph, values of r have been computed at these points, but now the comparison of theory and observation must be made, not only at the contour for $\cos\theta = 0{\cdot}238$, but also at $0{\cdot}391$. For in these cases, on some independent grounds, a value of either $1/n$ or ξ has been assumed, and the remaining quantity calculated from the contour at $\cos\theta = 1{\cdot}00$ alone.

The fit on the whole is surprisingly good and, as comparison with fig. 12 shows, definitely superior to that obtained with either the model of pure absorption or that of pure scattering. What is the origin of the still outstanding discrepancy? On the basis of the discussion in § 4.21 we may reject the possibility that a representation of $B(\tau)$, more exact than (30), will improve the fit appreciably. There is, however, involved in the mathematical treatment, a more serious injustice to the model of combined absorption and scattering. For reasons of mathematical convenience in the derivation of (35), we have assumed ξ and n to be constant with optical depth, whereas in its most general form the model requires a variation of these quantities with electron pressure—that is, with optical depth. To use (35), therefore, with the observed contours to calculate ξ and n means that the values so calculated are averages through the depth of the solar atmosphere. To what effective depth do these average values of ξ and n refer?

4.41. *Average Optical Depth.*—The average depth from which the emergent radiation comes is given by

$$\tau_m = \int_0^\infty \tau d\{I(\tau, \theta)e^{-n\tau\sec\theta}\} \Big/ \int_0^\infty d\{I(\tau, \theta)e^{-n\tau\sec\theta}\} \quad . \quad (37)$$

Using the equation of transfer (29), and assuming as before ξ and n constant with τ, we find

$$d\{I(\tau, \theta)e^{-n\tau\sec\theta}\} = -\left[a + b\tau + \frac{\sqrt{3}}{2}\frac{\frac{2}{3}\frac{b}{n} - a}{\xi + \sqrt{3}/2}(1 - \xi^2)e^{-n\xi\tau\sqrt{3}}\right]e^{-n\tau\sec\theta}n\sec\theta d\tau.$$

Substituting this in (37) and integrating we finally obtain

$$\tau_m = \frac{\cos\theta}{n} \cdot \frac{1 + \frac{2c}{n}\cos\theta + X}{1 + \frac{c}{n}\cos\theta + X(1 + \xi\sqrt{3}\cos\theta)} \quad . \quad (38)$$

where

$$X = \frac{\sqrt{3}}{2}\frac{\frac{2}{3}\frac{c}{n} - 1}{\xi + \sqrt{3}/2} \cdot \frac{(1 - \xi^2)}{(1 + \xi\sqrt{3}\cos\theta)^2}.$$

We note from (38) that, to a first approximation, the optical depth τ_m, to which the average values of ξ and n refer, varies as $\frac{\cos\theta}{n}$. Hence when (35) is used to calculate ξ and n, the first of the two equations, that for $\cos\theta = 1{\cdot}00$, refers to an effective optical depth which is greater than that for the second of the equations, with $\cos\theta = 0{\cdot}391$. This discrepancy will become the more serious the larger the value of $1/n$—that is, the farther out in the line wing (see the third column of Table VIII*c*., where $1/n$ steadily increases from zero in line centre to unity in wing). It is therefore scarcely surprising that in the line wing physically possible values of ξ and n, which simultaneously satisfy the two equations, cannot be found, and even less surprising that the thus predicted r at $\cos\theta = 0{\cdot}238$ differs as much as it does from the observed r.

The value of τ_m, which corresponds to the observed values of ξ and n, may of course be exactly calculated from (38). Choosing a place in the line wing at $\lambda(51)80{\cdot}80$, where from Table VIII*c*. $\xi = (\cdot000)$ and $1/n = (\cdot831)$, and a place in the line core at $\lambda(51)83{\cdot}40$, where $\xi = {\cdot}905$ and $1/n = {\cdot}025$, we find from (38),

$\lambda 5180{\cdot}80$;	$\cos\theta = 1{\cdot}00$	$\tau_m = 1{\cdot}33$
	$\cos\theta = 0{\cdot}391$	$\tau_m = 0{\cdot}44$
$\lambda 5183{\cdot}40$;	$\cos\theta = 1{\cdot}00$	$\tau_m = 0{\cdot}027$
	$\cos\theta = 0{\cdot}391$	$\tau_m = 0{\cdot}010$.

From this exact treatment, in confirmation of the foregoing approximate discussion, we find in the line wing a large difference of optical depth between solar centre and limb, and in the line core almost no difference. The optical depth in the line wing varies so much between centre and $\cos\theta = 0{\cdot}391$, that the failure to find physically possible values of ξ and n from two equations, referring to such different depths of the solar atmosphere, is not surprising, nor is it surprising that the values of r at $\cos\theta = 0{\cdot}238$, computed from such values of ξ and n, agree so poorly with the observed contour in the line wing.

It will be recalled that also in the line centre physically possible values of ξ and n could not be found from the simultaneous solution of the two equations, though here a natural assumption gave a good fit with observation. The difficulty in the line core cannot, of course, arise from differences in optical depth, but it may, with some probability, be due to errors in the observed contours. Thus if values of ξ and n are computed from the contours at $\cos\theta = 1{\cdot}00$ and $0{\cdot}238$, the contours with the smallest accidental error, physically possible values are found for all wave-lengths near the line centre except $\lambda\lambda(51)83{\cdot}62$, $83{\cdot}68$; this is to be contrasted with the results near the line centre in Table VIII*c*., where the contour, $\cos\theta = 0{\cdot}391$, with a large accidental error, was used. When the values of $1/n$ are as small as they are near the line centre, slight uncertainties in the observed contours are sufficient to make $1/n$ "spill over" into negative values.

4.42. It is of some interest to test the Eddington model on other lines of the *Mg b* triplet. Unfortunately such a test can only be carried

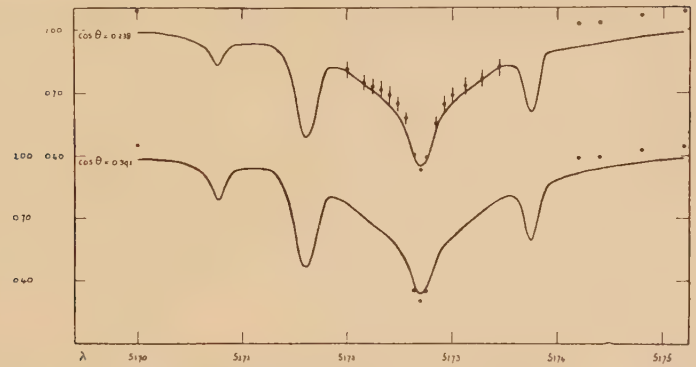

FIG. 14.—Comparison, principally at cos θ=0·238 for *Mg b*, λ5172·70, of the values of r as observed (continuous lines), and as predicted by the model of combined absorption and scattering (filled circles). Compare also fig. 13.

TABLE IX.

Values of r Computed on the Model of Combined Absorption and Scattering for λ5172·70.

λ.	ξ.	1/n.	cos θ = 0·391 Comp. r.	cos θ=0·238. Obs. r.	Comp. r.	
70·00	(·000)	(·882)	(1·053)	·984	(1·089)	
72·00	·470	·592	..	·802	·810	·041
72·16	·690	·430	..	·742	·751	·041
72·24	·805	·335	..	·714	·734	·042
72·32	·880	·248	..	·681	·719	·042
72·40	·890	·172	..	·640	·692	·041
72·48	·861	·093	..	·594	·649	·039
72·56	·770	·033	..	·518	·581	·035
72·64	(·494)	(·000)	(·359)	·393	(·405)	
72·70	(·390)	(·000)	(·301)	·356	(·335)	
72·76	(·480)	(·000)	(·353)	·381	(·396)	
72·84	·691	·065	..	·521	·557	·036
72·92	·820	·130	..	·603	·648	·040
73·00	·865	·190	..	·653	·691	·041
73·12	·845	·315	..	·704	·736	·042
73·28	·589	·501	..	·770	·770	·041
73·44	·000	·665	..	·820	·821	·041
74·20	(·000)	(·830)	(·991)	·914	(1·025)	
74·40	(·000)	(·836)	(·998)	·930	(1·032)	
74·80	(·000)	(·862)	(1·029)	·967	(1·064)	
75·20	(·000)	(·876)	(1·046)	·987	(1·082)	

out for λ5172·70, since λ5167·33 is badly distorted by the strong iron line at λ5167·51. The test for λ5172·70 was carried out in exactly the same way as for λ5183·62. There is no need to repeat the early part of the calculations, and in Table IX., which is arranged exactly similarly to Table VIIIc., there appear in successive columns the wave-length, the computed values of ξ and $1/n$, the value of r computed for $\cos\theta = 0{\cdot}391$, the observed value of r for $\cos\theta = 0{\cdot}238$ (from Table IV.), and the predicted value of r for this same solar position, together with its uncertainty computed from (36). The comparison is shown graphically in fig. 14, a figure arranged similarly to fig. 13. It will be noted that there is, on the whole, good agreement between observation and prediction.

4.5. The results of this section may now be briefly summarized. The observed behaviour of the *Mg b* lines, lines which meet the necessary theoretical requirements for such tests, has been compared with the limb behaviour predicted by the models of pure absorption, pure scattering, and combined absorption and scattering. The first two models failed to represent the observed behaviour, and this failure could not be attributed to any unfair treatment, mathematical or otherwise, of these models. The third model gave moderately satisfactory representation of observation, and the outstanding discrepancy in the line wings has been found to arise from a mathematical over-simplification in the treatment of the model. We therefore conclude that the *Mg b* lines are formed in the solar atmosphere in accordance with the Eddington model of combined absorption and scattering.

Section 5.—Consequences of the Investigation.

5.1. Before discussing the consequences of the investigation, it is useful to have an atomic picture of how such wide lines as these *Mg b* lines originate. A helpful way of looking at the problem is to regard the lower and upper energy levels, transitions between which produce a single line, not as infinitely sharp levels, but as continua. Consequently the absorption or emission line, which results from transitions between these levels, is not monochromatic but extends over a band of frequency or wave-length. Following Tolman and Badger,* in accordance with the original suggestions of Pauli, and Einstein and Ehrenfest, we shall assign transition coefficients b_{12}, a_{21}, b_{21}, which may vary continuously across the line, where the subscript 1 refers to the lower, and the subscript 2 to the upper of the two broadened states. Let $N_1(\nu)d\nu$ be the number of atoms in state 1, which may absorb radiation with frequency between ν and $\nu + d\nu$, and $N_2(\nu)d\nu$ be the number in the upper state, which may react with radiation in the same frequency interval; the total number of atoms in the lower and upper states will be represented by N_1 and N_2 respectively. If now the relations between these coefficients are

$$a_{21} = \frac{q_1}{q_2}\frac{8\pi h\nu^3}{c^3}b_{12}; \qquad q_1 b_{12} = q_2 b_{21} \quad . \quad . \quad (39)$$

* R. C. Tolman and R. M. Badger, *Physical Review*, **27**, 383, 1926.

we shall obtain Planck's law. The quantities q_1 and q_2 are the statistical weights of the two states. The ordinary Einstein coefficients may be regarded as average values of these new coefficients, defined in the following way:—

$$B_{12} = \frac{1}{N_1}\int_0^\infty b_{12}N_1(\nu)d\nu\,; \quad A_{21} = \frac{1}{N_2}\int_0^\infty a_{21}N_2(\nu)d\nu\,; \quad B_{21} = \frac{1}{N_2}\int_0^\infty b_{21}N_2(\nu)d\nu \qquad (40)$$

Bearing in mind this atomic picture with its consequent relations, we are now in a position to discuss the physical and astrophysical consequences of the fact that the Eddington model most satisfactorily represents the observed behaviour of the *Mg b* lines across the solar disc.

5.2. *Atomic Memory.*—The mathematical formulation of the model of combined absorption and scattering has depended upon an equation of transfer (29), in whose integration it has been assumed that there is a separate balancing in each frequency interval in the line between the energy scattered per unit mass into and out of the radiation field. In so far as the predictions of the model, calculated on this assumption, have been satisfactorily verified by observation, we conclude that this assumption is justified. The physical significance of this is that the atoms in the solar atmosphere act as if they had a memory, so that an atom, lifted to the upper state by the absorption of radiation of frequency ν, "remembers" the exact position of the lower state from which it came, and on de-excitation by emission returns exactly to that state. This result may be true for an individual atom, or merely statistically true for a collection of atoms. All that can be concluded from the present investigation is that atomic memory is at least statistically a justifiable conception.

5.3. *Atomic Life as a Function of Frequency.*—In so far as the Eddington model satisfactorily describes the observed behaviour of the *Mg b* lines, it follows that the absorption and scattering coefficients, calculated with its aid from these observed contours, have a physical significance. These coefficients are tabulated in Table X. for $\lambda 5183{\cdot}62$, and in Table XI. for $\lambda 5172{\cdot}70$. The first columns of these two tables contain the wave-length ($\Delta\lambda$) from the line centre, and the second and third contain the values of ξ and n respectively, taken from Table VIIIc. for $\lambda 5183{\cdot}62$ and from Table IX. for $\lambda 5172{\cdot}70$. The errors attached to these values of ξ and n have been computed from (36); these errors arise, of course, from the $\pm$ 5 per cent. uncertainty in the observed contours at $\cos\theta = 1{\cdot}00$ and $0{\cdot}391$, which observed contours are the basis of the whole calculation. The remaining three columns of the tables contain the values of $k/\bar{k}$, $s/\bar{k}$, s/k, which from (31) are given by—

$$\frac{k}{\bar{k}} = n\xi^2\,; \qquad \frac{s}{\bar{k}} = n(1-\xi^2)\,; \qquad \frac{s}{k} = \frac{1-\xi^2}{\xi^2} \qquad . \qquad (41)$$

Since these coefficients are averages over some range of optical depth in the solar atmosphere, and since, from the discussion in § 4.41, the effective optical depths at $\cos\theta = 1{\cdot}00$ and $\cos\theta = 0{\cdot}391$ differ the least for wave-lengths near the line centre, it follows that the

TABLE X.

Coefficients for the Line λ5183·62.

Δλ.	ξ.	n.	$k/\bar{k}$.	$s/\bar{k}$.	s/k.
−1·02	·000±·170	1·52± ·13	·000	1·52	∞
−0·82	·542 ·165	1·92 ·16	·564	1·36	2·40
−0·62	·780 ·144	2·84 ·29	1·73	1·11	·645
−0·42	·928 ·111	5·88 ·96	5·06	·818	·162
−0·30	·926 ·093	12·3 4·2	10·6	1·76	·167
−0·22	·905 ·078	40·0 32	32·8	7·24	·221
−0·14	(·692)	(∞)	(∞)	(∞)	(1·09)
−0·06	(·431)	(∞)	(∞)	(∞)	(4·38)
0·00	(·306)	(∞)	(∞)	(∞)	(9·64)
0·06	(·376)	(∞)	(∞)	(∞)	(6·09)
0·14	(·700)	(∞)	(∞)	(∞)	(1·04)
0·18	·840±·075	∞	∞	∞	·416
0·26	·918 ·086	18·5 ± 9·0	15·6	2·91	·186
0·34	·911 ·102	8·13 2·1	6·75	1·38	·205

TABLE XI.

Coefficients for the Line λ5172·70

Δλ.	ξ.	n.	$k/\bar{k}$.	$s/\bar{k}$.	s/k.
−0·70	·470±·170	1·69± ·13	·373	1·32	3·53
−0·54	·690 ·155	2·33 ·22	1·11	1·22	1·10
−0·46	·805 ·140	2·98 ·31	1·93	1·05	·543
−0·38	·880 ·128	4·03 ·51	3·12	·911	·292
−0·30	·890 ·110	5·81 1·0	4·60	1·21	·263
−0·22	·861 ·093	10·7 4·3	7·97	2·78	·349
−0·14	·770 ·075	30·0 30	18·0	12·3	·686
−0·06	(·494)	(∞)	(∞)	(∞)	(3·10)
0·00	(·390)	(∞)	(∞)	(∞)	(5·58)
0·06	(·480)	(∞)	(∞)	(∞)	(3·35)
0·14	·691±·075	15·4 ±30	7·34	8·04	1·10
0·22	·820 ·101	7·69 2·4	5·17	2·52	·488
0·30	·865 ·115	5·26 ·88	3·94	1·33	·337
0·42	·845 ·140	3·17 ·34	2·27	·908	·400
0·58	·589 ·163	2·00 ·16	·693	1·30	1·88
0·74	·000 ·170	1·50 ·13	·000	1·50	∞

coefficients, which are calculated from values of r at these two points on the sun by means of (35), will only have a physical meaning in the same central portions of the line. Outside of this central region, as Tables VIII*c*. and IX. show, the difference of effective optical depth

at $\cos\theta = 1{\cdot}00$ and at $\cos\theta = 0{\cdot}391$ is so great that it is impossible to solve the two equations (35) simultaneously with physically real values of the averaged coefficients. Consequently in Tables X. and XI. the coefficients are given only for line regions within one angstrom of the centre.

In order to interpret the remarkable variations of these macroscopic coefficients across the line, we must find their atomic significance. From the discussion in § 5.1, neglecting for simplicity stimulated emission, we find in the usual way, from a consideration of the absorption of radiation in a layer of gas of thickness dx and density ρ, that

$$k + s = \frac{h\nu}{c} b_{12} \frac{N_1(\nu)}{\rho} = \frac{h\nu}{c} b_{12} \frac{\epsilon_1(\nu)}{m},$$

where $\epsilon_1(\nu)$ is that fraction of the total mass of atoms per cubic cm. which can absorb radiation of frequency ν to $\nu + d\nu$, and m is the mass of an individual absorbing atom. Further, we may assume that $\bar{k}$, the average coefficient of absorption outside of the line, is proportional to the pressure P of free electrons. Hence we have

$$n = \frac{k+s}{\bar{k}} = \alpha \frac{b_{12}\epsilon_1(\nu)}{P} \quad . \quad . \quad . \quad (42),$$

where α is a constant. Considering next the quantity s/k, it is clear that s, the coefficient of scattering, varies directly as a_{21}, and inversely as the pressure of free electrons, P; similarly k, the coefficient of absorption, varies directly as the life time in the upper state, that is as $1/a_{21}$, and directly as the pressure of free electrons. Hence

$$\frac{s}{k} = \beta \frac{a_{21}}{P}; \qquad \xi^2 = \frac{k}{k+s} = \frac{1}{1 + \beta \frac{a_{21}}{P}} \quad . \quad . \quad (43),$$

where β is another constant. The remaining coefficients, $k/\bar{k}$, $s/\bar{k}$, more complicated functions of the atomic quantities, need not be explicitly given, since, by (41), they are implicitly contained in n and either ξ or s/k.

Let us first consider the variation of s/k, shown in Tables X. and XI., as a function of the distance ($\Delta\lambda$) from the line centre. We have already noted several times that the coefficients n, ξ, and hence, by (41), s/k are averages throughout the solar atmosphere, and refer to an effective optical depth τ_m, which, by (38), is greatest outside the line and steadily decreases towards the line centre. Decrease of optical depth is accompanied by decrease of electron pressure, and hence s/k, which by (43) varies as a_{21}/P, will on this account tend to increase towards the line centre. Actually s/k decreases from a maximum in the line wings ($\Delta\lambda \gtrless 0{\cdot}70$ A.) to a minimum at $\Delta\lambda = 0{\cdot}30$ A., and only from this point on increases towards the line centre. This observed variation of s/k can only mean that, in the wings of the line, a_{21} decreases more rapidly than the effective electron pressure, and that only at the very centre of the line does the decrease of electron pressure take the upper hand. Variation of the atomic quantity a_{21} means

variation of the life time of the atom in the excited state, and we conclude that the life time of the atom increases from a minimum in the line wings to a maximum towards the line centre.

From (42), n depends upon the product of the two factors b_{12}/P, which from (39) is proportional to a_{21}/P, and $\epsilon_1(\nu)$. The first of these factors, as we have just seen, has a minimum at $\Delta\lambda = 0{\cdot}30$ A. Since the observed variation of n shows no such minimum, we conclude that its steady and rapid increase towards the line centre is due to the dominance of the factor $\epsilon_1(\nu)$. This latter factor, the fraction of atoms per cubic cm. capable of absorbing radiation of frequency ν, must therefore increase more rapidly towards the line centre than a_{21}, and hence b_{12}, decreases.

The observed behaviour of the coefficients, shown in Tables X. and XI., is from this discussion to be attributed in part to increase of atomic life towards the line centre, and in part to an even more rapid increase in the same direction of the numbers of atoms capable of absorbing radiation of frequency ν. Independent confirmation of this increase of life time towards the line centre, already foreshadowed by Eddington,* is contained in an important investigation by Pannekoek.† In this paper Pannekoek has studied the theoretical contour of an absorption line in a stellar atmosphere in which the absorption and scattering coefficients vary with optical depth, and has come to the conclusion from his quadratures that, if the line be widened as a result of thermal agitation and damped oscillations, the contour will have zero central intensity. This result, contrary to the results of all observational investigations, including the present one, appears to have resulted from Pannekoek's explicit assumption that the electron pressure Q, "for which half of the energy of the excited atom is removed by collisions, half is radiated," is constant for a given line—that is, the atomic life time is constant across the line. If Q actually decreases towards the line centre, as the present investigation suggests, then reference to Pannekoek's Table II. shows that, for a given value of $k + s$, the ratio of intensity r in the line to that in the adjacent continuous spectrum, increases with decrease of Q. In other words, the theoretical line contour agrees with the observed contour in showing residual central intensity if (and from Pannekoek's careful discussion of other sources of central intensity, only if) the atomic life increases sufficiently rapidly towards the line centre. Indeed, it would be possible by an extension of the quadratures to use the observed contours to determine quantitatively the variation of life time across the line. It is to be hoped that this may be done, since the present investigation gives only a rough qualitative result. Thus from laboratory results we know that the life time, averaged across the whole line in accordance with (40),

$$A_{21} = \frac{I}{N_2}\int_0^\infty a_{21}N_2(\nu)d\nu$$

* A. S. Eddington, *Monthly Notices*, **89**, 620, 1929.
† A. Pannekoek, *ibid.*, **91**, 139, 1930.

is of the order of 10^{-8} sec. On account of the undue weight given the central part of the line by the rapid increase, indicated in our discussion, of the weighting factor $N_2(\nu)$, this life time will be practically that of the central portion of the line. Using this result, and the actual variation of s/k shown in Tables X. and XI., it follows that the life time in the wings cannot be greater than 10^{-10} sec., or at most 10^{-9} sec.

5.4. *The Interpretation of Spectroheliograms.*—The "flocculi" observed in the wings of lines, for example H_1 and K_1, have been interpreted in two different ways. On the one hand Evershed * regards them simply as faculæ, while Hale and his collaborators,† on the other hand, have adopted as a working hypothesis the view that they have their origin in low-lying vapour (of calcium in the case of H_1 and K_1). Important evidence on this difficulty of interpretation has recently been secured by d'Azambuja.‡ Placing the second slit of his spectroheliograph successively closer to the line centre, he has been able to show that the "flocculi" have two maxima of visibility, one when the second slit (in the case of *Mg b*, $\lambda 5183{\cdot}62$) is placed at a distance $\Delta\lambda = 0{\cdot}3$ A. from the line centre, and the other when the second slit is placed exactly in the centre. On Hale's working hypothesis, as the second slit is placed successively closer to the line centre, we are seeing the *Mg* atoms emitting the *b* lines at higher and higher levels in the solar atmosphere; on this view d'Azambuja's beautiful and well-established observation can only be accounted for if these *Mg* atoms are concentrated at two levels, separated by a region where there are practically no emitting *Mg* atoms. Such a picture of the solar atmosphere seems highly artificial, and in the light of d'Azambuja's work it seems preferable to adopt Evershed's hypothesis, that the "flocculi" in the line wing are actually faculæ.

The present investigation makes it clear why faculæ can be seen in the wings of a line, even at the solar centre. Faculæ clearly occur at small optical depth, with a surface brightness greater than that characteristic of the continuous radiation appropriate to that depth. It is for this reason that, in continuous or total radiation, they are seen only near the limb of the sun, in so far as radiation emerging at large angles with the outgoing normal comes effectively from a small optical depth. On the basis of the present investigation, an equally good method of reaching a small optical depth is to enter an absorption line, for, if the absorption line be formed on the Eddington model, then the effective optical depth τ_m varies, to a first approximation, as $\frac{\cos\theta}{n}$ (§ 4.41), and with increasing n towards the line centre, the level to which we see draws closer and closer to the boundary of the solar atmosphere. The maximum of visibility of the faculæ, found by d'Azambuja at a position $\Delta\lambda = 0{\cdot}30$ A., indicates the optical depth at which the faculæ occur, namely, from § 4.41 at $\tau = 0{\cdot}03$. As we pass further into the line centre, we move above the level at which the faculæ are localized,

* J. Evershed, *Observatory*, **27**, 164, 1904.
† G. E. Hale, *Astroph. Journ.*, **21**, 261, 1905.
‡ L. d'Azambuja, *Annales de l'Observatoire de Paris*, **8**, 69, 1930.

and enter finally at the line centre the region of flocculi, where, for some still unknown reason, the faculæ super-excite the various atoms to give emission lines. If this interpretation be correct, further observations by d'Azambuja's method, giving the position in the line of the maximum visibility of the faculæ, will yield much information as to the physical nature of these peculiar objects. Does the optical depth of a facula vary with its age, with the co-existence of spots, with latitude and in the sun-spot cycle ? We do not know, but by virtue of d'Azambuja's discovery we can now find out, and hence make a start at the physical investigation of faculæ.

5.5. *The Limb Spectrum.*—In a well-known paper, Hale and Adams * describe the spectrum of the solar limb as characterized by two features, —the tendency towards a sun-spot spectrum, and the disappearance of the wings of strong lines. Both these phenomena are explicable in the light of the present investigation. The explanation of the low excitation limb spectrum, in terms of the model of combined absorption and scattering, is due to Unsöld.† From (34) we have

$$r(\theta) = \frac{a + \frac{b}{n}\cos\theta + \frac{\sqrt{3}}{2}\,\frac{\frac{2}{3}\frac{b}{n} - a}{\xi + \sqrt{3}/2}\cdot\frac{1-\xi^2}{1+\xi\sqrt{3}\cos\theta}}{a + b\cos\theta} \quad . \qquad (34)$$

from which we see that the more nearly ξ approaches unity, the more nearly does the intensity ratio r approach that for the pure absorption model, namely, from (20)

$$r(\theta) = \frac{a + \frac{b}{n}\cos\theta}{a + b\cos\theta} \quad . \quad . \quad . \quad . \quad (20)$$

and hence the more nearly do the lines tend to disappear at the limb. Considering the line as a whole, in order to have ξ nearly unity, collisions of the second kind must be very numerous. As Unsöld points out, however, Born's theoretical investigation of collisions shows that the effective cross-section of an atom, for a successful inelastic or super-elastic impact, increases in the following order : (1) neutral atoms in their normal state, (2) neutral atoms in excited states, (3) ionized atoms in normal states, and (4) ionized atoms in excited states. In short the more highly excited the atom, the better is the chance of a collision of the second kind, hence the more nearly ξ approaches unity, and so finally the weaker the line appears at the limb. Accordingly the Eddington model, and Born's theory, inevitably require the observed phenomena of predominance of King's low temperature class lines at the limb.

Next consider the various parts of a single line. The discussion of § 5.3 shows that the life time in the excited state decreases as the line centre is approached. With increase of life time comes increased

* G. E. Hale and W. S. Adams, *Astroph. Journ.*, **25**, 300, 1907.
† A. Unsöld, *Sommerfeld Festschrift*, p. 95, 1929.

probability of a collision of the second kind, and we have, as we approach the line centre, two opposing factors at work. The increased chance of a collision of the second kind means that the absorption coefficient k increases, hence so also does ξ, but as the absorption coefficient increases, the optical depth to which we see decreases. In short, as we pass into the line, the increasing atomic life first makes collisions of the second kind more probable, but also this increases the opacity of the atmosphere, so that we only see to a depth where the electron pressure is such that collisions of the second kind reach a limiting value. We would therefore anticipate, that, as we entered the line, k would build up to its limiting value, and $\xi = \dfrac{k}{k+s}$ would decrease very slowly from its value unity in the adjacent continuous spectrum; these outer portions of the line, it follows from (34), would therefore tend to disappear at the limb. As we pass closer to the line centre the value of k still retains its limiting value, but ξ, on account of a steady increase of $k+s$ towards the centre, rapidly decreases; hence from (34) the line centre strengthens at the limb. In short, at the limb the lines should show a core, which, as figs. 6 and 7 indicate, is what they do. In fact it was the very existence of that core which enabled us to deduce the variation of atomic life across the line. The consequence of this appearance of the lines at the limb will be that ordinary direct photographs of limb spectra will show a strongly condensed central portion bounded by weak wings. This is exactly what the photographs of Hale and Adams show (see their plate xx. for example), and is the phenomena which they describe as the disappearance of the wings.

5.6. *Numbers of Atoms.*—The basic problem of stellar spectroscopy is the determination of the surface temperatures and pressures, or gravities, of the stars. Following the classical investigations of Saha and Fowler and Milne, it was generally hoped that the total absorption, or some other measurable parameter of an absorption line, could be used to deduce the number of atoms, in the lower of the two stationary states, per square cm. column of the stellar atmosphere, and that from the distribution of the numbers of atoms thus found among the various states of excitation and ionization, the temperature and pressure could be determined from an application of thermodynamical theory. The basis of this hope was an analogy with terrestrial absorption spectra and the beautiful experiments of Fuchtbauer * (rediscussed by Tolman) and Minkowski.† In Fuchtbauer's experiments, for example, in front of a definitely localized source of continuous spectrum was placed a tube containing a column of absorbing atoms. For an infinitesimal layer of thickness dx and density ρ, the relation between the absorption coefficient k, the transition coefficient b_{12} (see § 5.1), and the number of atoms $N_1(\nu)$ per cubic cm. is as usual given by

$$\rho k = \frac{h\nu}{c} b_{12} N_1(\nu) \quad . \quad . \quad . \quad . \quad (44)$$

* R. C. Tolman, *Physical Review*, **23**, 693, 1924.
† R. Minkowski, *Zeitschr. f. Phys.*, **36**, 839, 1926.

From the simple equation of transfer applicable to this experiment, namely, $dI = -k\rho I dx$, we find that r is given by

$$r = \frac{I}{I_0} = e^{-\int k\rho dx} = e^{-\frac{h\nu}{c}B_{12}N_1'(\nu)} \quad . \quad . \quad (45)$$

where $N_1'(\nu)$ is the number of atoms, in the whole length of the tube, capable of absorbing radiation of frequency ν. Hence, integrating over the whole line and using the first of (40), we obtain

$$\int_0^\infty \log_e r d\nu = -\frac{h\nu_0}{c}B_{12}N_1' \quad . \quad . \quad . \quad (46)$$

a simple relation between the total absorption of the line, the Einstein transition coefficient B_{12}, and the total number of atoms N_1' in the tube.

Though it was generally realized that this terrestrial analogy was misleading, it was hoped that the formation of absorption lines in stellar atmospheres could be adequately described by some simple model, such as that of pure absorption or pure scattering. In the latter event, for example, using the Schuster approximation (26) at an average point on the stellar disc where $\cos\theta = 2/3$, and the relation (44), we find the equivalent of our terrestrial (46), namely,

$$\int_0^\infty \left(\frac{I}{r} - 1\right) d\nu = \frac{3}{4}\frac{h\nu_0}{c}B_{12}N_1' \quad . \quad . \quad . \quad (47)$$

from which we can find the total number of atoms, N_1', per square cm. column.

The present investigation has shown conclusively, however, that these simple models do not adequately describe the formation of the *Mg b* lines, nor presumably the formation of any other solar or stellar lines. Consequently, if we wish to determine numbers of atoms from some measured parameter of an absorption line, we must use the Eddington model of combined absorption and scattering. Just as soon as we attempt to do so, however, there occur three difficulties, any one of which is, apparently, insuperable. The first and third of these have been fully discussed by Eddington,* and need only be mentioned here. These difficulties are—

(1) On the Eddington model the strength of an absorption line depends, not only upon the number of atoms in the lower state, but also upon the number in the upper state. In view of the fact that atoms can get into the upper state, for an ordinary spectrum line, in many other ways than by absorption of the line under investigation, the determination of the number of atoms in the lower state, from a measure of the absorption line, becomes indeterminate. It is true that, for this case, the equation of transfer becomes

$$\cos\theta\frac{dI}{\rho dx} = (k+s)I - akB - asJ \quad . \quad . \quad (48)$$

* A. S. Eddington, *Monthly Notices*, **89**, 620, 1929.

where a is the fraction of atoms in the upper state, unity for the case of the number in the upper state solely determined by the absorption line under investigation. If this equation can be integrated, and Eddington has already treated a simple form of it, it would be possible, by measuring contours at three points on the solar disc, to find a as well as k and s. From this it might be possible to find the distribution of atoms amongst the stationary states, by measuring a sufficient number of lines. Such a method is not, however, applicable to the stars, where the contour at effectively only one point on the disc can be found.

(2) On the Eddington model the strength of an absorption line depends upon the frequency of collisions of the second kind—that is, it depends upon our quantity ξ. If we differentiate (35) with respect to ξ, we obtain an expression of the form

$$\frac{\partial r}{\partial \xi} = \frac{\left(\alpha_1 - \frac{\alpha_2}{n}\right) + 2\xi\left(\beta_1 - \frac{\beta_2}{n}\right) + \xi^2\left(\gamma_1 - \frac{\gamma_2}{n}\right)}{a + \beta\xi + \gamma\xi^2} \quad . \quad (49)$$

where the quantities α, β, γ are all positive, and where those with the subscript 2 are larger than those with subscript 1. Consequently, weak lines (small value of n) become stronger with increase of ξ, that is with increase of collisions of the second kind, and similarly, strong lines become weak. Three consequences immediately follow. First, in a stellar atmosphere in which collisions of the second kind take place, the weak lines of a multiplet will be strengthened and the strong lines weakened (the Minnaert *–Woolley † effect). Secondly, in a stellar atmosphere, from Born's results, collisions of the second kind will be more numerous the greater the excitation potential of the upper level of the line, with the same two effects on weak and strong lines. This result seems to be obscurely related to the anomalous Boltzmann distribution of Adams and Russell. Finally, line strength will depend upon electron pressure in the atmosphere, and to find the numbers of atoms we will have to know the electron pressure, one of the very quantities whose magnitude we are trying to determine from the numbers of atoms in various stages of ionization.

(3) Finally, the strength of an absorption line depends upon the effective depth at which it occurs in the stellar atmosphere—that is, upon the variation of the microscopic co-efficients of absorption and scattering throughout the depth of the stellar atmosphere. In general, following the exhaustive treatment of Eddington,‡ we may say the greater the depth the weaker the line, and conversely.

From this brief discussion it is clear that, to find the numbers of atoms from some measured parameter of an absorption line, we shall have to know completely all the physical circumstances of the stellar

* M. Minnaert and G. F. W. Mulders, *Zeitschr. f. Astroph.*, **1**, 192, 1930; M. Minnaert, *Zeitschr. f. Phys.*, **45**, 610, 1927; M. Minnaert and B. van Assenbergh, *ibid.*, **53**, 248, 1929.

† R. V. d. R. Woolley, *Astroph. Journ.*, **72**, 256, 1930; **73**, 194, 1931.

‡ A. S. Eddington, *Monthly Notices*, **89**, 620, 1929.

atmosphere, not only the stellar temperature and pressure but the variation of these quantities and numbers of atoms with atmospheric depth. In short, we cannot hope to determine the number of atoms from an absorption line without an intimate knowledge of the very stellar physical conditions we hoped to ascertain when we had found the number of atoms.

Summary and Conclusion.

This investigation, undertaken to discover the model of absorption line formation which most accurately described the behaviour of the theoretically suitable *Mg b* lines across the solar disc, has been characterized by the following features:—

1. The contours of the *Mg b* lines have been determined from spectra made with the solar equipment of the Dominion Observatory, Ottawa. The wedge method of spectrophotometry has been used, and the transmission of the wedge, upon which the accuracy of the whole investigation depends, has been determined by an essentially new and accurate method.

2. The plates so obtained were measured with the Moll microphotometer of the Harvard College Observatory. Precautions necessary in the use of this apparatus are discussed, and the method of plate reduction indicated. The resulting mean values of r, the ratio of intensity in the line to that in the adjacent continuous spectrum, are summarized in Table IV., and graphically illustrated in figs. 5, 6, and 7 for points on the solar disc where $\cos\theta = 1{\cdot}00$, $0{\cdot}391$, and $0{\cdot}238$.

3. The accidental and systematic errors of the resulting contours are fully discussed. It is concluded that the values of r have a total error not greater than $\pm$ 5 per cent. In the course of this study of systematic errors a method has been developed, applicable to any spectroscope, for finding the distortion in line contour due to finite slit width and finite resolving power.

4. The observed variation of the contours of these lines, across the solar disc, has been compared with the predictions of the models of pure absorption, pure scattering, and combined absorption and scattering. This comparison has led to the rejection of the first two models. The third model, due to Eddington, satisfactorily represents the observations, and the still outstanding anomalies may be accounted for by simplifications introduced for mathematical convenience.

5. This verification of the Eddington model has had five consequences: (i) Atoms which absorb radiation off the line centre, reemit the radiation, statistically at least, in the same frequency; (ii) the life time of an atom in the excited state increases from the line wings in towards the line centre, with the result that collisions of the second kind also increase in the same direction; (iii) the spectroheliographic observation of faculæ in the wings of lines, up to the centre of the solar disc, is accounted for; (iv) the Eddington model and Born's collisional theory accounts in detail for the observed limb spectrum; (v) if absorption lines are formed in the way indicated in the body of the paper, it is impossible to determine the number of atoms from

the strength of an absorption line without knowing in detail the physical conditions of the stellar atmosphere.

In conclusion, the consequences of this study of line contours seem sufficiently significant to justify further work on this difficult observational problem. It is to be hoped that this basic problem of line formation, which can only be solved by solar studies, may be attacked with independent technique by other investigators. Indeed, in the present state of astrophysics, spectroscopic investigations of the sun seem likely to yield more information about stellar physics than spectroscopic studies of the stars themselves.

I wish to acknowledge again the generosity of Mr. R. M. Stewart and Dr. R. E. DeLury of the Dominion Observatory, Ottawa, in allowing me to use the magnificent solar equipment of that institution. I am greatly indebted to Prof. E. A. Milne for his helpful suggestions in the computational treatment of the model of combined absorption and scattering. Finally, to Dr. Harlow Shapley acknowledgment is due for his interest and encouragement during this protracted study.

Harvard College Observatory,
Cambridge, Massachusetts :
1931 *May* 10.

Faint Stars in the Selected Areas with Large Proper Motion. Revised List from the Radcliffe Observatory, Oxford. By H. Knox-Shaw and H. G. Scott Barrett.

Four lists containing the stars from 51 of the Selected Areas with proper motions as large as 0″·1 per annum have already been published, but the proper motions given therein were affected by a magnitude equation.* As it is now possible to eliminate this error, the corrected results from these 51 areas, together with those from 22 additional areas, are included in the present list. In these 73 areas, covering 54 square degrees, 21,070 stars have been measured down to a mean limiting magnitude of 15·3, and of these 101 have been found to have proper motions as large as 0″·096. In addition 14 stars outside the areas systematically measured have been included in the list. Except in the case of some of the very faint stars, the proper motions are the means of two independent values. The discordances between these two values provide a measure of the probable error, the mean value of which for the 73 areas is ± 0″·0048 in R.A. and ± 0″·0050 in Declination.

The table requires but little explanation. The star number is that in the Harvard-Groningen Durchmusterung of Selected Areas, from which the positions of the stars have been taken. The magnitudes are on the international scale, and the proper motions are relative to the mean of the comparison stars.

* *M.N.*, **87**, 439, 1927.

Selected Area No.	Area measured.	No. of Stars measured.	No. of Comparison Stars.	Mean Mag. of Comparison Stars.	Limiting Magnitude.	Star No.	Magnitude.	R.A. 1900·0.	Dec. 1900·0.	Annual Proper Motion. μ_α.	μ_δ.	μ.
	′ ′							h m s	° ′	″	″	″
1	50×50	239	89	14·0	16·2	196	12·6	6 36 6	+89 1·6	−0·047	−0·098	0·109
						130	15·6	6 50 0	+88 49·8	+ ·051	+ ·146	·155
2	40×40	227	76	13·3	15·3	—						
4	50×50	279	108	13·2	15·3	26	12·1	8 0 24	+74 28·0	− ·065	− ·264	·272
5	60×60	248	117	13·5	15·9	299	9·4	12 28 6	+75 2·6	− ·136	− ·044	·143
6	50×50	232	72	13·3	15·6	85	15·2	16 10 18	+74 35·0	− ·026	− ·174	·176
						181	12·0	16 17 0	+74 42·1	− ·144	+ ·063	·157
						369	12·9	16 19 0	+75 11·2	− ·150	+ ·078	·166
7	50×50	379	152	13·8	15·6	944	14·6	20 19 18	+75 34·8	− ·101	− ·250	·270
						598	13·7	20 22 18	+75 18·4	+ ·035	+ ·118	·123
						431	13·2	20 23 42	+75 6·4	+ ·100	+ ·170	·197
8	40×40	761	282	13·7	15·7	—	15·0	0 57 58	+60 32·9	+ ·105	+ ·003	·105
10	40×40	203	100	14·0	15·5	136	7·4	5 8 33	+60 4·3	+ ·041	− ·151	·156
						336	14·6	5 9 32	+60 23·6	− ·008	− ·113	·111
						342	15·2	5 9 44	+60 23·9	+ ·184	− ·462	·497
11	50×50	296	141	13·6	15·3	—	12·0	7 3 32	+59 26·2	+ ·095	− ·285	·300
						240	7·0	7 7 11	+59 48·9	− ·101	− ·229	·255
						643	15·0	7 10 12	+60 15·9	+ ·135	− ·087	·164
12	60×60	183	118	13·7	15·2	199	8·7	9 2 9	+59 33·5	− ·151	− ·006	·153
						216	10·9	9 4 16	+59 31·8	− ·078	− ·192	·200
						371	13·0	9 6 18	+60 6·2	− ·052	− ·152	·160
14	60×60	237	98	13·7	15·8	175	15·0	13 25 55	+59 22·9	+ ·066	− ·086	·108
15	60×60	174	80	13·2	15·0	555	11·6	15 17 29	+60 13·2	− ·156	− ·180	·238
						289	14·6	15 18 17	+59 44·2	− ·058	+ ·076	·096
						563	14·8	15 18 39	+60 15·2	− ·139	− ·339	·366
						152	15·0	15 19 48	+59 23·0	+ ·004	− ·115	·111
						161	12·1	15 20 28	+59 29·4	− ·038	− ·197	·200
16	50×50	227	120	13·5	15·3	—						
17	40×40	301	101	13·2	15·2	—						
18	40×40	568	234	13·9	15·8	171	11·7	21 24 27	+59 54·1	† ·094	+ ·058	·111
20	40×40	408	150	13·7	15·7	265	15·7	0 39 19	+45 29·4	+ ·119	− ·008	·111
26	40×40	383	174	14·1	15·8	—						
30	60×60	142	80	13·3	15·4	399	13·8	10 35 13	+45 33·4	− ·089	− ·115	·14
31	60×60	127	53	13·3	15·3	75	15·2	11 35 37	+44 24·1	− ·085	− ·052	·10
						253	8·0	11 39 1	+45 2·8	− ·175	+ ·031	·17

* Measured on one plate only.
† Star is outside the area given in the second column.

Selected Area No.	Area measured.	No. of Stars measured.	No. of Comparison Stars.	Mean Mag. of Comparison Stars.	Limiting Magnitude.	Star No.	Magnitude.	R.A. 1900·0.	Dec. 1900·0.	Annual Proper Motion. μ_α.	μ_δ.	μ.
	′ ′							h m s	° ′	″	″	″
33	60×60	157	58	13·5	15·6	138	14·8	13 47 33	+44 52·5	+0·069	−0·093	0·116
						267	9·8	13 50 7	+45 12·9	− ·144	+ ·056	·155
34	60×60	129	60	13·3	15·0	242	11·0	14 47 14	+44 51·1	+ ·030	− ·199	·201
35	60×60	204	88	13·7	15·3	291	15·3	15 51 5	+44 46·6	− ·108	+ ·057	·122*
						225	10·2	15 52 31	+44 31·5	− ·167	+ ·033	·170†
						474	13·0	15 52 38	+45 2·2	− ·071	− ·204	·216†
36	50×50	166	88	13·5	15·2	190	14·9	16 46 19	+45 12·0	− ·039	− ·090	·098
38	40×40	219	82	12·6	14·6	—	11·0	18 44 40	+45 33·9	− ·182	− ·042	·187†
39	40×40	761	254	13·8	15·3	999	12·7	19 47 48	+44 55·5	− ·081	− ·058	·100
40	40×40	386	122	12·8	15·1	548	9·7	20 45 2	+45 17·0	+ ·009	+ ·120	·120
41	40×40	485	174	13·3	15·0	384	10·0	21 49 36	+44 58·9	+ ·069	− ·089	·113
42	40×40	444	140	13·7	15·6	—						
43	40×40	214	83	12·9	14·7	—						
44	50×50	252	99	13·3	15·3	—						
45	50×50	295	93	13·5	15·7	349	8·6	1 24 13	+30 29·4	+ ·238	+ ·016	·239
						262	10·0	1 24 16	+30 17·3	+ ·110	− ·035	·115
						368	15·3	1 25 21	+30 28·0	+ ·222	− ·062	·230*
						207	9·8	1 26 9	+30 6·6	+ ·092	− ·030	·097
						309	12·2	1 26 33	+30 14·2	+ ·127	+ ·015	·128
46	50×50	263	81	13·2	15·6	—						
51	50×50	396	140	13·5	15·2	—						
54	60×60	148	54	13·4	15·3	125	13·4	10 24 28	+29 46·7	− ·079	− ·072	·107
						165	10·4	10 25 28	+29 57·6	− ·099	− ·067	·120
55	60×60	159	79	14·0	15·9	57	13·4	11 27 40	+29 39·2	− ·086	− ·043	·096
						303	15·2	11 29 46	+30 28·2	− ·100	− ·002	·100
						169	10·0	11 29 48	+29 58·7	+ ·123	− ·084	·149
						33	15·0	11 30 52	+29 24·0	+ ·285	− ·835	·882†
						318	12·4	11 31 51	+30 21·3	− ·142	− ·005	·142
56	60×60	142	68	13·7	15·5	27	14·7	11 57 16	+29 8·7	− ·796	− ·017	·796†
						210	12·4	11 57 42	+29 40·6	− ·131	− ·103	·167
						166	14·7	11 58 4	+29 34·5	− ·197	+ ·059	·206
						168	11·6	11 58 7	+29 34·2	− ·191	+ ·058	·200
						102	15·5	12 0 26	+29 17·4	− ·097	+ ·017	·098*
58	60×60	155	52	13·2	15·4	299	14·6	14 1 0	+29 56·1	+ ·047	− ·084	·096

* Measured on one plate only.
† Star is outside the area given in the second column.

Selected Area No.	Area measured.	No. of Stars measured.	No. of Comparison stars.	Mean Mag. of Comparison Stars.	Limiting Magnitude.	Star No.	Magnitude.	R.A. 1900·0.	Dec. 1900·0	Annual Proper Motion. μ_α.	μ_δ.	μ.
	′ ′							h m s	° ′	″	″	″
59	60×60	144	82	13·9	15·2	354	14·2	15 0 8	+29 52·4	+0·239	−0·173	0·295
						210	13·9	15 2 58	+29 35·8	− ·298	+ ·034	·300
60	60×60	149	83	13·3	14·8	275	12·6	15 56 32	+29 49·2	− ·169	− ·013	·169
						604	12·8	15 58 12	+30 21·9	+ ·063	− ·076	·099
61	50×50	201	106	13·4	15·4	—						
62	50×50	507	146	13·3	15·3	801	13·7	17 54 18	+30 8·0	+ ·127	− ·003	·127
						888	14·8	17 55 49	+30 1·4	− ·074	− ·143	·161
						221	7·2	17 56 48	+29 34·3	− ·161	+ ·177	·239
						226	14·0	17 56 55	+29 33·9	− ·144	+ ·178	·229
						1206	11·4	17 56 55	+30 19·2	− ·081	+ ·091	·122
63	40×40	374	180	13·1	14·7	—						
64	40×40	1166	354	13·4	15·5	—	6·6	19 59 31	+29 37·7	+ ·695	− ·536	·878
65	40×40	339	214	13·7	15·2	—						
66	50×50	358	174	13·1	14·9	348	12·6	21 57 42	+29 51·0	+ ·101	+ ·066	·12
67	50×50	311	167	13·7	15·4	—						
68	60×60	194	78	13·0	15·2	179	10·4	0 10 13	+15 15·0	+ ·105	+ ·038	·11
						384	10·8	0 10 54	+15 42·8	− ·008	− ·149	·14
						335	10·0	0 12 24	+15 33·2	− ·041	− ·099	·10
						398	7·2	0 12 38	+15 46·6	+ ·221	− ·020	·22
69	60×60	178	68	13·1	15·3	240	13·6	1 14 20	+15 26·4	+ ·093	− ·065	·11
						246	13·6	1 14 48	+15 28·1	+ ·183	− ·029	·18
						26	8·9	1 16 38	+14 39·2	+ ·255	+ ·016	·25
73	40×40	294	132	14·2	15·7	—						
74	40×40	407	172	13·7	15·5	—						
75	40×40	428	180	13·7	15·5	—	10·8	7 12 56	+15 12·0	+ ·092	− ·147	·17
82	60×60	104	48	13·2	14·8	375	14·5	14 15 57	+15 44·2	− ·088	+ ·066	·11
						259	9·8	14 16 36	+15 21·1	− ·083	+ ·074	·11
84	60×60	238	91	13·2	14·9	636	11·8	16 13 24	+15 28·2	− ·106	+ ·123	·16
87	40×40	308	95	13·4	15·3	—						
88	40×40	324	164	13·2	14·8	559	11·4	20 11 4	+15 3·3	+ ·006	− ·172	·17
89	50×50	417	153	13·5	15·4	50	11·4	21 6 59	+14 46·3	+ ·039	− ·100	·10
						—	11·6	21 10 17	+15 37·6	+ ·104	− ·140	·17
90	50×50	243	130	13·5	15·5	251	15·0	22 11 8	+15 3·5	+ ·153	− ·028	·15
						166	15·0	22 12 27	+14 51·7	+ ·203	− ·065	·21
						110	11·3	22 14 27	+14 49·1	+ ·154	− ·052	·16

* Star is outside the area given in the second column.

Selected Area No.	Area measured.	No. of Stars measured.	No. of Comparison stars.	Mean Mag. of Comparison Stars.	Limiting Magnitude.	Star No.	Magnitude.	R.A. 1900·0.	Dec. 1900·0.	Annual Proper Motion. μ_α.	μ_δ.	μ.
	′ ′							h m s	° ′	″	″	″
91	60×60	128	64	13·0	14·7	578	13·5	23 14 20	+14 51·7	+0·059	−0·132	0·145
92	60×60	134	60	13·2	15·3	409	11·9	0 50 6	+ 0 23·6	− ·236	− ·123	·266
96	50×50	236	110	13·2	15·0	871	13·5	4 46 51	+ 0 21·4	+ ·167	+ ·118	·204
98	40×40	1013	389	13·6	15·6	358	15·2	6 47 52	− 0 24·7	+ ·159	− ·021	·160
101	60×60	202	94	13·5	15·1	361	11·5	9 53 7	+ 0 6·7	− ·083	+ ·053	·098
						216	12·4	9 53 10	− 0 15·0	+ ·051	− ·095	·108
102	60×60	164	58	13·3	15·1	620	11·4	10 49 59	− 0 16·4	− ·228	+ ·007	·228
						679	10·9	10 51 50	− 0 18·8	+ ·071	− ·130	·148
						680	12·2	10 51 52	− 0 19·0	+ ·082	− ·131	·155
104	60×60	131	70	13·3	15·0	133	13·6	12 36 34	− 0 24·0	+ ·005	− ·124	·124
						460	14·0	12 37 56	+ 0 4·5	− ·101	+ ·031	·106
105	60×60	146	72	13·3	14·9	214	7·2	13 31 8	− 0 25·1	− ·192	− ·053	·199
106	60×60	159	61	13·6	14·9	432	13·9	14 37 37	− 0 17·2	− ·102	+ ·007	·102
						1124	12·0	14 38 9	+ 0 23·9	− ·098	− ·046	·108
107	60×60	178	66	13·3	15·0	580	12·8	15 33 22	+ 0 5·8	+ ·147	− ·201	·249
						595	8·0	15 33 55	+ 0 1·0	− ·194	− ·078	·209
110	50×50	79	49	12·5	14·3	122	12·6	18 35 46	− 0 13·5	− ·045	− ·088	·099
						409	11·8	18 36 29	+ 0 15·3	− ·060	− ·155	·166
						246	13·1	18 36 44	− 0 0·4	− ·071	− ·167	·181
111	40×40	242	80	13·4	15·2	—						
112	50×50	321	122	12·8	15·0	1805	11·4	20 37 59	+ 0 11·5	+ ·100	− ·042	·108
113	50×50	252	86	13·3	15·4	—						
114	60×60	259	98	13·7	15·4	151	11·5	22 36 27	− 0 10·6	+ ·013	− ·115	·116
						668	13·2	22 36 58	+ 0 37·3	+ ·096	+ ·020	·098
						669	14·9	22 36 59	+ 0 39·4	+ ·107	− ·141	·177
						272	8·8	22 37 50	− 0 7·1	+ ·143	− ·176	·227
115	60×60	153	66	13·0	15·0	331	11·6	23 37 0	+ 0 25·8	+ ·092	− ·098	·134
						496	13·2	23 37 17	+ 0 40·4	− ·052	− ·086	·100
						525	13·6	23 39 38	+ 0 40·9	+ ·101	− ·015	·102

Radcliffe Observatory, Oxford:
1931 *June* 1.

The Effect of Atmospheric Absorption in Stellar Spectrophotometry. By W. M. H. Greaves, M.A.

In *Monthly Notices*, **91**, 549, 1931, J. Dufay publishes a critical paper on this subject. He points out that the atmospheric absorption, expressed in magnitudes, is not a linear function of the reciprocal of the wave-length, and deduces that the method of treating it as a gradient is incorrect and vitiates the accuracy of the reductions.

The fact that the absorption does not vary linearly with $1/\lambda$ is, as M. Dufay says, well known. It is, however, easy to see that, provided the absorption is derived from measures at the same wave-lengths as those used for the gradients to which it is to be applied, no inaccuracy is introduced into the final results of colour-temperature observations by solving the absorption measures for a linear gradient. If, for example, a star is being compared with a terrestrial standard, the atmosphere introduces curvature into the comparison, and also into the measures taken to determine the absorption. When the gradient for star *minus* standard is corrected by the absorption gradient these curvatures cancel one another.

The curvature in question is thus immaterial if it is merely desired to derive colour-temperatures from measures at a selected series of wave-lengths. It becomes important if it be desired to investigate the closeness with which the energy distribution of the stars conforms to the black-body law. It then becomes necessary to evaluate for each wave-length the residuals from the derived gradient between star and standard source, and to correct them by the corresponding residuals (multiplied by the appropriate factor) of the absorption measures. This procedure is in effect that recommended by M. Dufay, with the exception that it is applied to the residuals of the least-squares solutions for linear gradient, and not to the original measures.

Royal Observatory, Greenwich:
1931 *June* 11.

Note on Dr. Kreiken's Paper: "On the Dwarf Nature of Spectroscopic Binaries." By W. J. Luyten.

In *Harvard Bulletin*, 870 (1929 October), I wrote a short criticism of Kreiken's paper: "On the Dwarf Nature of Spectroscopic Binaries" (*M.N.*, **89**, 589, 1929). Recently Kreiken has written a reply to these criticisms (*M.N.*, **90**, 760, 1930). It is evident from this reply that he has misunderstood my remarks, since he has interchanged our points of view, abandoning his, and taking over mine; he has then proceeded to accuse me of committing the very error I have pointed out to him. It will therefore be necessary to repeat some of my previous remarks, as well as some statements made by Kreiken. In what follows, his

original paper will be referred to as I., with page number, his reply as II., with page number.

In *H.B.*, 870, I wrote: "There seems to be a slight confusion at the outset. Kreiken states that in the evaluation of the mass of a spectroscopic binary from the quantity $m \sin^3 i$, the mean value of $\sin i$ is usually taken equal to 2/3 and hence that the mean value of $\sin^3 i$ is taken equal to 0·296. But since the mean of the cubes is not equal to the cube of the mean . . .," etc. Further on I wrote: "Moreover, it is not usual, in the writer's opinion, to take the mean value of $\sin i$ equal to 2/3. Usually it is assumed that the discovery chance . . .," etc.

In his first paper Kreiken himself wrote: "Usually the mean value of $\sin i$ is put equal to $2/3 = 0{\cdot}667$, and the masses of the stars are derived by multiplying the numerical values of $m_1 \sin^3 i$ and $m_2 \sin^3 i$ by $(1/0{\cdot}667)^3$." (I. p. 589.) Later, in the same paper he writes: "In the following I tried to fix the exact value of $\overline{\sin i}$. It appeared that the value of $\overline{\sin i}$ is much larger than the one used up till now." (I., p. 589.)

Clearly, my quotation of Kreiken's statement is fair and correct. His statement is erroneous, as it is distinctly *not* usual to take either $\overline{\sin i} = 0{\cdot}667$, or to put $\overline{\sin^3 i} = (\overline{\sin i})^3$; this may be verified anywhere in the literature (*cf.* Aitken's *Binary Stars*).

Later on in his reply Kreiken objects to my determining a mean value from his absolute magnitudes in Table VI. (paper I.). His absolute magnitudes were derived from the masses by means of Eddington's mass-luminosity curve. These masses, in turn, had been derived from the values of $m \sin^3 i$ by the application of a constant correction. This constant correction had been determined empirically, by comparing the relation between spectral class and $\log (m \sin^3 i)$ with that between spectral class and $\log m$ (fig. 1, and Tables II., III., IV., first paper). It is clear, therefore, that the constant correction takes care of any dispersion or any peculiar behaviour of $\sin^3 i$, and the logarithms of the masses thus determined should be observationally correct in the *mean*. Consequently, the absolute magnitudes derived from these masses should likewise be observationally correct in the mean, except in so far as the relationship between absolute magnitude and logarithm of mass is not linear. The error arising from this source is very small and may well be neglected.

Again, I think I may say that my taking a *mean* value of Kreiken's absolute magnitudes is an entirely legitimate procedure.

That Kreiken himself took this view in his first paper is evident from the fact that he used these absolute magnitudes, or rather the logarithmic distances derived from them, for a direct comparison with logarithmic distances derived from trigonometric parallaxes. Furthermore, Kreiken uses the small *mean* difference (0·062 in $\log r$ corresponding to 0·3 in the absolute magnitudes) between these two sets of logarithmic distances, to claim: "We thus obtain a second *proof* that the spectroscopic binaries are dwarfs" (I., p. 601, italics mine).

In his reply Kreiken suddenly claims that a systematic error resulting from the dispersion in sin i is affecting these absolute magnitudes, and determines this error at approximately $2^{m}\cdot5$ (compare with the *mean* difference of $0^{m}\cdot3$ above). In addition he writes: "The mean magnitude derived in such a way has only a complicated relation to the true mean, which cannot be determined from it unless the distribution of the frequencies of the actual values of sin i is known. It was for this reason that I did not give this mean in my paper."

Summary.

(*a*) My remarks concerning Kreiken's confusion between $\overline{\sin^3 i}$ and $(\overline{\sin i})^3$ were entirely correct.

(*b*) Kreiken's absolute magnitudes, since they are derived in an empirical way, should be free from systematic errors arising from source (*a*), and my use of them in taking the mean, etc., was entirely correct.

(*c*) After my pointing out (*a*), Kreiken discovers a systematic error, due to (*a*), in his absolute magnitudes, and objects to my using them to derive a straight-mean absolute magnitude for the A- and B-stars, and adds: "Dr. Luyten then proceeds to derive from my data the mean absolute magnitude, and it has evidently escaped his attention that he thus commits the error against which he thinks he is warning me." (II., p. 760.)

It is clear from the foregoing that Kreiken's view is incorrect on all counts.

As far as Kreiken's data go, it might be stated that in his first paper, in Table VI., No. 24 (I., p. 598), he uses for the star Boss 1457 (136 Tauri), $4^{m}\cdot5$, A0–A5, a trigonometric or group parallax of $1''\cdot0$, or a distance of *one parsec*. The only trigonometric parallax I have been able to find for this star is Allegheny, No. 676, viz. $0''\cdot016 \pm 0''\cdot006$ (relative).

Comparing the data for star 33 in Tables I. and VI. of his first paper we notice that he has calculated the distance of this star by using the *absolute* magnitude of the M-*companion* to Alpha Geminorum, and the *apparent* magnitude of the brighter *component* of Castor itself, and hence derives distances for this star of *four parsecs* and *one parsec*, by treating it as a "giant" (*sic*) and as a "dwarf" respectively.

In Kreiken's first paper (I., Table VI., p. 599) data are entered for the companion to Alpha Geminorum, in the columns labelled *giants*, as well as in columns labelled *dwarfs*. The same applies to Alpha Aurigæ. The numbers of these stars in these tables are Nos. 33 and 20 respectively.

Hence my remark in *H.B.*, 870: "It is not usual, however, to include Alpha Aurigæ among the dwarfs, or the companion to Alpha Geminorum among the giants," which remark, as must be quite clear, was entirely justified by the facts.

In his reply, however, Kreiken not only denies having included Alpha Aurigæ in his dwarf scheme, but, as far as the companion to Alpha Geminorum is concerned, attempts to reverse the situation by saying: "I do not think that it is quite usual to consider a star of

this absolute magnitude to be a giant *as is done by Luyten.*" (Italics mine.)

The aim of the present note is merely to point out the *facts* of the case, and not to enter into any further arguments on the subject, as it is abundantly evident from the foregoing that Kreiken has completely misunderstood not only my criticisms but his own papers as well.

Observations of Nova Persei (1901), 1930–1931.

By W. H. Steavenson.

Most of the estimates given below were made with the 20½-inch Hindle reflector. They are fewer in number than in previous years, partly owing to unfavourable weather, and partly because the telescope was not erected until early in 1930 November. The observations of 1930 November 22 and 23 were made with Mr. A. F. Bennett's 6-inch Cooke refractor at Leiston, Suffolk, while for that of 1931 January 24 the late Mr. J. Player's 6-inch Cooke refractor at Cheltenham was used.

The usual irregular variability of the nova was maintained during the period covered by the observations, the extreme range recorded being $1^{m}.8$.

Date.	Mag.	Date.	Mag.
1930 Nov. 15	13·28	1931 Feb. 12	13·37
22	13·57 B	13	13·67
23	13·37 B	19	13·28
25	13·47	21	13·08
Dec. 8	13·37	22	13·03
13	12·86	23	12·98
25	13·30	26	12·96
26	13·67	Mar. 8	13·13
27	13·72	14	12·64
29	13·18	15	12·79
30	13·03	17	12·79
1931 Jan. 24	13·97 P	21	12·17
Feb. 10	13·37	31	12·98
11	13·32	Apr. 5	13·67

Rapidly Moving Spots on Jupiter's North Temperate Belt.

By B. M. Peek. (Plate 14.)

The following discussion of the rapidly moving spots which appeared at the south edge of Jupiter's north temperate belt during the apparition of 1929–30 has been undertaken at the request of three other British

observers, Fellows of the Society, who together with the writer were engaged in making systematic observations of the planet at the time in question.

Before the work of reduction was commenced, a request was made in a letter to *The Observatory* that other observers would submit any records dealing with the phenomena under discussion, for incorporation with the data already to hand; as, however, no communications on the matter have been received, and as the spots required instruments of at least moderate dimensions for their visibility, it seems probable that very little in the way of observational material, obtained in the British Isles, can have been omitted.

The apparition of 1929–30 was only the third occasion on which such rapidly moving spots had been detected in this latitude of the planet. The first occasion was in 1880, when Mr. W. F. Denning derived for a number of minute dark spots, which he described as looking "like a train of sunspots," a rotation period slightly exceeding $9^h\ 48^m$.* The next recorded outbreak of similar dark spots was in 1891; these were dealt with by Professor E. E. Barnard in *M.N.*, **52**, 7, 1891, and by Professor G. W. Hough on p. 410 of the same volume. Professor Barnard found that these spots decreased their longitude by $9^\circ{\cdot}8$ daily when referred to the meridian of System II.; this gives a rotation period of $9^h\ 49^m{\cdot}1$. The phenomena of both 1880 and 1891 were observed by Mr. A. Stanley Williams (whose Jupiter records begin in 1877); his observations of 1880 are to be found in full in *English Mechanics* of 1880 and 1881, and there are notes by him in *The Observatory* of 1891.

The early detection of the 1929 spots was entirely due to the vigilance and experience of Mr. Stanley Williams, and testifies not only to the unimpaired acuity of his vision, but also to his quick appreciation of their significance. The following quotation from his note-book speaks for itself: "1929 Oct. 10–11. The appearance of the N.T.B. has so closely resembled (on a smaller scale) that presented during the great disturbance of 1891–2, that it seemed desirable to ascertain as soon as possible if the dark spots on the southern edge of the belt did not rotate at, very approximately, the same rate as that of System I., instead of that of System II. If the former, the spot 3 of Oct. 8–9 should have been in mid-transit at about $4^h\ 42^m$ on Oct. 11. The night was almost hopelessly cloudy, but the spot was seen distinctly several times during instants of partial clearance, and its transit time estimated at $4^h\ 36^m$. Rotation period $9^h\ 48^m{\cdot}8$ very approximate."

In general appearance the spots presented the form of dark projections from the south edge of the north temperate belt, interspersed here and there with white "bays." Plate 14 is a reproduction of a "strip-sketch" of the belt made by Phillips, using the 18-inch reflector, at Headley on 1929 November 14; it gives an excellent idea of the general character of the disturbance.

The observational records, which represent the work of Mr. F. J. Hargreaves, Rev. T. E. R. Phillips, Mr. A. Stanley Williams, and the

* *M.N.*, **41**, 44 and 358, 1880–81.

Fig. 1.- Portion of North Temperate Belt.
(Longitudes according to System I.)

writer, consist chiefly of the longitudes determined for the various spots as they crossed the central meridian. These longitudes, referred to System I., are shown plotted against the time in fig. 2, where about thirty spots seem well enough represented to allow of a determination of their rotation periods. By assigning weights to these in proportion to the length of time over which each spot was observed, a carefully determined mean rotation period of $9^h\ 49^m\ 16^s$ was derived; but as a few of the identifications may be based on somewhat scanty material, the publication of the details of this analysis hardly seems justifiable, particularly as Phillips, from a consideration of the movement of the group as a whole, found independently a mean rotation period of $9^h\ 49\frac{1}{4}^m$. At the suggestion of Williams a third value was obtained by considering only the twelve best-observed spots; this gave the period as $9^h\ 49^m\ 11^s$. It is evident therefore that $9^h\ 49\frac{1}{4}^m$ represents the mean rotation period of the group with a satisfactory degree of accuracy.

It is to be noted that System I. has been preferred for plotting the longitudes, since its zero meridian makes a complete revolution in $9^h\ 50^m\ 30^s$, whereas that of System II. rotates in $9^h\ 55^m\ 40^s$ approximately. Normally System I. is applicable only to the equatorial regions of the planet; all other latitudes, including those under discussion, move approximately at the rate of System II. The broken line in fig. 2 represents a rotation in accordance with System II., and consequently the approximate movement of the other surface details in the vicinity. It is remarkable, however, that spots and streaks at the north edge of the north temperate belt, immediately contiguous to the disturbed region, of which there were several normal examples in 1929–30, have a period longer than that of any other latitude of the planet—almost exactly $9^h\ 56^m$.

The two most rapidly rotating spots were those designated A and B on the plate, the former being a dark and the latter a white one closely following it; their rotation periods were $9^h\ 48^m\ 48^s$ and $9^h\ 48^m\ 52^s$ respectively. The dark spot C, however, appears to have rotated during part of its history—namely, in December 1929—in $9^h\ 48^m\ 40^s$.

Turning now to the group as a whole, an inspection of the plate shows immediately that the distribution of the spots in longitude was by no means fortuitous. With the exception of a very few spots, none of which appears to have been of a permanent character, the whole disturbance was confined to a region extending over about 240° of longitude, the remaining 120° being practically unaffected. The active region made a complete circuit of the planet, relative to System II., in about 38 days—Barnard found 37 days for the 1891 spots.

In 1880 Denning was able to observe the gradual extension of the group in longitude as it developed; he noted that on October 29 of that year the disturbed region passed the central meridian in less than an hour; on November 8 it took double that interval; and on November 23 its passage occupied $3^h\ 19^m$. No such lengthening of the disturbance is apparent in 1929, as the earlier observations, though somewhat scanty, show the same distribution in longitude; it is

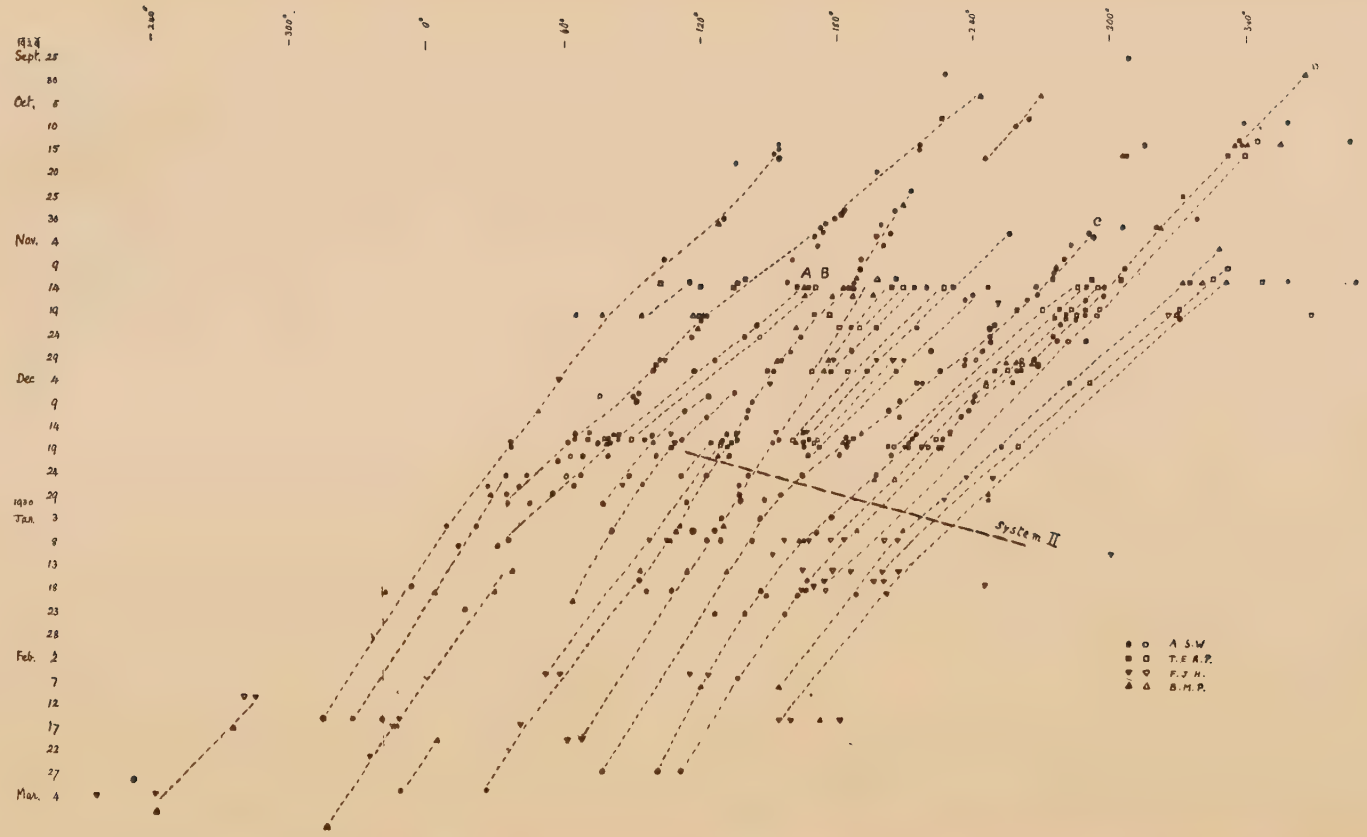

FIG. 2.—Rapidly moving North Temperate Spots, 1929.

possible, however, that the incipient stages were missed owing to the proximity of Jupiter to the sun.

It is evident that during the latter half of the apparition there was some slowing down of the rapid rotation throughout the disturbance. This seems first to have affected the spots near the preceding end of the group and to have spread later through its entire length ; but it does not seem possible to connect the points on the chart, where the change of motion for the various spots first became apparent, by a line that could have any physical meaning. It is to be regretted that during January and February 1930, after this slower motion had set in, a spell of very bad observing weather, coupled with the absence from his telescope of Rev. T. E. R. Phillips owing to ill-health, greatly reduced the number of observations, so that several of the identifications after the end of January may be regarded as not being conclusively established. The decline in the number of objects, however, is real, and the disturbance was by this time definitely on the wane, the spots being smaller and more difficult to observe. The converging of some of the lines on the chart suggests that occasionally two spots may have coalesced, thus bringing about the reduction observed in their number, but it is not known whether this actually occurred, or whether one or other of the spots simply faded out ; it can only be stated that the disturbance must have been at a maximum about the middle of December 1929.

As has already been remarked, the current to the north of this region was quite normal in 1929–30. Immediately to the south of it we have the north tropical current, whose rotation period is usually found to be about $9^h\ 55^m\ 30^s$. This current was well observed, and gave a period of approximately $9^h\ 55^m\ 29^s$; but certain well-defined spots in the same latitude provided clear evidence that, apparently superimposed upon the normal current, there was a secondary drift with the unusually long rotation period of about $9^h\ 55^m\ 46^s$. In view of the fact that this secondary current had a motion slower than the normal, it seems difficult to connect it in any way with the rapidly moving outburst to the north of it.

It remains to examine whether we may properly consider the outbreak of these spots and their extremely rapid rotation to be abnormalities, or whether there is anything in the nature of a more or less regular surface current of short rotation period in this particular latitude of the planet, which may be observed whenever the visible features are sufficiently well defined for correct identification of the details to be made from night to night—a somewhat rare occurrence for the south edge of the north temperate belt.

In a paper published in *M.N.*, **59**, 76, 1898, Denning suggested a possible periodicity in the outbreaks of these objects, but Phillips, in a letter to *The Observatory* of 1929 December, points out that during the long interval between 1891 -2 and 1929 a recurrence of the disturbance could scarcely have passed unnoticed.

Two or three examples in recent years are undoubtedly of importance. The 1929–30 disturbance can hardly be said to have lasted

into the 1930–31 apparition, as irregularities at the south edge of the north temperate belt were then rare and extremely difficult to observe; but in one or two instances, where the recognition of a feature after a short lapse of time was possible, the rapid rotation was still indicated. In 1928 there was a definite thickening of the belt in one region, the preceding end of which was fairly well defined; from a combination of visual observations with measurements of photographs obtained at the Lowell Observatory, Phillips has derived for this a rotation period of $9^h\ 53^m\ 10^s$, a rate intermediate between that of 1929 and the normal for System II. This might be considered to represent the stage then reached by a current that was in process of acceleration towards a maximum in 1929–30, but a further investigation by Phillips has revealed the fact that in 1926 there was a dark projection from the south edge of the belt rotating in $9^h\ 49^m\ 3^s$.* Hence it appears possible that more of these objects might have been recorded in the past had their significance and importance been fully appreciated; they should not escape detection in the future, but until more is known about the behaviour of such isolated objects as may from time to time appear, it will be impossible to decide whether or not the rapid drift that has been observed in this latitude may be regarded as one of the planet's permanent surface currents.

Summary.

1. A discussion is undertaken of the outbreak in 1929 of rapidly moving spots at the south edge of Jupiter's north temperate belt, similar to those which appeared in 1880 and 1891.

2. The observed longitudes of the individual spots are plotted against the time, and a mean rotation period for the disturbance, closely approximating to $9^h\ 49\frac{1}{4}^m$, is derived.

3. The disturbance was at a maximum about the middle of December 1929.

4. In the early part of 1930 there was a noticeable decrease in the rapid rate of rotation exhibited by the spots. These became fewer in number and more difficult to observe.

5. The disturbed region extended over about 240° of longitude, the remaining 120° being comparatively quiet. The above distribution was maintained, in spite of the large difference in rotation periods between this and the neighbouring zones. If a gradual increase in total longitude covered by the disturbance took place in the early stages of its development, as in 1880, this must have occurred while the planet was too near the sun for observation.

6. The disturbance cannot be said to have lasted into the 1930–31 apparition, but one or two isolated markings in the same latitude indicated that the rapidly rotating current still persisted.

7. The normal rate of drift of the surface markings in the latitudes immediately contiguous to that of the disturbance was apparently unaffected.

8. It is possible that a narrow zone in this latitude of the planet may

* *B.A.A. Memoirs*, **29**, pt. iii., 1930, "Jupiter."

have a permanent surface current whose rotation period is in the neighbourhood of $9^h\ 49^m$. Previous observations do not negative this assumption, but the positive evidence is too meagre to be considered as definitely favouring it. Should there be such a current, careful observation during the next few apparitions should serve to place its existence beyond doubt, provided that this region does not remain entirely devoid of observable detail.

Photographies de la planète Mercure. Par F. Quénisset.

(*Communicated by Dr. A. C. D. Crommelin.*)

On sait que la photographie de l'aspect physique de Mercure est extrêmement difficile, surtout sous nos latitudes, car cette planète est toujours plus ou moins plongée dans le rayonnement solaire et, même aux moments de ses plus grandes élongations (de 18° à 28° du Soleil, suivant les cas), elle reste encore très basse sur l'horizon. Ses images

Dessin de Mercure exécuté d'après une série de six photographies obtenues le 11 Avril 1931 de $18^h\ 57^m$ à $19^h\ 8^m$.

sont donc presque toujours violemment agitées par les vagues atmosphériques, particulièrement si fortes dans les couches inférieures de l'air. L'idéal serait d'obtenir des photographies en plein jour vers son passage au méridien. Je vais entreprendre des essais dans cette voie, qui présente aussi quelques difficultés, que je ne crois pas, cependant, insurmontables aujourd'hui avec le développement de la technique photographique.

Le 30 Avril 1930 j'avais déjà obtenu quelques photographies de Mercure à son élongation du soir, mais les images étant très onduleuses aucun détail n'avait été enregistré. Le 11 Avril dernier, l'air étant beaucoup plus calme, j'ai entrepris, de nouveau, de photographier la planète avec l'objectif Viennet photographique, monté sur l'équatorial de l'Observatoire Flammarion de Juvisy. Cet objectif a un diamètre de $0^m,160$ et une distance focale de $2^m,900$. A l'aide d'un système optique positif, constitué par deux lentilles plan-convexes, j'agrandis l'image focale 9 fois. Ce jour-là Mercure avait un diamètre de $7''{\cdot}9$. Les

plaques photographiques employées étaient des plaques ultra-sensibles, de rapidité environ 700 H et D ; elles ont été exposées au nombre de quatre : à $18^h\ 57^m$ trois images posées de 3 à 4 secondes ; à $18^h\ 59^m$ deux images posées de 3 à 4 secondes ; à $19^h\ 8^m$ trois images posées 2 à 3 secondes, et à $19^h\ 15^m$ deux images posées de 1 à 3 secondes. J'ai donc obtenu le 11 Avril 1931, entre $18^h\ 57^m$ et $19^h\ 15^m$, dix photographies de la planète Mercure.

Ces dix images photographiées présentent des nettetés assez variables suivant l'état d'agitation des vagues atmosphériques du moment. Deux d'entre elles sont assez satisfaisantes, quatre sont moins bonnes mais présentent encore quelques détails, et les quatre autres, très vagues ou manquant de pose, sont inutilisables. Les meilleures sont celles que j'ai obtenues à $18^h\ 57^m$ et ce sont celles-ci que nous allons examiner.

Je dois dire tout d'abord qu'une observation visuelle à l'équatorial de $0^m,240$ m'avait révélé immédiatement l'existence, à la surface de Mercure, d'une région blanche un peu au Sud du centre du quartier non loin du terminateur, ainsi qu'une tache australe assez foncée au-dessus de cette tache blanche. Cette dernière était encore limitée au Nord par une autre tache foncée, moins étendue et moins sombre que celle australe. C'est donc surtout cette vision de détails bien marqués à la surface de la planète qui m'a engagé à tenter aussitôt la photographie.

Six images photographiées montrent incontestablement les détails vus à l'équatorial. La région blanche centrale semble même déborder légèrement du terminateur par irradiation combinée avec l'assombrissement des taches qui la bordent au Sud et au Nord. J'ai tiré des contretypes, puis des agrandissements de ceux-ci, qui font ressortir encore les détails des clichés originaux. Mais comme les reproductions de ces photographies seraient très difficiles à cause de leur petite échelle, j'ai dessiné le plus exactement possible sur le croquis ci-joint, les détails que l'on peut y observer avec quelque attention. Je répète que c'est le résultat de l'examen, non pas d'une seule photographie, mais de *six* des meilleures obtenues le 11 Avril 1931.

Je crois que c'est la première fois que l'on arrive à obtenir quelque chose à la surface de Mercure. J'étais arrivé, aussi le premier, à photographier des taches sur Vénus en 1911 et en 1921.*

Nous nous plaisons à rappeler que la plaque sensible se révèle souvent supérieure à l'œil pour enregistrer les faibles différences de tonalités qui existent à la surface des planètes. J'en ai eu maintes fois la preuve dans mes nombreuses photographies planétaires.

Pour Mercure ce n'est qu'un début et j'espère obtenir de meilleurs résultats dans l'avenir. Mais, dès aujourd'hui, je tiens surtout à signaler ces nouvelles photographies aux grands observatoires, qui sont mieux outillés et surtout mieux placés que nous, tant en latitude qu'en altitude.

Observatoire de Juvisy.

* Voir les *Comptes-Rendus de l'Académie des Sciences de Paris*, 1911, tome 153, page 1208, et 1921, tome 172, No. 26 ; ainsi que les *Bulletins de la Société Astronomique de France*, 1913 février, page 53, et 1922 Mars, page 126.

Occultations of Stars by the Moon, observed at the University of London Observatory during the Year 1930.

(*Communicated by the Director.*)

No.	Star.	Mag.	Phase.	Date.	G.M.T.	Telescope.	Observer.
1	24 G Sco.	6·2	D	June 9	23 6 22·68	24-inch Cass.	C. C. L. G.
2	B.D.+24° 674	6·3	R	Sept. 15	0 23 8·96	,,	C. C. L. G.
3	112 B Aur.	5·7	R	Sept. 15	23 26 36·90	,,	C. C. L. G.
4	B.D.+19° 511	7·2	D	Dec. 31	21 47 43·08	8-inch Ref.	F. R.
5	63 Ari.	5·2	D	Dec. 31	22 48 27·34	,,	F. R.

The error and rate of the synchronome clock are determined by the B.B.C. wireless signals, and no correction has been applied to the observed times for lag, personal error, etc. Eye and ear is the method adopted by C. C. L. G.; eye and stop-watch by F. R.

The co-ordinates of the 24-inch Cassegrain are given in the *N.A.*, 1932. From this the 8-inch bears N. 200° E. (true) 17 metres, and this small difference has been disregarded.

In the reduction of the above observations a correction of $0^h{\cdot}0030$ to allow for an error of 6″ in the mean longitude of the Moon has been included as suggested by Professor E. W. Brown.

No.	χ.	ρ.	$\sigma'-\sigma$.	$\chi-\rho$.	$\cos(\chi-\rho)$.	Computer.
	° ′	° ′		° ′		
1	102 48	105 40	0·0	−2 52	+0·999	T. L. MacD.
2	241 0	77 59	−0·2	163 1	−0·956	F. R.
3	223 54	84 28	+2·4	139 26	−0·760	T. L. MacD.
4	137 38	70 39	+0·2	66 59	+0·391	F. R.
5	117 49	70 52	−0·3	46 57	+0·683	F. R.

For Star No. 2, B.D. + 24° 674, the *N.A.* gives no co-ordinates. They were obtained from Greenwich 1910, Heidelberg 1900, Washington 1900, using P.M. from Greenwich 1910 in each case.

The occultation of B.D. + 19° 511 was not predicted. Its disappearance was noted by the observer while waiting for D of 63 Ari, and the star was identified later, by the aid of the B.D. maps and the G.F.H., as Abbadia 1480 and Cincinnati publication 15, No. 615. Its position for 1900·0 is $3^h\ 15^m\ 6^s{\cdot}47 + 20°\ 8'\ 53''{\cdot}9$.

University of London Observatory,
Mill Hill Park, N.W. 7:
1931 *June* 10.

Errata.

p. 465, right-hand column of table, "Composite I," *for* "homogeneous core" *read* "relativistically degenerate core."

p. 735, before line 9 from bottom, insert:—The probable error of one distance measured with the Cape heliometer is—